The Filamin A Actin Binding Domain Structure and Function:

Implications for a gain-of-function mechanism for the otopalatodigital syndrome spectrum disorders

A dissertation presented in partial fulfilment of the requirements for the degree of

Doctor of Philosophy

in

Biochemistry

at Massey University, Palmerston North, New Zealand

Alice Rosemary Clark

2009

Abstract

The filamin family act as scaffolding proteins associating with actin filaments, acting through a highly conserved actin binding domain (ABD). The ABD of the filamins is homologous to that found in other F-actin binding proteins such as dystrophin. Mutations in the filamin A gene cause a wide range of disease symptoms in humans reflecting the diversity of the roles that filamin A has in cell structure and signalling pathways. The diseases fall into two separate phenotypic groups. Periventricular nodular heterotopia (PVNH) generally results from the complete loss of filamin A protein, and affects the central nervous system. The clinically separate otopalatodigital disorders (OPD) spectrum disorders are skeletal disorders and were hypothesised to be gain of function phenotype diseases. At the beginning of this work, there was very little structural data available for the human filamins, and none for the crucial highly conserved actin binding domain. This lack of structural data limited the interpretation of the biochemical and genetic data and constrained our understanding of the disease associated mutations that cluster in this domain. These studies aimed to provide insights into the structure and mechanism of actin binding domains, and thus provide a better understanding of the diseases caused when this domain is mutated.

A secondary structural analysis and crystal structures of the wildtype and OPD2 associated mutant ABDs were obtained. The overall fold of the three proteins was equivalent as determined by circular dichroism spectroscopy and x-ray crystallography. The ABD from filamin A E254K showed 3.7 fold increased F-actin affinity, accompanied by a reduced thermostability (of 5.6 °C). Western blotting of OPD2, frontometaphyseal dysplasia (FMD) and PVNH patient fibroblast lysates showed similar levels of filamin A compared to the control cells. In addition the OPD and PVNH patient fibroblasts were able to adhere to fibronectin and migrate with an equivalent rate to control cells.

Together these results have allowed correlations to be developed between structure, protein stability, actin affinity, cellular phenotype and the overall clinical phenotype. Showing that, at least in one example, OPD2 may be due to an increased actin affinity providing further evidence for a gain of function mechanism of OPD2.

Διά τὸ θαυμάζειν ἡ σοφία

Wisdom begins in wonder

Socrates

Acknowledgements

This thesis would not have been possible without the help, guidance and support of many people, and I would like to acknowledge some of these people.

Firstly to my supervisor Dr Andrew Sutherland-Smith, whose patience, kindness and enthusiasm made this project a joy to be involved in. Thank you so much. To my co-supervisor Dr Gill Norris, thank you for your many kind and wise words and for letting me use your lab. You have taught me a lot about biochemistry and life!

To all the members of the Centre for Structural Biology – thank you all so much. I do not consider you my work mates, but rather my dear friends. I will miss Fridays at the Celtic. Your support, both in science matters and as friends, has made this work what it is, and has made me the happy person I am today. To all the members of the Sutherland-Smith group, Jan, Ben, Carlene and Muthu: Thanks for all the lab fun we had! I would especially like to mention Greg – who shared my frustration with the assay, and helped me in so many ways. I would also like to thank; Matt, Brian, Geoff, Simon and Trevor whose guidance (particularly in computer matters) is much appreciated. To the girls in our lab; Meekyung, Jana, Judith, Komala, Ursula and Kristy who I will miss so, so much, thank you for your love and support. To the NMR boys; Jo and Martin. Thanks for your help in all things magnet related (and non-magnet related issues). I would also like to thank everyone else in IMBS who helped me, and there are many of you. But I would especially Kathryn and Natisha who let me use their tissue culture facility, and have supported me in so many ways throughout my time at Massey.

To all my amazing friends - thanks so much! But especially Sacha and Mat – this work would not have been possible without your love and support. Ben and Nicole – thanks for feeding me and letting me chop your gorse. Your friendship means a lot to me.

To my family; Di, John, Helen, Robin and Lily. Your endless support and love means so much to me – I am lucky to have such a wonderful family.

Table of Contents

List of Figures

List of Tables

Abbreviations

ABD	Actin binding domain
ABS	Actin binding sequence
Amp	Ampicillin
ADP	Atomic displacement parameter
BCA	Bicinchoninic acid
BLAST	Basic local alignment search tool
BMD	Becker muscular dystrophy
BSA	Bovine serium albumin
CaM	Calmodulin
cDNA	Complementary DNA
CD	Circular dichroism
CH	Calponin homology domain
C-terminal	Carboxyl terminal
CV	Column volume
DMD	Duchenne muscular dystrophy
DMEM	Dulbecco's modified eagle media
DNA	Deoxyribonucleic acid
dNTP	Deoxy-nucleotide tri-phosphate
DTT	Dithiothreitol
E. coli	*Escherichia coli*
EDTA	Ethylene diamine tetraacetic acid
EGTA	Ethylene glycol tetraacetic acid
F-actin	Filamentous actin
FMD	Frontometaphyseal dysplasia
g	Gravitational field, unit of
G-actin	Globular (monomeric) actin
GOF	Gain of function
IPTG	Isopropyl-β-D-thiogalactopyranoside
kb	Kilobase pairs (of DNA)
K_d	Dissociation constant
LOF	Loss of function

M2	Human melanoma derived cell lines
MCS	Multiple cloning site
MEF	Mouse embryonic fibroblasts
MNS	Melnick Needles syndrome
NCS	Non crystallographic symmetry
N-terminal	Amino terminal
OMIM©	Online mendelian inheritance in man
OPD	Otopalatodigital syndrome
ORF	Open reading frame
PAGE	Polyacrylamide gel electrophoresis
PBS	Phosphate buffered saline
PCR	Polymerase chain reaction
PDB	Protein database
PIP_2	Phosphotidylinositol 4,5-bisphosphate
PVNH	Periventricular nodular heteropia
RMSD	Root mean square deviation
RNA	Ribonucleic acid
SDS	Sodium dodecyl sulfate
TEMED	N, N, N', N'-tetramethylethylenediamine
Tris	Tris-(hydroxymethyl)-aminomethane
V	volts
WT	Wildtype

Related Publications

Clark, A. R., Sawyer, G. M., Robertson, S. P., Sutherland-Smith, A. J. (2009). Skeletal dysplasias due to filamin A mutations result from a gain-of-function mechanism distinct from allelic neurological disorders. Human Molecular Genetics Advance Access published September 22, 2009, 10.1093/hmg/ddp442

1 Introduction

1.1 The Actin Cytoskeleton

The cytoskeleton of cells is constructed of filamentous polymers composed of actin, intermediate filament proteins or tubulin proteins. Filamin A binds two actin fibres, cross linking actin to form the networks found in cells (Nakamura *et al.*, 2007). The actin cytoskeleton is a dynamic and highly regulated entity involved in many cellular processes such as motility, endocytosis, phagocytosis, adhesion (Figure 1-1).

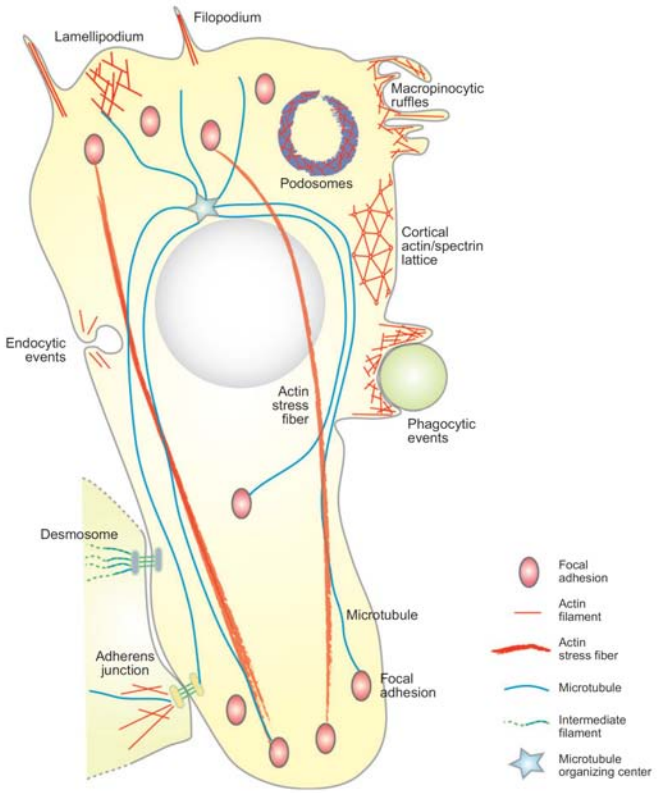

Figure 1-1. Roles of the Actin Cytoskeleton.

This stylised eukaryote cell shows the different roles of actin in the cell. Actin is involved in phagocytic events, membrane ruffles, filopodium, lamellipodium, endocytic events, stress fibres, and mediating cell-cell contacts.

Doherty and McMahon, 2008

Actin forms a mesh of filaments that associate with the plasma membrane, helping to maintain the cellular shape and form. Actin is also involved with endocytic and phagocytic structures at the cell membrane, and long actin filaments are seen in filopodia. There is an actin network at the leading edge of migrating cells and long bundles of actin fibres form cables (stress fibers) that anchor to sites of adhesion (focal adhesions) in migrating cells (reviewed in Doherty and McMahon, 2008).

1.2 Regulation of Filamin A

1.2.1 Gene Expression

The family of filamins (filamin A, B and C) are a widely expressed family of actin binding proteins. The filamin A gene (filamin A; 300017) is encoded on chromosome Xq28 and is expressed in tissues almost ubiquitously from early development onwards. Filamin A and filamin B have similar patterns of expression in many tissues (Xu *et al*., 1998), with filamin C expression is restricted to muscle tissues (Dalkilic *et al*., 2006). However, despite the similarities between filamin A and B, the two proteins clearly have distinct functional roles as seen in the distinct diseases associated with each.

Filamin mRNA also uses a number of alternative poly(A) signals, which results in different turnover rates of mRNA (Takafuta *et al*., 1998). Alternative splicing in the mRNA was identified, enabling cells to produce a number of different filamin isoforms (Gorlin *et al*., 1990). The filamin A splice variants were at relatively low levels, but were expressed throughout the body. In two heart-specific filamin B splice variants the dimerisation domain is absent and the function of these is not well understood (Xu *et al*., 1998).

1.2.2 Post Translational Regulation

1.2.2.1 Phosphorylation and Proteolysis

Filamin A is regulated by post-translational modifications such as proteolysis and phosphorylation (Gorlin *et al*., 1990; Woo *et al*., 2004; Sharma and Goldmann, 2004). Phosphorylation near the hinge regions decreases the actin binding activity and regulates filamin A-integrin interactions (Ohta and Hartwig, 1996; Goldmann, 2001).

Phosphorylation at repeat 23 regulates membrane ruffle formation and cytoskeletal reorganisation (Vadlamudi *et al*., 2002). Filamin A is a caspase and granzyme B substrate, and is cleaved during apoptosis (Browne *et al*., 2000).

1.2.2.2 Phosphatidylinositol (4,5)-bisphosphate 2

Phosphotidylinositol (4,5)-bisphosphate 2 (PIP_2) is a phospholipid that plays a signalling role in cell division and proliferation, membrane trafficking, endocytosis and exocytosis, cell adhesion and polarisation. The general PIP_2 binding site is not a specific amino acid sequence, and is thought to be a lysine-rich basic region (reviewed in Bella, 2005).

To remodel the actin cytoskeleton PIP_2 dissociates the profilin:actin and gelsolin:actin complexes, *in vitro*, to promote actin polymerisation (Moens and Bagatolli, 2007). PIP_2 also inhibits the actin crosslinking activity and the F-actin-binding activity of smooth muscle filamin (Furuhashi *et al*., 1992). The mechanism by which PIP_2 inhibits the α-actinin-3 F-actin interaction is well characterised (Franzot *et al*., 2005). Disruption of this PIP_2 α-actinin-3 interaction has been implicated as a mechanism of some disease causing mutations within α-actinin (Fukami *et al*., 1996).

1.3 The Structure of the Filamin A Homodimer

1.3.1 Domain Structure in the Dimer

The filamin A open reading frame (ORF) encodes a 280 kDa monomer which forms tail to tail homodimers through the C-terminal domain. The filamin A dimer forms a 'V' shape as observed by electron microscopy (Tyler *et al*., 1980) (Figure 1-2a). Each filamin A monomer is composed of a C-terminal dimerisation domain, rod/repeat domains and a N-terminal F-actin binding domain (ABD) (Hock *et al*., 1990) (Figure 1-2b).

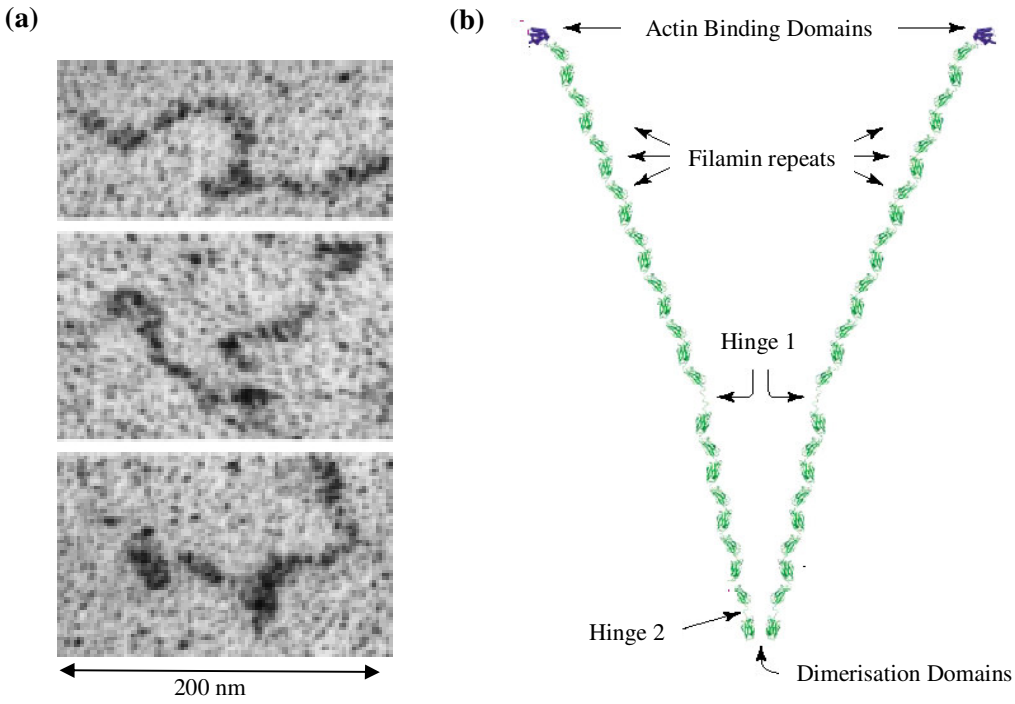

Figure 1-2. Electron Micrographs of Filamin A Dimers and a Model of the Filamin A Dimer.

a) Electron micrographs of tantalum–tungsten-cast filamin A dimers from rabbit macrophage (Tyler *et al*., 1980).

b) Model of the filamin A structure, two monomers associate through the dimerisation domain at the C-terminus forming a V-shaped dimer. The two hinge regions allow flexibility. The ABD is located at each N-terminus. The ABD is linked to the dimerisation domain through the rod domain, which is constructed of 24 filamin repeats. This model is derived from homology studies only (and not experimental data).

The rod domain determines the flexibility, orientation and spacing of the F-actin cross-linkage (Weihing, 1988; Furuike *et al.,* 2001). The repeats of this domain have an Ig like domain fold, with a predominantly β-sheet structure, which are interrupted by two hinge regions that form the V-shape that the filamin requires for correct function (Bork *et al.,* 1994; Fucini *et al*., 1997) (modelled in Figure 1-2). The dimerisation domain (repeat 24) is located at the C-terminus, and the structure of this domain in filamin C has been solved (PDB code 1VO5). Unlike some actin binding proteins, such as α-actinin and spectrin, the filamins all lack a calcium-responsive domain (van der Flier and Sonnenberg, 2001).

1.3.2 The Actin Binding Domain (ABD)

1.3.2.1 Interactions with Actin

Filamin A is a cytoskeletal protein that binds to the dynamic actin filaments as a homodimer through the ABD, (Nakamura *et al*., 2007). The ABD is comprised of two calponin homology (CH) domains (Gimona *et al*., 2002). The filamin A:actin interaction is thought to occur though the actin residues 105-120 and 360-372 (Mejean *et al.,* 1992). One filamin A monomer binds to an actin filament, with the second monomer binding another actin filament. This interaction crosslinks the actin filaments into an orthogonal network (Nakamura *et al*., 2007), with filamins the only proteins that organise actin in this way (Figure 1-3). Filamin A also helps to stabilize the actin filaments by slowing actin depolymerization (Koteliansky *et al*., 1981), and in actin crosslinking studies, increasing filamin A concentrations lead to tighter actin bundles (Brotschi *et al.,* 1978; Dabrowska *et al.,* 1985; Niederman *et al.,* 1983).

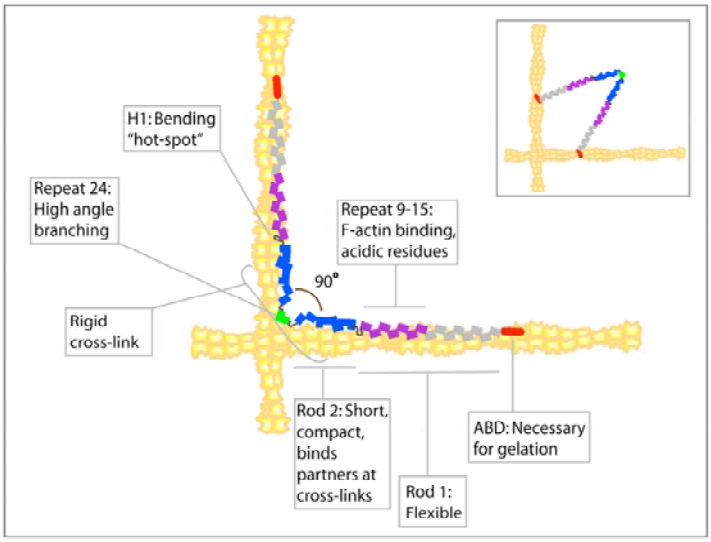

Figure 1-3. The Filamin A Dimer Bound to Actin.

Two actin fibres (yellow) are shown cross linked by a filamin A homodimer. The domains of filamin A are labelled accordingly. The insert shows the alternative binding mechanism that has not been observed.

Osborn 2007

1.3.2.2 Interactions with Calmodulin

Increasing the Ca^{2+} concentration, in the presence of calmodulin (CaM), was shown to inhibit filamin A gelation of actin. However, in pull down assays CaM did not bind the native filamin A (Nakamura *et al.,* 2005). When seven acidic residues, (Asp and Glu), were removed from the loop between the two calponin homology (CH) domains, CaM bound to the filamin A, in the presence of Ca^{2+} (Nakamura *et al.*, 2005). Based on data from the α-actinin structure, the authors speculated that the loop between CH domains may block CaM binding to filamin A. In the α-actinin structure (PDB 1WKU) the loop between CH1 and CH2 lies close to the core ABD structure, and is located near the C-terminus of the ABD. Because the CaM only binds native filamin A in the presence of F-actin, it was thought that this acidic loop may block CaM access to the binding site by binding to the basic C-terminus.

1.3.2.3 Homology and Evolution of the ABD

Many cytoskeletal proteins share a highly conserved ABD. This group of proteins include all three filamins (A, B and C), α-actinin, dystrophin, utrophin, fimbrin and β-spectrin. The ABD is formed by the two sub-domains, CH1 and CH2 (Castresana and Saraste, 1995) (Figure 1-4). Each CH sub-domain shares high sequence similarity with a domain of the smooth muscle protein calponin.

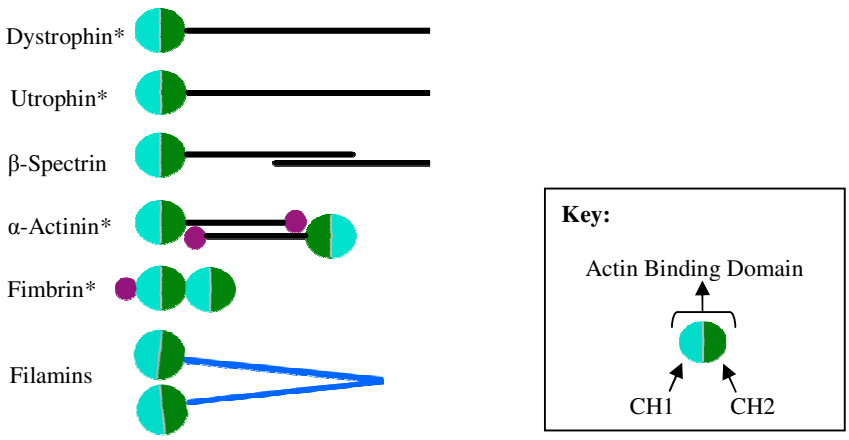

Figure 1-4. Schematic of the Actin Binding Domains in Proteins.
Shown here are the F-actin binding proteins: filamins, α-actinin, dystrophin, utrophin, fimbrin and β-spectrin. The location of the ABD is indicated within the overall protein architecture. The two sub-domains that make up the ABD, CH1 and CH2 are also shown. *Indicates the structure of the ABD had been determined before this work.

Sequence comparisons show there is more similarity between the CH1, or the CH2, domains of different members of the F-actin binding family than between the CH1 and CH2 domains from the same protein. During early evolution, the fimbrin ABD was further duplicated, and the resulting ABD pair is present in the fimbrin of all phyla. Following this evolutionary event, plants and fungi have almost completely lost the single ABDs (Korenbaum and Rivero, 2002). The diversity of ABD-containing proteins is thought to have occurred through gene duplication followed by shuffling and intragenic multiplication (Dubreuil, 1991; Leung *et al.*, 2001). The *Dictyostelium* filamin (APB120) is the archetype filamin protein; this protein is thought to have given rise to the animal filamins by multiplication of filamin repeats (Korenbaum and Rivero, 2002).

1.3.2.4 The General Structure of the ABD

The ABD is typically composed of two CH domains. Each CH subdomain typically contains four main α-helices and two shorter, less regular α-helices, designated A to G. Three α-helices (C, E and G) form a triple helical bundle with the N-terminal α-helix (A) lying perpendicular to this bundle. These helices are connected by variable loops

and two small helices B (only in CH2) and F (Franzot *et al*., 2005; Goldsmith *et al*., 1997).

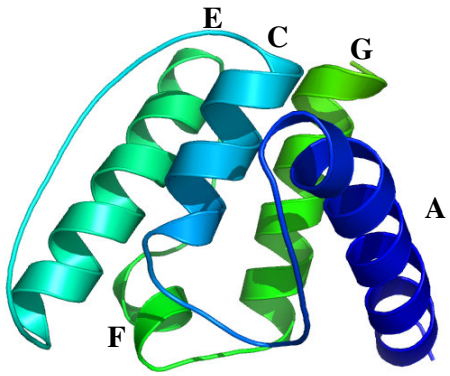

Figure 1-5. The Conserved Helical CH Domain Structure.
The α-Actinin CH1 domain is shown (1WKU), the helices are labelled A to G. The small B and D helices are absent in this domain structure.

1.3.2.5 The Actin Binding Surface of Filamin A

The ABD binds filamentous actin, rather than actin monomers. Deletion studies of dystrophin revealed residues in three separate sites within the ABD were important for actin affinity (Corrado *et* al., 1994; Fabbrizio *et* al., 1993). The actin:utrophin ABD interaction was disrupted using antibodies to investigate the residues involved (Morris *et al.,* 1999). Mutagenesis studies of the α-actinin ABD (Kuhlman *et al*., 1992; Hemmings *et al*., 1992) and filamin isolated from smooth muscle (Lebart *et al*., 1994) and Dictyostelium filamin (Bresnick *et al*., 1991) showed that the sequence 119 - 146 (actin binding site 2, ABS2) is absolutely required and it is also a highly conserved region of the ABD (see alignment page 31).

When the two CH domains of dystrophin are separated CH1 (containing ABS1 and 2) binds to actin, but CH2 (containing ABS3) does not, indicating that CH1 is the major contributor to the actin binding surface. However, the domains bind with a greater affinity when together as the complete ABD (Winder *et al*., 1997; Gimona *et al*., 1998), and the ABS are not functionally interchangeable (Lorenzi and Gimona, 2008). The filamin C:actin interaction, in contrast to α-actinin, is affected by ionic strength. Therefore, in addition to the hydrophobic residues, hydrophilic residues in filamin C are critical for the actin binding (Lebart *et al*., 1994). Studies of fimbrin have shown

conformational rearrangements between the CH1 and CH2 sub domains with the ABD, though the functional significance of this remains unclear (Klein *et al.,* 2004). NMR studies of the amino acids involved in the actin:dystrophin interface further highlighted the residues in ABS2, and confirmed the importance of ABS1 (Levine *et al*., 1990, 1992). When the ABS surface is mapped to the ABD structure of fimbrin (PDB code 1AOA) the residues do not form a continuous surface (Goldsmith *et al*., 1997). To study the interface between the ABD and actin the structure of the fimbrin ABD was fitted to electron density data and diffraction from 2D arrays, with good agreement (Hanein *et al*., 1998; Volkmann *et al*., 2001).

In contrast to the fimbrin ABD, the way in which the utrophin and dystrophin ABDs bind to actin is less clear. The utrophin and dystrophin ABDs crystallised in a dimer in which the CH1 and CH2 domains are swapped (1QAG, Keep *et al*., 1999; 1DXX, Norwood *et al*., 2000). This structure was referred to as the 'open' or 'extended' form of the ABD. The CH1/CH2 interface is formed by the same region as α-actinin and fimbrin, but the CH1 forms an interaction with CH2 of the adjacent molecules in the crystal. In 2002 Galkin *et al*., modelled the 'open' utrophin structure into the electron density from negatively stained electron microscopy reconstruction. This showed the ABS was able to be modelled at the interface. However, data from another study supported the 'compact' monomer form of the utrophin ABD binding to actin (Sutherland-Smith *et al*., 2003; Lehman *et al*., 2004) (Figure 1-6a-c). This bound form of the utrophin ABD was a ‘lozenge-like’ shape, and like the other ABD-actin electron microscopy studies, correlated with a closed/compact ABD. This led the authors to propose a general mechanism by which this pair of CH domains (ABD) binds to F-actin (Figure 1-6d). However, an intrinsic flexibility of the CH1 and CH2 domain must exist to allow the domain swapping in dystrophin and utrophin to occur (Bennett *et al*., 1994). In addition to the uncertainty surrounding the residues of the ABD that contact actin, other domains at the N-terminus (adjacent to the ABD) are also implicated in the actin binding in utrophin and filamin A (Sutherland-Smith *et al*., 2003; Nakamura *et al*., 2007).

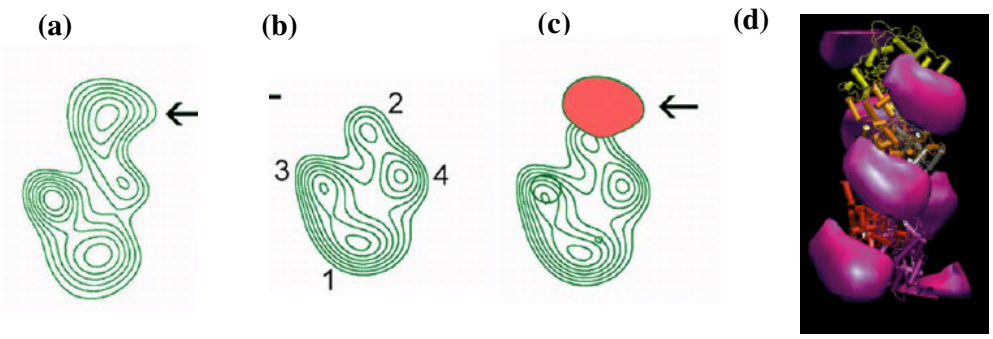

Figure 1-6. The Transverse Sections Reconstructed from EM Data of Utrophin Bound to Actin and the Resulting Model.

a) A section through the actin fibre with the utrophin ABD bound. Note the mass contributed by utrophin, (arrow) when compared to section (b).

b) Undecorated F-actin, actin sub-domains are numbered 1-4.

c) Difference densities (arrow) were constructed by subtracting maps of F-actin from those of the F-actin-utrophin map.

d) The resultant model of utrophin (pink) binding to F-actin.

Sutherland-Smith *et al.*, 2003, Lehman *et al.*, 2004

1.4 Cellular Roles of Filamin A

1.4.1 Filamin A Binding Partners

The filamin A homodimer binds not only to actin, but also to many signaling and membrane bound proteins in the cell, playing a role in integrating signaling and cytoskeletal remodeling for processes such as cell locomotion, organelle transport and cell division (Stossel *et al*., 2001) (Figure 1-7).

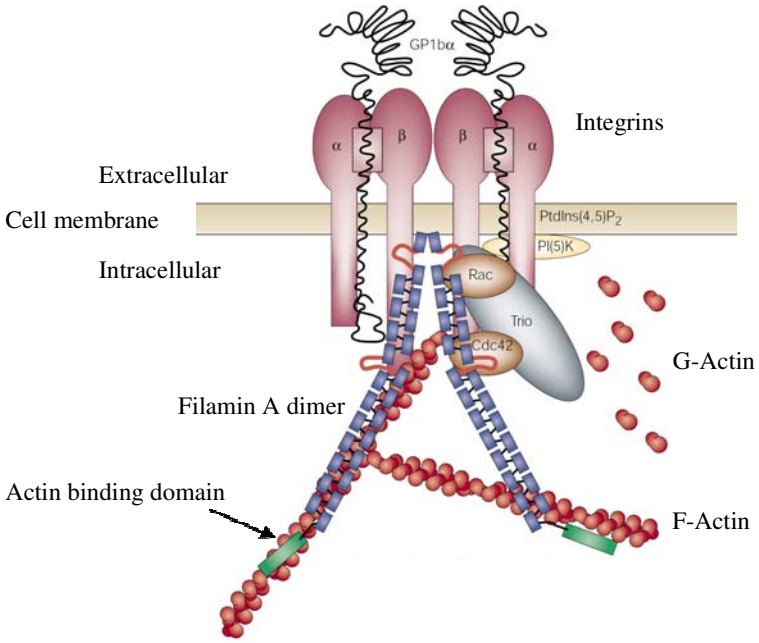

Figure 1-7. Model of the Filamin A Homodimer Interactions.

The actin binding domain (ABD) in green is located at the N-terminus of filamin A (blue). The two filamin A monomers associate through the C terminal dimerisation domain. Monomeric globular (G) and filamentous (F) actin are shown in red. Some other interaction partners of filamin A are also shown, the signaling proteins Rac, Trio, cdc42 and the integral membrane receptors, integrin and GP1bα.

Stossel *et al*., 2001

These filamin binding partners include cytoskeletal, signalling and sorting and trafficking proteins (Nakamura *et al*., 2005; Hayashi and Altman 2006; Liu *et al*., 1997; Hjalm *et al*., 2001; Nagano *et al*., 2004; Calderwood *et al*., 2001; Loo *et al*., 1998; Sharma *et al*., 1995; Lad *et al*., 2008; Ohta *et al*., 1999; Bellanger *et al*., 2000; Stahlhut

et al., 2000) (Figure 1-8). The nature and abundance of these interactions highlight the diverse roles of filamin A in cells (reviewed in Revenu *et al.,* 2004).

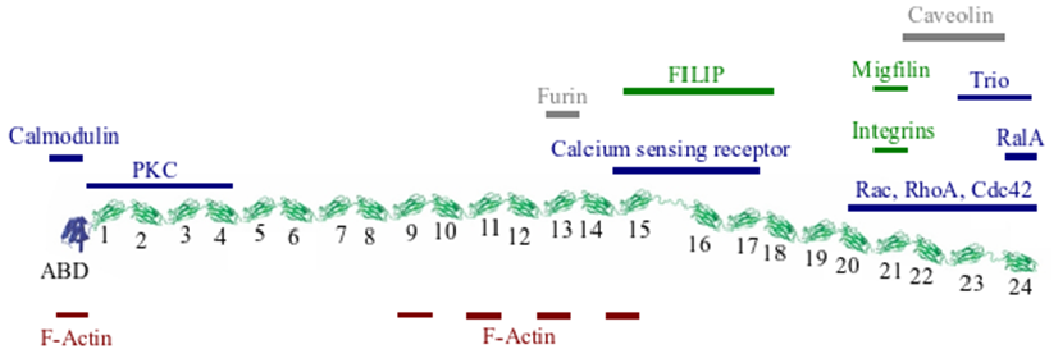

Figure 1-8. Selected Filamin A Binding Partners.

The filamin A monomer is shown with the ABD and the repeat domains numbered 1-24. The binding sites of proteins are indicated and coloured by function. Red: Cytoskeletal. Blue: Signalling. Green: Motility. Grey: Sorting/Protein transport.

1.4.2 Membrane Stability

In addition to a role in the cytoskeleton, filamin A is also implicated in membrane stability and structure (reviewed in Feng and Walsh, 2004). Human melanoma cell lines that naturally lack filamin A show cytoskeletal blebbing (Cunningham *et al.*, 1992; Stossel *et al.,* 2001). When a mechanical force is applied to the membrane of human fibroblasts and osteoblast cells, filamin A expression is upregulated (D'Addario *et al.*, 2001; Jackson *et al.*, 2008). Filamin A also has an integrin dependent role in mechanoprotection in human melanoma cells, organising actin at the sites of force (Glogauer *et al.*, 1998). Taken together, these results highlight the role of filamin A in membrane structural integrity.

1.4.3 Sorting and Protein Transport

Filamin A also has a role protein sorting within cellular compartments and organelles. Furin, which cycles between cellular compartments, requires filamin A for correct cell localisation and rate of internalisation (Liu *et al.*, 1997). In addition to furin, filamin A

interacts with caveolin, a protein involved in endocytosis of proteins from the cell membrane (Stahlhut *et al.*, 2000).

1.5 X-linked Filamin A Associated Diseases

1.5.1 Pathogenic Filamin A Mutations

Mutations in Filamin A are associated with otopalatodigital disorders 1 and 2 (OPD1; OMIM 311300, OPD2; OMIM 304120), frontometaphyseal dysplasia (FMD; OMIM 305620) and Melnick Needles syndrome (MNS; OMIM 309350), periventricular nodular heterotopia (PVNH; OMIM 300049) (Figure 1-9). A number of the mutations cluster in the ABD, highlighting the importance of this domain for the correct function of filamin A.

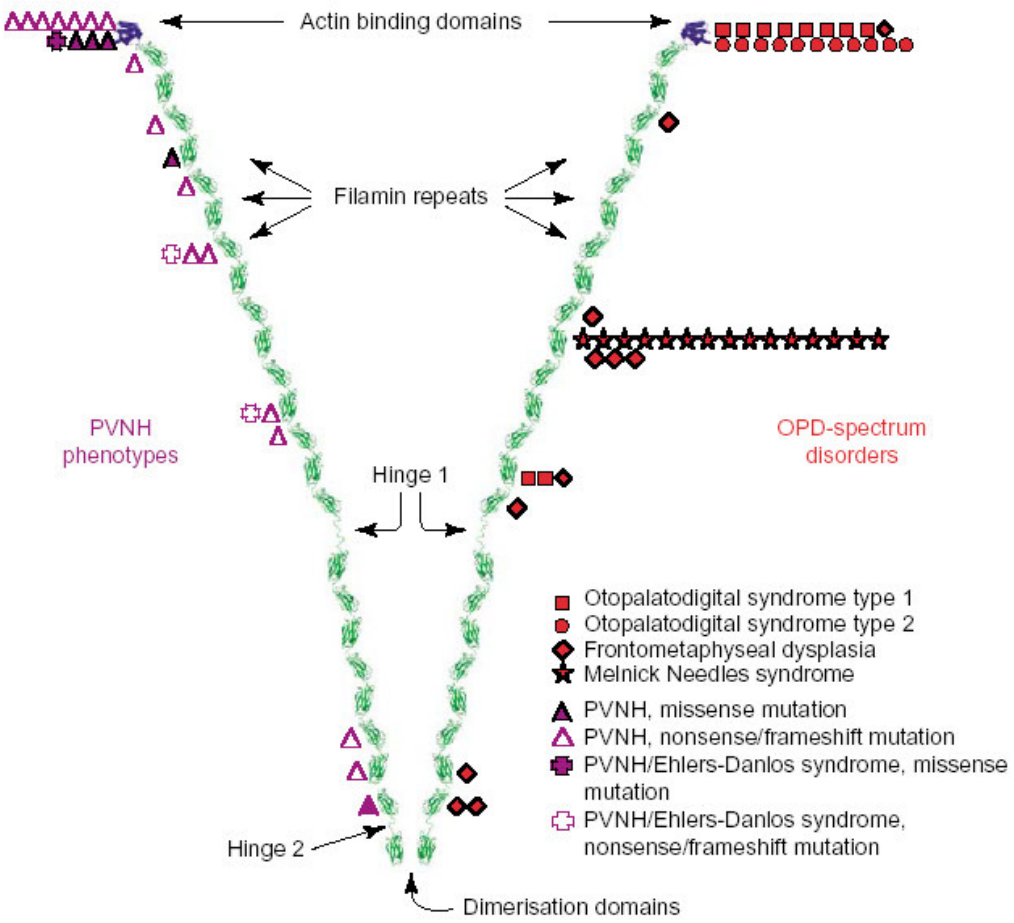

Figure 1-9. The Location of Pathogenic Point Mutation Sites in Filamin A.

The sites of pathogenic mutations and the diseases that are caused are indicated. Disease mutations cluster in discreet domains. On the left are the PVNH (loss of function) associated mutations, and on the right are the OPD-spectrum disorders (OPD1, OPD2, FMD and MNS).

Robertson, 2005

1.5.2 The ABD and Disease

The ABD is also associated with disease associated mutations in other proteins. Mutations in the filamin B ABD cause three distinct skeletal disorders, Larsen syndrome (OMIM 160250) and atelosteogenesis I and III (AOI, OMIM 108720 and AOIII, OMIM 108721) (Krakow *et al.,* 2004; Zhang *et al.,* 2006). Some of the mutations that cause these disorders are analogous to those found in filamin A that are associated with disease. Filamin C is critical to correct muscle development and maintenance of muscle structural integrity. There are no reported pathogenic mutations

in the ABD of filamin C; however, mutations in other domains of filamin C are associated with myofibrillar myopathy (Vorgerd *et al*., 2005; Dalkilic *et al.,* 2006).

Dystrophin contains analogous ABD mutations to those of filamin A that cause neuromuscular disease, enabling a comparison between the filamin A and dystrophin ABDs (Tyler *et al,* 1980; Roberts *et al.*, 1994). Point mutations in the dystrophin ABD are associated with both Duchenne and Becker muscular dystrophy. The severity of these diseases ranges from the Duchenne form with a life expectantly of about 20, to the milder Becker form for which life expectancy can be in excess of 40-50 years old. Generally the Duchenne form is associated with deletions and frame shift mutations, resulting in the complete loss of dystrophin protein. However, both diseases are a "loss of function" phenotype (Murray *et al*., 1982; Prior *et al*., 1993; Emery, 2002).

In the β-spectrin, ABD point mutations are associated with a hemolytic anemia disorder, hereditary spherocytosis (Agre *et al*., 1986), and, in α-actinin-4, mutations in the ABD are associated with the kidney disorder, focal segmental glomerulosclerosis (Kaplan *et al*., 2000). When these pathogenic point mutations are mapped to the ABDs most cluster in the CH2 domain (Figure 1-10).

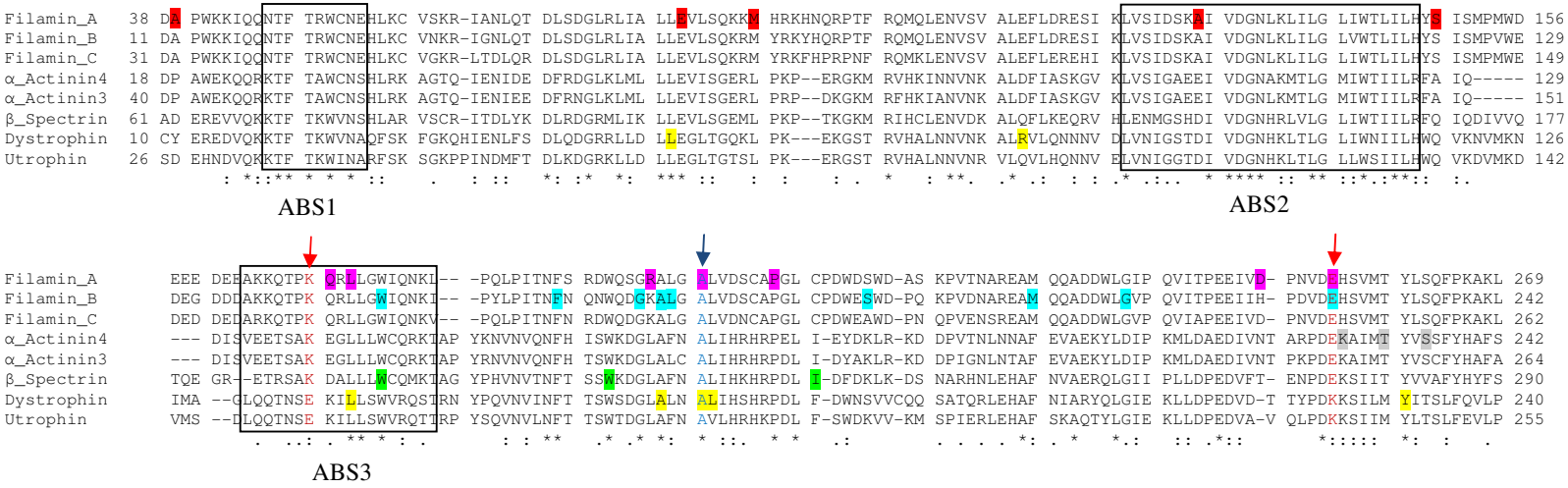

Figure 1-10. Alignment of the Conserved ABD.

The actin binding sites 1-3 (ABS1-3) are shown (section 1.3.2.5), and the CH1 domain (top) and CH2 domain (bottom) are shown separately. The sites of pathogenic mutations are coloured by associated disease. PVNH is shown in red; OPD spectrum disorders in purple; the Larsen, boomerang, AO1; and AO3 syndromes are shown in blue; focal segmental glomerulosclerosis are shown in grey; hereditary spherocytosis is shown in green; muscular dystrophy in yellow. Two residues associated with OPD2 (E254K and A200S) are highlighted: The pair of residues that contribute to the conserved salt bridge between E254 and K169 is shown in red text/arrow. The conserved A200 is shown in blue text/arrow.

1.5.3 Loss of Function Phenotype: PVNH Disease

PVNH female patients present with normal intelligence but suffer from late onset epilepsy and are diagnosed by the presence of periventricular nodules in the brain, which can be visualised with MRI (magnetic resonance image) (Poussaint *et al*., 2000; Sarkisian *et al*., 2008) (Figure 1-11). The epilepsy is attributed to the periventricular nodules in the brain, which are formed during foetal development, when morphologically normal neurons fail to migrate correctly (Fox *et al*., 1998).

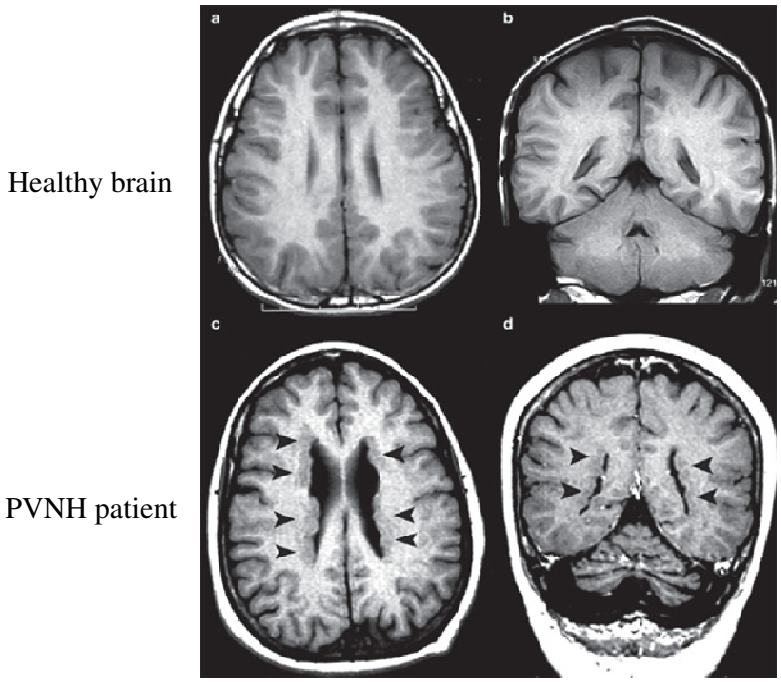

Figure 1-11. Magnetic Resonance Image of the Brain of a PVNH Patient and a Healthy Brain.
Images of the brain of a healthy patient (top two panels) and a female PVNH patient (lower panels) showing multiple nodules of gray matter (arrows).

Feng and Walsh 2004

PVNH patients also have extracerebral features, heart anomalies, a tendency to premature strokes, small joint hyperextensibility and gut dysmotility (Kakita, *et al.,* 2002; Robertson *et al.,* 2003; Moro *et al.,* 2002). This disease is associated with a loss of filamin A function (or partial loss of function). However, there is a cluster of missense point mutations found in the CH1 domain of the ABD, highlighting the functional importance of this domain: A39G (Sheen *et al*., 2005), E82V (Moro *et al*.,

2002), M102V and S149F (Guerrinni *et al*., 2004) and A128V (Gomez-Garre *et al*., 2006). In male patients PVNH is generally lethal before birth or during early infancy. However, in rare cases of PVNH in boys who survive some neurone's are able to migrate, despite a lack of filamin A expression in these cells (Sheen *et al*., 2001).

In an interesting parallel to PVNH, neuronal migration during brain development is also misfunctional in lissencephaly disease. This inherited brain disorder results from mutations in the microtubule binding proteins LIS1 and DCX and the disease is thought to arise from incorrect regulation of the microtubule cytoskeleton (Olson and Walsh 2002). Given that PVNH is thought to be due to the incorrect regulation of the actin cytoskeleton, this highlights the importance of the cytoskeleton regulation in neuronal migration during brain development.

1.5.4 Cell Motility and Shape

Tumour cell lines that lack filamin A show no locomotion when compared to other melanoma cell lines that express filamin A. Transfection of one of the filamin A deficient human melanoma derived cell lines (M2) was able to rescue the cells, with the ability of the cells to migrate being proportional to the level of filamin A protein. Overexpression of filamin A (above WT filamin A levels) resulted in decreased locomotion, indicating the delicate balance of filamin A levels that is required in cells (Cunningham *et al*., 1992; Sarkisian *et al*., 2008). Mouse embryonic fibroblasts that lack filamin A are able to migrate; however, the mouse model of PVNH (filamin A null) does not result in missfunctional neuronal migration (Hart *et al*., 2006). When the amount of filamin A within the rat brain periventricular zone is varied, the polarity and orientation of neurons within this region change (Nagano *et al*., 2004). The filamin A binding protein FILIP induces filamin A degradation within the cortical ventricular zone of rat and mice brains. This filamin A - FILIP interaction controls the start of neuron cell migration from the ventricular zone (Nagano *et al*., 2002).

Taken together, this evidence supports a role for filamin A in the integration of signals within the reorganisation of neuronal shape and position during motility (Robertson, 2005). Filamin A has been shown to have roles in the MAP kinase pathway (Sarkisian *et al*., 2006), Wnt-c-Jun N-terminal kinase pathway (Nomachi *et al.,* 2008) and an

interaction with CEACAM1 (Klaile *et al.*, 2005) and integrin (Travis *et al.*, 2004), which are all involved in the regulation of cell migration. Integrin is particularly important during development (Figure 1-12), which is when the filamin A associated diseases are manifested.

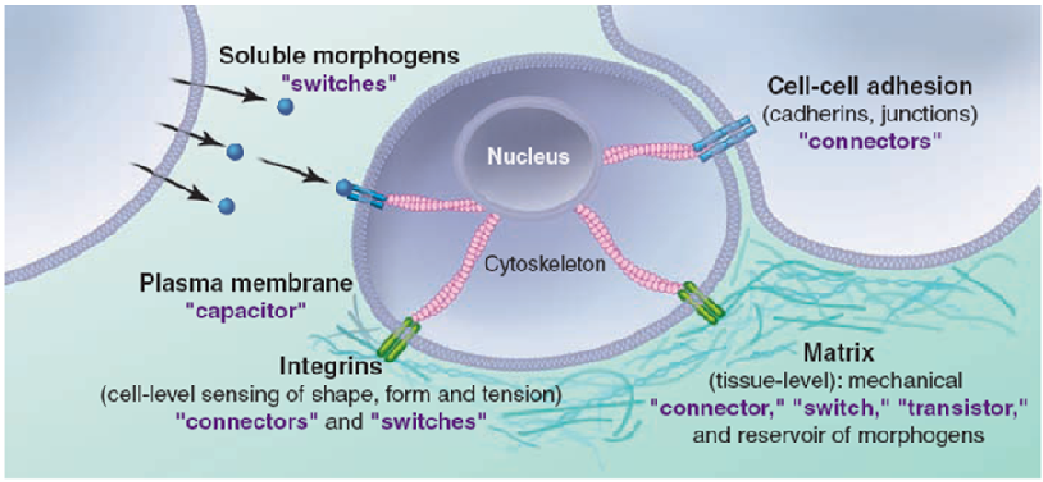

Figure 1-12. Cell Adhesion and Shape During Development.

Integrin plays a role in maintaining cell shape, cell-cell and cell-matrix adhesion by modifying the actin cytoskeleton. Integrin also integrates extracellular signals such as cytokine stimulation. These complex interactions control how cells are arranged during development.

Engler *et al.*, 2009

The disorder PVNH is a result of defective neuron migration. However, in a separate filamin A associated disorder, OPD2, bone development is affected. While it is unclear why some mutations in filamin A may affect bone development, given what we know about PVNH, it seems reasonable to suspect that the migration of osteoblasts may be affected in OPD2.

1.5.5 The Otopalatodigital Spectrum Diseases (Gain of Function)

1.5.5.1 Gain of Function Disease and Filamin A

These diseases have a distinct and separate phenotype to the loss of function disease (PVNH). The gain of function OPD spectrum diseases (FMD, OPD and MNS) are all skeletal disorders. Most of the symptoms can be attributed to defective intramembranous ossification of bone during development, as the diseases are not progressive (Robertson, 2007; Robertson, 2005). In females the genotype-phenotype

correlation between certain filamin A mutations is often less predictable than would be expected, and skewed X-inactivation occurs in females with these filamin A linked diseases (Hidalgo-Bravo *et al*., 2005; Sheen *et al*., 2002; Robertson, 2005).

1.5.5.2 OPD1 and OPD2

Male OPD1 patients have conductive deafness, congenital dislocations of hips and knees, long metacarpals, spatulate thumbs, scoliosis, and craniofacial anomalies (Figure 1-13). Patients with OPD2 have more severe symptoms and typically have skeletal dysfunction, bowed limbs, small head circumference, mental retardation and craniofacial disorders (Robertson, 2007; Robertson *et al*., 2003) (Figure 1-13).

Mutations associated with OPD1 occur only in CH2 of filamin A. Mutations associated with OPD2 occur in CH2 and repeats 14-15. All these domains are thought to participate in actin binding (Nakamura *et al*., 2007); however, the underlying molecular basis of these mutations is unknown. This work will focus on the molecular basis of two OPD2 associated mutations, E254K and A200S (residues are shown in Figure 1-10). Both these pathogenic mutations occur in the CH2 domain within the ABD. E254K was predicted to disrupt a salt bridge between E254 and K169, and A200 is a highly conserved residue (Figure 1-10).

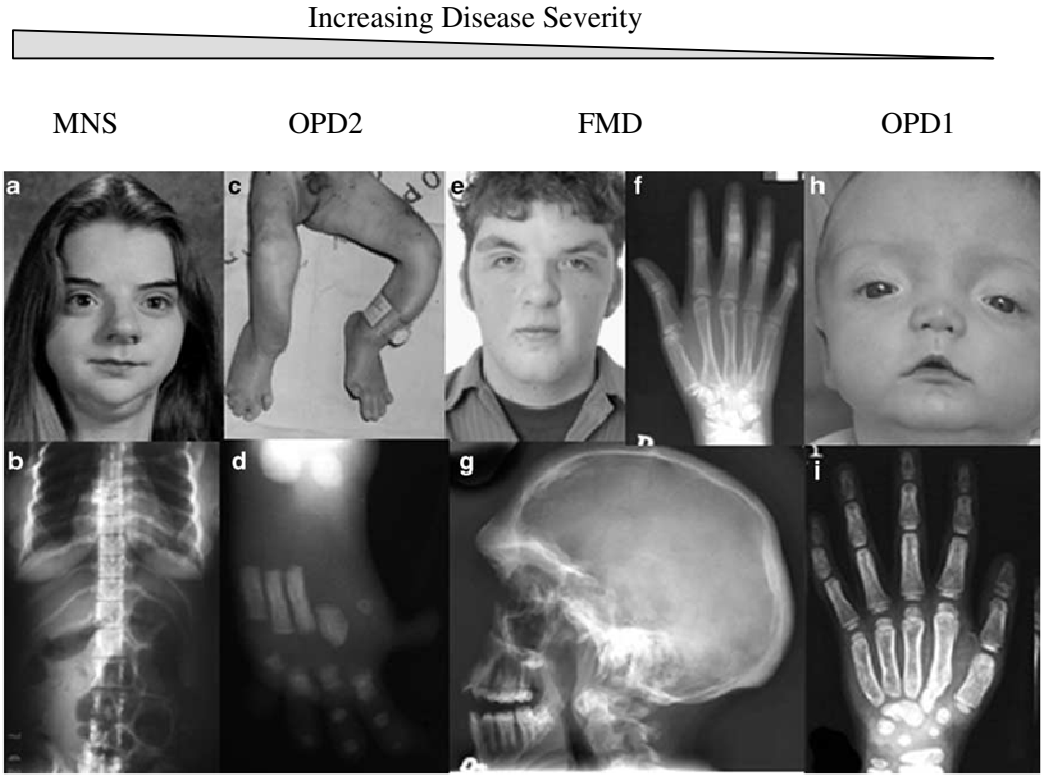

Figure 1-13. Gain of Function Diseases Associated with Filamin A.

a) Facial appearance in MNS
b) Decreased lung size, irregular ribs and curved spine in MNS
c) Bowed long bones and under development of the big toe in OPD2
d) Pattern defects in the foot of a male with OPD2
e) Facial features in FMD
f) Metacarpal and phalangeal modeling anomalies in FMD
g) Skull base tissue hardening and supraorbital excessive bone growth in FMD
h) Facial appearance in OPD1
i) Metacarpal and phalangeal modeling anomalies in OPD1 including accessory growth plate ossification centre of metacarpal

Robertson, 2007

1.5.5.3 FMD

FMD is part of the OPD – type range of disorders, with FMD patients showing striking overgrowth of frontal facial bones and displaying features of OPD including deafness, bony dysplasia and digital anomalies (Figure 1-13) (Robertson *et al.*, 2003). FMD associated mutations are distributed in CH2, repeats 3, 9-10, 14-15, and 22-23 of filamin A.

1.5.5.4 MNS

MNS is similar to OPD but symptoms also include deformities in ribs, clavicles, scapulae, pelvis, and bowed long bones (Robertson, 2007) (Figure 1-13). This is the most severe phenotype of the gain of function mutations and in males causes death in neonatal or in the first months of life. All mutations causing MNS are localised to the region encoding filamin repeat 10, suggesting a specialised role for this region of the protein (Robertson, 2007; Robertson, 2005).

1.5.5.5 Bone Development

Our lack of understanding about the role filamin A plays in bone development is limiting our understanding of the OPD spectrum disorders. Intramembranous bone ossification, which is defective in the OPD spectrum disorders, occurs during development by direct ossification of embryonic connective tissue and forms the membrane bones such as those of the skull (Roberson *et al.*, 2003). Filamin A is also expressed in the cytoplasm of chondrocytes in the developing growth plate, and at the edges of the proliferating cells, indicating an additional role in endochondral bone development (Krakow *et al.*, 2004).

During intramembranous bone development osteoblasts are highly motile, which requires many cytoskeletal rearrangements, and these cells move through a number of cell transformations to become osteocyte cells (reviewed in Franz-Odendaal *et al.*, 2006) (Figure 1-14). Filamin A is also upregulated in osteoblast cells when a physical stress load is applied to the cells (Jackson *et al.*, 2008).

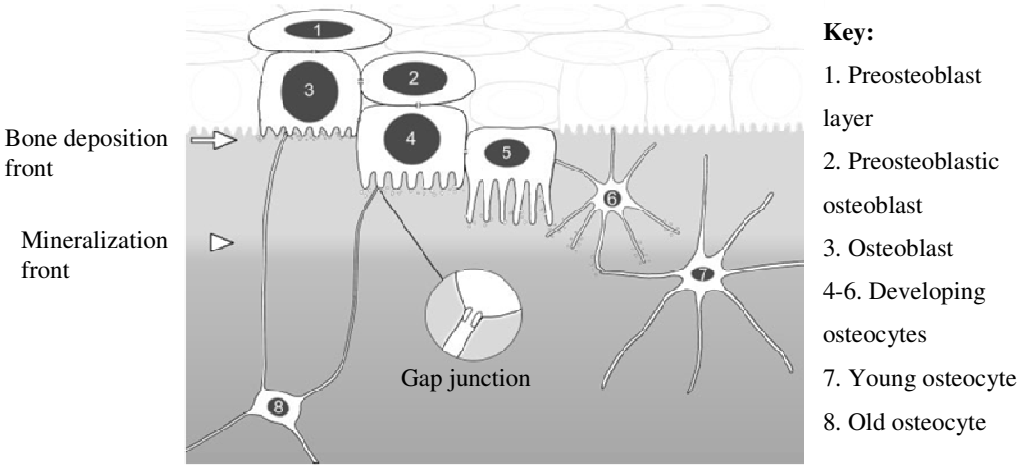

Figure 1-14. Cell Transformation during Intramembranous Bone Development.
This shows the cell types between preosteoblasts and osteocytes during intramembranous bone ossification. A gap junction (for direct cell communication) is shown between an osteocyte and an osteoblast that is embedding. During this transformation process, cellular organelles decrease and the volume of the cell decreases substantially.

Franz-Odendaal *et al*., 2006

Following the morphogenesis, in intramembranous bone development, osteoblast cells lay down the organic fibres of bone, such as collagen. The osteoblasts then either retreat or become entrapped as osteocytes in the bone. These organic bone fibres are calcified from the inorganic salts transported in the blood. These salts are deposited as fine crystals (hydroxyapatite crystals) within the collagenous fibers, and form the bone matrix (reviewed in Franz-Odendaal *et al*., 2006).

The way in which bone cells migrate and adhere is slightly different to other cell types. Instead of focal adhesions, these bone cells mainly use podosomes for migration, adhesion, and bone absorption (Reviewed in Jurdic *et al*., 2006) (Figure 1-15). Podosomes are composed of an F-actin cone, the 'podosome core', containing actin polymerisation promoting proteins, surrounded by an actin network concentrating regulatory proteins and adaptor proteins (Saltel *et al*., 2004) (Figure 1-15). This structure is linked to the integrins in the cell membrane. Given that filamin A associates with integrins, Cdc42, RhoA and actin (see section 1.4.1) and is involved in cell migration it seems likely that filamin has a role in podosomes.

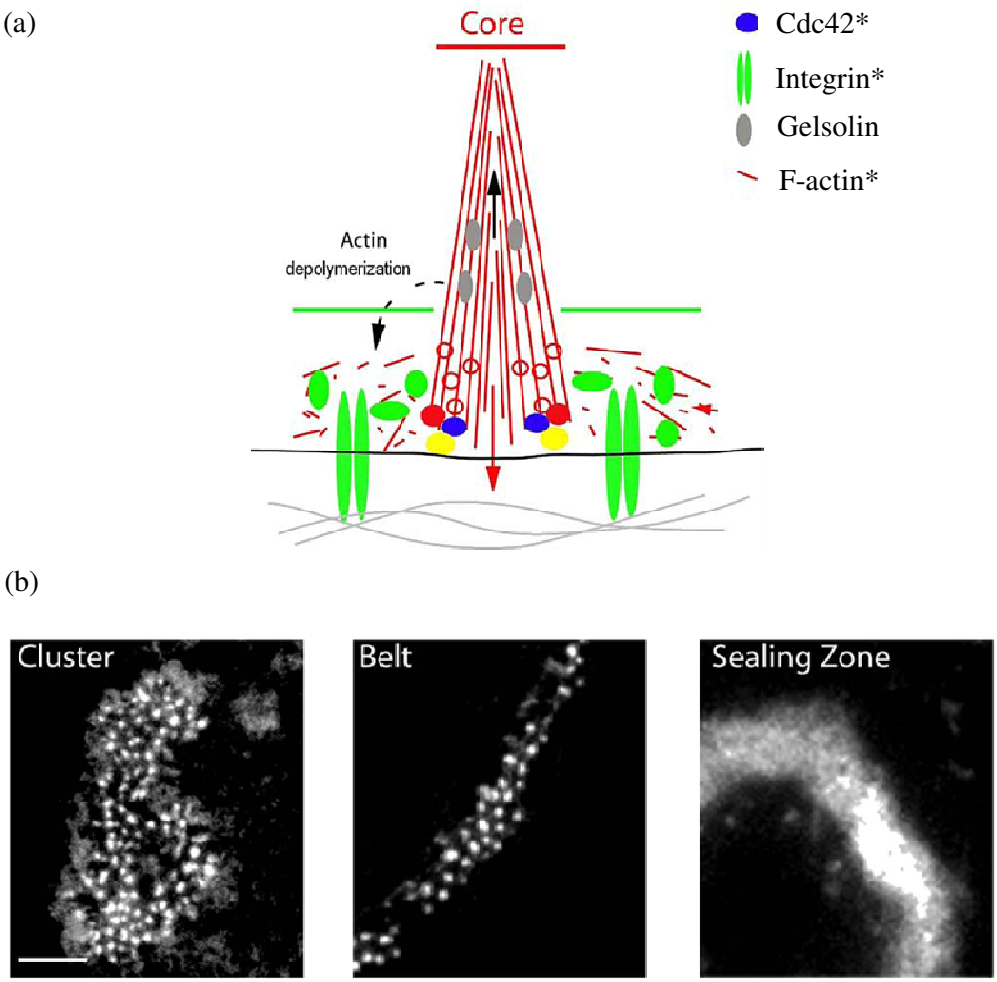

Figure 1-15. Podocyte Stuctures in Osteoclasts.

a) The protein composition of podosomes. Asterisks indicate filamin A binding partners.

b) The different actin structures (visualised with the actin stained) observed during osteoclast differentiation and activation. At the beginning of the differentiation, podosomes are organized in clusters, which develop into dynamics rings. The rings are stabilized at the cell periphery, forming a podosome belt. When osteoclasts are adherent on surfaces containing apatite crystals, a sealing zone is formed for bone resorption.

Jurdica *et al.*, 2006

1.6 Aims

This work aimed to complete structural and functional studies of filamin A – particularly focusing on the ABD, with a view to improving our understanding of the associated diseases. During this work there were six main aims:

1. **Clone the WT, E254K and A200S ABD and express soluble recombinant protein**.

Expression in *E. coli* can provide a ready source of recombinant protein for studies and allows the use of affinity tags for the rapid production of pure protein. The actin binding assay and the crystal trials ideally require large amounts (>20 mg) of highly pure active protein.

2. **Determine the crystal structure of the WT, E254K and A200S filamin A ABD**

Before this work the structure of the WT ABD structure had not been determined for any of the filamins. A structural model would enable a better understanding of disease associated residues that cluster in this domain. Therefore a primary aim of this project was to determine the X-ray structure of the WT filamin A ABD.

In addition to the WT structure, solving the X-ray structures of two OPD2 associated mutations (E254K and A200S) was an aim. This was also to enable a comparison with the WT structure. These mutations result in the same disease, allowing the two mutant structures to be compared and contrasted – to highlight any common structural changes. This structural work, particularly when coupled with biochemical data, also aimed to increase our understanding of the way in which filamin A binds to actin.

3. **Determine the solution structure of the WT and E254K filamin A ABD using circular dichroism spectroscopy**

To allow a comparison of the secondary structure of the WT and E254K proteins in solution the CD spectra of each protein was determined. This study also enabled the crystal structures and the secondary structures to be compared and contrasted.

4. Measure the actin affinity for the WT and E254K filamin A ABD

The primary characterised role of the filamin A ABD is F-actin binding. Therefore the actin affinity (K_d) of the filamin A ABD was determined for the WT and E254K domain, to determine if the disease associated mutation changed the activity of this domain.

5. Determine the thermostability of the WT and E254K filamin A ABD

The E254K mutation results in the loss of the conserved salt bridge that links two helices. This salt bridge is predicted to have a structural role, and the loss of it may affect the stability of the domain. Therefore the difference in thermal stability between the WT and E254K was analysed by circular dichroism and differential scanning fluorimetry.

6. Analyse the phenotype of fibroblast cells from patients with the filamin A associated diseases OPD2, FMD and PVNH.

The molecular/physiological mechanism behind OPD2 is unknown, so three cellular phenotypes were chosen to study based on what was known about filamin A. Filamin A has a role in mobility and adhesion in cells, and results from this study showed a loss in thermal stability in the E254K mutant. Therefore the mobility, adhesion and the filamin A level of fibroblast cells was determined for WT and patient cells.

2 Experimental Procedures

2.1 Water

All water used for this work (referred to as milli-Q) was purified over two ion-exchange filters and two organic filters in a Barnstead NANOpure II system (Thermoscientific).

2.2 Chemicals

Chemicals used in this work were the highest grade available.

2.3 Agarose Gel Electrophoresis

Gels were made with 1 % agarose (w/v) (Roche) in 1X TAE buffer (40 mM Tris.HCl, 20 mM acetic acid, 2 mM EDTA, pH 8.0), which was heated until the agarose had dissolved. Sample was mixed 1:1 with loading dye (0.2 % w/v bromophenol blue, 50 % v/v glycerol). Gels were run at 80V in an Easy-cast electrophoresis system (Owl Scientific). A 1 Kb Plus DNA ladder was run on all gels (Invitrogen). The DNA was visualised by staining the gels with ethidium bromide stain (0.5 µg/mL) for 15 min, followed destaining in water for 15 min. The images were captured under ultraviolet light on a GelDoc (BioRad), using QuantityOne software (BioRad).

2.4 Media for *E. coli* Growth

The Luria Broth (LB) media (Invitrogen) was made up in milli-Q water at 25g/L and autoclaved at 121 °C for 15 min before use. To make LB agar, 1 % agar was added to the broth before autoclaving.

2.5 Antibiotics

Ampicillin (Amp) (100 µg/mL) was added to the LB growth media to maintain plasmids in *E. coli*. The Amp was stored as a filtered stock solution (100 mg/mL) at -20 °C and added to the media directly before inoculation.

2.6 PCR amplification

A pRSET plasmid containing a fragment from the 5' end of the filamin A cDNA was a kind gift from Prof. Stephen Robertson (Otago University). The actin binding domain (encoding residues 2-269) of filamin A was PCR amplified with the foward primer AGAAT TCAAG CTTTT ACAGC TTGGC CTTGG GGAAC TGGGA (*Nco*I) and the reverse primer TAAAC CATGG CAAGT AGCTC CCACT CTCG (*Hind*III) using the Pwo polymerase (Roche). The following program in a Tgradient thermocycler (Biometra) was used for the amplification: 94 °C for 5 min – for one cycle, then 94 °C for a min, 54 °C for a min, 72 °C for a min for 30 cycles. This was followed by incubation at 72 °C for 5 min. The PCR products were analysed by agarose gel electrophoresis, then purified using a high pure PCR product purification kit (Roche) according to the manufacturer's instructions and eluted in 50 µL water.

2.7 Digestion with Restriction Endonucleases

The vector (pProEX™ HTb, LifeTechnologies) and PCR products were digested with the restriction endonucleases *Nco*I (Invitrogen) and *Hind*III (Roche). The following typical reaction was incubated at 37 °C for 3 ½ hours.

Tube number	**1 (Vector)**	**1 (Insert)**	**2**	**3**	**4**
10x Buffer 2 (Invitrogen)	3 µL	3 µL	3 µL	3 µL	3 µL
DNA	8 µL vector	8 µL insert	3 µL vector	3 µL vector	3 µL vector
*Nco*I	1 µL	1 µL		1 µL	
*Hind*III	1 µL	1 µL			1 µL
H_2O	17 µL	17 µL	24 µL	23 µL	23 µL
Reactions			Control reactions		

An agarose gel was run to confirm both enzymes were active. This was determined by the single enzyme digests in tubes 3 and 4, when compared to tube 2, the uncut vector. Following this, 20 µL of the reaction was loaded onto an agarose gel, the gel run stained and the bands cut out and purified using high pure PCR product purification kit (Roche) according to the manufacturer's instructions and the DNA was eluted into 50 µL water.

2.8 DNA Ligation

The purified products from the restriction digest (vector and insert) were mixed 3:1 insert to vector molar ratio. The reaction was incubated at 18 °C for 3 hours with 5U (1 µL) of T4 DNA ligase (Invitrogen) and 3 µL of the accompanying 5X buffer.

2.9 Competent *E. coli* cells

E. coli cells (either BL21(DE3) or Top10) were grown to an OD_{600} of 0.5-0.8 in 200 mL of LB broth at 37 °C. The cells were centrifuged at 4000*g* for 10 min at 4 °C and resuspended in 80 mL of ice cold buffer 1 (7.5 mM KOAc, 25 mM $RbCl_2$, 10 mM $CaCl_2$, 50 mM $MnCl_2$, 75 % v/v glycerol, pH 5.8). The cells were incubated on ice for 5 min and then centrifuged at 4000*g* for 10 min. The supernatant was removed and the cells were resuspended in ice cold buffer 2 (0.1 mM MOPS, 0.75 mM $CaCl_2$, 0.1 mM $RbCl_2$, 15 % v/v glycerol, pH 6.5). The cells were then incubated on ice for 15 min, and stored in 100 µL aliquots at -80 °C.

2.10 Transformation of Plasmid DNA into *E. coli* Cells

The plasmid DNA transformations were based on the method of Hanahan *et al.* (1991). The competent cells (50 µL per reaction) were thawed on ice for 30 min, 2 µL of DNA was added and the mixture gently mixed. The cells and DNA were incubated on ice for 30 min and then placed in a 42 °C waterbath for 45 sec and then cooled on ice for 20 min. Then 200 µL of LB media was added and the cells incubated with shaking for 1 hour. The transformed cells were plated on prewarmed LB/agar plates containing the appropriate antibiotics and incubated overnight at 37 °C.

2.11 Isolation of Plasmid DNA from *E. coli* cells

A single *E. coli* colony from an agar plate was picked and incubated overnight in 5 mL of LB broth at 37 °C with the appropriate antibiotics. Using 3 mL cells of this culture, the plasmid DNA was extracted using the high pure plasmid isolation kit (Roche), according to the manufacturer's instructions.

2.12 Determination of DNA Concentration

The DNA concentration of a solution, unless specified otherwise, was determined by absorbance at 260 nm on a nanodrop spectrophotometer (NanoDrop® ND-1000). The conversion value used (for dsDNA) was 50 µg/mL = 1 absorbance unit.

2.13 DNA Sequencing

DNA sequencing of the expression plasmids was performed at the Allan Wilson Sequencing service, at Massey University, on an ABI Prism 3730 capillary sequencer, using BIGDYE labelled dideoxy termination (Applied Biosystems).

2.14 Centrifugation

All centrifugations were performed in one of four centrifuges. In a SORVALL Evolution RC centrifuge with either the GS3 fixed angle rotor (at 6000*g*) or the SS34 fixed angle rotor (at 30000*g*). Also used was a benchtop Centrifuge 5702 (Eppendorf) with an A-4-38 swinging bucket rotor (at 1700*g*). Smaller volumes (<1.5 mL) were centrifuged in a benchtop Minispin Plus centrifuge (Eppendorf). Ultracentrifuge spins (in the actin co-sedimentation assay) were performed in a TL Benchtop Ultracentrifuge (Beckmann Coulter) with a TLA100 fixed angle rotor (used at 214000*g*).

2.15 Sonication

Cells and cell lysate were sonicated by an Ultrasonic Processor (Misonix), at power level 4 on ice for 15-20 sec bursts, with one min rests on ice to allow the sample to cool.

2.16 Glycerol Stocks

E. coli cells were grown to log phase in LB broth at 37 °C, then mixed with 10 % glycerol and stored at -80 °C.

2.17 Growth of *E. coli* for Protein Expression

The LB media (1 L) and appropriate antibiotic was inoculated with 10 mL of an overnight culture of *E. coli* BL21(DE3) cells containing the expression plasmid. The

cells were grown with constant shaking at 37 ° for 2 hours then transferred to 25 °C to continue growing (for approximately one hour) to an OD_{600} of 0.6-0.7. The recombinant protein expression was induced with the addition of 0.1 mM IPTG and the cells grown for a further 5 hours at 25 °C.

2.18 Sodium Dodecyl Sulfate Polyacrylamide Gel Electrophoresis (SDS PAGE)

SDS PAGE was based on the method of Laemmli (1970). Gels were 12.5% w/v acrylamide, with a 4% w/v stacking gel, unless stated otherwise. Samples were mixed 1:1 with 5X loading buffer (60 mM Tris.HCl, pH 6.8, 50% v/v glycerol, 10% w/v SDS, 0.5 M DTT, 0.1% w/v bromophenol blue) and boiled for 5 min, then loaded onto the gel along with precision plus protein™ molecular mass standards (Biorad). All gels were run in running buffer (25 mM Tris, 0.2 M glycine, 0.1% SDS) in a mightly small II tank (Amersham). Gels were run at 200V until the dye reached the end of the gel, then stained (0.125% w/v Coomassie brilliant blue R250, 40% v/v ethanol, 10% v/v acetic acid) for 1 hour and destained for at least 3 hours in destain solution (20% v/v ethanol, 10% v/v acetic acid).

2.19 Lysis of *E. coli* Cells for Protein Purification

The cells were lysed by passing twice through a French press (at 5000 psi), followed by a 15 second sonication to shear the nucleic acids.

2.20 Ni^{2+} Affinity Chromatography of Filamin A ABD

Ni^{2+} affinity chromatography was performed at room temperature over a 5 mL HisTrap™ HP column (Amersham) using a peristaltic pump. The *E. coli* cell pellet was resuspended in 50 mL of ice cold lysis buffer (50 mM K_2HPO_4/KH_2PO_4, 0.5 M NaCl, 10 mM imidazole, 1 EDTA free protease inhibitor tablet (Roche), pH 8). Following cell lysis (section 2.19) the resulting solution was then centrifuged at 30000*g* for 30 min at 4 ° C, to remove insoluble protein and cellular debris. The cleared cell lysate was filtered through a 0.45 µm filter and loaded onto the column at 1 mL/min. The resin was then washed at 2 mL/min with purification buffer (50 mM potassium phosphate buffer, 0.5 M NaCl and increasing concentrations of imidazole, pH 8). The purification was

analysed by SDS PAGE and the fractions containing approximately >80 % protein of the expected molecular weight were pooled and concentrated. Following purification the column was washed with 500 mM imidazole, rinsed with water and stored in 20 % ethanol.

2.21 Determination of Protein Concentration by A_{280}

The protein concentration of a solution, unless specified otherwise, was determined by absorbance at 280 nm on a nanodrop spectrophotometer (NanoDrop® ND-1000). The absorbance was converted into mg/mL using Beers law: Protein concentration (mg/mL) = (absorbance$_{280}$ X molecular weight) ÷ (molar extinction coefficient$_{280}$ X pathlength). The molar extinction coefficient (0.527 L/mol) and molecular weight (30 000 Da) of each protein was determined using ProtParam (ExPASy http://www.expasy.org/tools/protparam.html).

2.22 Protein Concentration Determination by Bicinchoninic Acid

The peptide bonds in protein reduce Cu^{2+} ions to Cu^{1+}, and this copper reduction is proportional to protein concentration. Bicinchoninic acid then chelates the Cu^{1+} ions, forming a complex that absorbs light at 562 nm (Smith, *et al*. 1985). To determine the protein concentration of a solution, the BCA™ Protein Assay Kit (Pierce) was used according to the manufacturer's instructions. A BSA standard curve of absorbance at 562 nm was plotted (appendix 9.3), and the protein concentration of each unknown read off this graph.

2.23 rTEV Production

The plasmid containing rTEV open reading frame (pET19b-TEV) was transformed into BL21 (DE3+pARG). The cells were grown in a 5 L flask containing 1L of LB broth containing the antibiotics tetracycline and ampicillin. Cells were grown at 37 °C to an OD_{600} of 0.7, induced with 0.1 mM IPTG and expressed at 25 °C overnight. Cells were then centrifuged at 6000*g* for 30 min and lysed by French press (section 2.19) in lysis buffer (50 mM K_2HPO_4/KH_2PO_4, 0.5 M NaCl, 1 mM $MgCl_2$, 10 % glycerol, 0.05 % Tween-20, 0.25 TCEP, 1 mM Benzamidine.HCL, 1 mM PMSF, pH 8). The lysate was then spun at 30000*g* for 30 min, to remove insoluble cell debris. The cleared lysate was

then loaded onto the HisTrap™ HP column at 1 mL/min. The column was washed with 10 CV of lysis buffer then followed by stepwise elution (20, 50, 100, 150, 500 mM imidazole) in wash buffer also containing (50 mM K_2HPO_4/KH_2PO_4, 0.5 M NaCl, 1 mM $MgCl_2$, 10 % glycerol, 0.25 TCEP, pH 8), with 6 CV of buffer at each wash step. The purification was confirmed by SDS PAGE and the fractions containing the 30kDa rTEV were combined and dialysed overnight into 2X storage buffer (25 mM Tris.HCl, 0.5 NaCl, 1 mM $MgCl_2$, 10 % glycerol, 1 mM DTT, 0.5 EDTA, pH 8). The protein was then concentrated to 2 mg/mL, mixed with an equal volume of glycerol, snap frozen and stored at -80 °C.

2.24 rhCalmodulin Production

The pET23a(+) vector containing the open reading frame cloned from human calmodulin cDNA clone (source identifier 4801400) was a kind gift from Fumihiko Nakamura (University of Harvard). The rhcalmodulin was purified as previously described (Gopalakrishna and Anderson, 1982). Holocalmodulin has a hydrophobic cleft that binds to hydrophobic phenyl-sepharose resin. Apocalmodulin does not have a hydrophobic cleft, and does not bind the phenyl-sepharose resin. These properties were exploited to purify the protein in one step. The human calmodulin was expressed in *E. coli* BL21(DE3) for 5 hr at 37 °C and resulting cell lysate was passed over a 10 mL phenyl-sepharose (Sigma) column in a buffer containing $CaCl_2$ (50 mM TrisHCl, pH 7.5, 1 mM β-mercaptoethanol, 5 mM $CaCl_2$). The resin (with the calmodulin bound) was then washed with a high salt buffer (50 mM TrisHCl, pH 7.5, 1 mM β-mercaptoethanol, 5 mM $CaCl_2$, 0.5 M NaCl). The calmodulin was then eluted in buffer containing EGTA (50 mM TrisHCl, pH 7.5, 1 mM β-mercaptoethanol, 1 mM EGTA).

2.25 Cleavage of the N-terminal Hexa-His Tag

The ABD protein eluted from Ni^{2+} affinity chromatography was exchanged into rTEV buffer (50 mM K_2HPO_4/KH_2PO_4, 150 mM NaCl, 0.25 mM TCEP, pH 8). The rTEV was added at a 1:50 w/w ratio and the reaction incubated overnight at 10 °C and His tag removal was confirmed by SDS PAGE (Carrington and Dougherty, 1988). Following rTEV cleavage the protein was exchanged into buffer (50 mM K_2HPO_4/KH_2PO_4, 0.5 mM NaCl, 20 mM imidazole, pH 8) and run through a HisTrap HP column at 1

mL/min, the flow through was collected and concentrated. This step removes the His tagged rTEV, the cleaved His tag and any protein still containing a His tag.

2.26 Protein Concentration and Buffer Exchange

Protein was concentrated and/or the buffer exchanged using Vivaspin centrifugal concentrators (GE Healthcare) with a 10 kDa molecular weight cut off, following the manufacture's instructions. With buffer exchange at least four >5 fold serial dilutions were made. After use, the filters were rinsed in milliQ water and the concentrator stored in 20 % ethanol. Each concentrator was only reused with the same protein, to avoid cross contamination between different proteins.

2.27 Gel Filtration Chromatography

Protein was concentrated to >5 mg/mL and DTT added to a final concentration of 5 mM. Protein samples were loaded onto the Superdex 75 gel filtration column (Amersham Biosciences) in 250 µL aliquots on an AKTA Explorer system (Amersham Biosciences) at 4 °C. Buffer (50 mM K_2HPO_4/KH_2PO_4, 150 mM NaCl, 5 mM DTT, pH 8) was run at 0.5 mL/min and the elutant collected in 0.5 mL fractions. To determine the molecular mass of the recombinant filamin A ABD the column was calibrated with molecular mass standards run on the column, to construct a standard curve (Appendix 9.1). This standard curve then allowed the molecular mass of unknowns to be determined from the elution volume.

2.28 Crystallisation

Protein for crystal trials was exchanged into crystallisation buffer (20 mM HEPES, pH 7.4, 100 mM NaCl) at concentrations varying between 4 - 15 mg/mL. The hanging drop crystal trials were set up with 500 µL of mother liquor in the wells of 24 well VDX plates (Hampton). Reservoir solution (from each well) was mixed 1:1 with protein (1 µL + 1 µL) on siliconised cover slips (Molecular Dimensions), and sealed with petroleum jelly (Shell). For screens at 4 °C the plate was set up sitting on ice, before being moved into the 4 °C cold room directly after setting up the screen. Solutions screened were from the kit "Crystal Screen" (Hampton). Plates were examined under the microscope immediately after setting up, the following day, then at 2-3 day intervals

over a 2 week period. Conditions that gave crystals (or microcrystals) were identified by eye under a microscope (20X magnification) and further screens around these conditions were set up.

2.29 X-ray Data Collection

Crystals were briefly soaked by picking the crystal up in a nylon loop then dragging it through a cryoprotectant solution for approximately 10 seconds (if required), and then flash frozen in liquid nitrogen, before mounting into a stream of 120K nitrogen cooled gas for data collection. The X-ray diffraction data were collected on a R-Axis IV^{++} detector using a Rigaku MicroMax007 copper rotating anode generator with a copper rotating anode generating K_α radiation, which was monochromated with Osmic blue optics to a wavelength of 1.54 Å. Data collection was under the control of CrystalClear 1.3.2 (Rigaku), and images were collected to insure at least 95 % completeness and 4 times redundancy in the data.

2.30 Actin Binding Assays

An actin co-sedimentation assay based on the methods of Moores and Kendrick-Jones (2000) and Nakamura *et al*. (2005) was used to determine the F- actin binding affinity (K_d) of the WT and E254K proteins. Monomeric actin (Cytoskeleton) is polymerised, and incubated with the protein of interest. The solution is then spun in an ultracentrifuge to pellet the actin and any proteins bound to the actin. The pellet and soluble fraction can then be analysed by SDS PAGE to determine the amount of protein bound to actin.

To polymerise the actin, 31.5 µL of monomeric actin (4 mg/mL as a suspension in water) was mixed with 3.5 µL of 10x F buffer (20 mM $MgCl_2$, 10 mM ATP, 500 mM KCl, 20 mM Tris.HCl, pH 8) and incubated for 1 hour at room temperature. The filamin A ABD, in ligand buffer (20 mM Tris.HCl, 6.25 mM DTT, 120 mM NaCl, pH 8), was spun at 214000*g* for 30 min. This step removes any precipitated/insoluble protein. Then 40 µL supernatant is transferred into a clean centrifuge tube and mixed with 5 µL actin (3.6 mg/mL suspension in water) and 5 µL of binding buffer (120 mM Tris.HCl, 1.5 M NaCl, 20 mM $MgCl_2$, 10 mM ATP, 1 mM $CaCl_2$) to give a final concentration of actin binding buffer (36 mM Tris.HCl, pH 8, 108 mM NaCl, 5 mM

DTT 2 mM $MgCl_2$, 1 mM ATP). The assay was incubated at 25 ºC for 30 min, then centrifuged at 214000*g* for 30 min. The entire supernatant was carefully pipetted away from the pellet, and the pellet mixed with an equal volume of ligand buffer. The soluble and pellet fractions were loaded onto an SDS PAGE gel, stained and the density of the protein bands in the supernatant and pellet fractions was determined using the QuantityOne software (Biorad). As a background control, the percentage of filamin A ABD that was in the pellet in absence of actin was subtracted from the pellet with each assay and was typically between 1-3 %. As an additional control, the F-actin in the absence of filamin A ABD was assayed to insure that the filamin A ABD did not alter the actin polymerisation.

The percentage of actin and filamin A ABD in the pellet and supernatant (as determined by the densitometry) was calculated. Since the total concentration of each protein was known, to determine the mol/mol ratio of filamin ABD bound to actin the percentage of each protein in the pellet was used to determine the number of moles of each protein in the pellet. This allowed the ratio of filamin ABD:actin (mol/mol) to be calculated, which is the value graphed against the moles of filamin A ABD in the supernatant (free filamin A ABD).

2.31 Actin Binding Assay with PIP_2 or Calmodulin

When PIP_2 (Sigma) or calmodulin was added to the assays the assay was done as described above (section 2.30), with the addition of PIP_2 or calmodulin (instead of ligand buffer) made before the first centrifuge step. The actin binding assays testing PIP_2 were set up based on the method of Furuhashi *et al*. (1992). The actin binding assays testing calmodulin were set up based the method of Nakamura *et al*. (2005). The filamin ABD used in this assay contained a His tag, to enable immunodetection with an antiHis antibody (Sigma). Two sources of calmodulin were tested: recombinant human calmodulin (purified from *E. coli* - section 2.24) and native bovine calmodulin (Sigma). Apo or holo calmodulin (either bovine or human) was added to the assay (in place of ligand buffer) before the first centrifugation step (section 2.30). The resulting supernatant and pellet fractions from the assay were then run on a 15 % acrylamide gel. Proteins were then transferred from the gel onto Hybond-C nitrocellulose membrane (Amersham) in a mini Trans-Blot® tank (BioRad) overnight at 30V, in transfer buffer

(25 mM glycine, 20 mM Tris.HCl, 7.6 mM SDS, 20 % methanol). The membrane was removed and stained with ponceau stain (2 % ponceau S (Sigma), 30 % w/v trichloracetic acid, 30 % w/v sulfosalicylic acid) to confirm the even transfer of proteins. The membrane was then blocked in 5 % w/v skim milk powder and TBST (20 mM Tris.HCl, 150 mM NaCl, 0.05 % Tween20, pH 7.5) for 1 hr. Then the blocking solution was removed and the membrane rinsed with TBST and incubated with the antiHIS primary antibody (Sigma H1029) diluted 1/3000 in TBST for 1.5 hr. The membrane was rinsed 6 times for 5 min with TBST. The blot was then incubated with secondary mouse antibody (Sigma) diluted to 1/6000 in TBST. The blot was then rinsed 6 times for 5 min in TBST. The detection system was the horseradish peroxidase reaction using the SuperSignal® west pico chemiluminescent substrate solution (Pierce), according to the manufacturer's instructions. Images were captured by exposure to light sensitive film (Fujifilm).

2.32 Differential Scanning Fluorimetry

To determine the thermal stability of the proteins Sypro orange melts were performed in a RotorGene6000 thermocycler (Corbett). Assays were based on the method of Yeh *et al*. (2006) and Niesen *et al.* (2007). To assay the melting point, 13.5 µL of protein at 2 mg/mL in ligand buffer (20 mM Tris.HCl, 6.25 mM DTT, 120 mM NaCl, pH 8) was mixed with 1.5 µL of Sypro orange dye (Sigma) at 100x concentration in water (sonicated briefly to solubilise), to make a final concentration of dye at 10x. The dye and protein solution was transferred into 0.3 mL PCR tubes (Axygen) and the tubes placed in a 36 well carousel. The thermocycler was programmed to heat from 30 °C up to 90 °C, at 1 °C steps (over 18 min). Data were collected with excitation at 470 nm and detection at 510 nm with a gain of 5. A background control of 'buffer and dye' along with a negative control containing 'protein and buffer' and a positive control with 'lysozyme and dye' were also run.

2.33 Circular Dichroism (CD) Spectroscopy

To study the secondary structure of the proteins, circular dichroism spectra were collected on a Chirascan CD spectrophotometer (AppliedPhotophysics) in a 0.1 mm quartz precision cell (Hellma). The sample compartment was purged with O_2-free N_2

before use, to remove the oxygen absorption. A spectrum of the sample buffer (20 mM K_2HPO_4/KH_2PO_4, pH 8, 20 mM NaCl) was also measured and this was used to baseline correct the experimental data. The melting temperature was determined by taking a scan over 200 - 240 nm, from 5 °C - 90 °C in 5 °C steps. All data were processed (baseline correction and averaging) on the Chirascan software (AppliedPhotophysics).

2.34 Fibroblast Cell Culture

Fibroblast primary cells were grown in Dulbecco's Modified Eagle Media (DMEM) (GIBCO) in 20 % fetal calf serum (GIBCO) with pen/strep (10 units of penicillin and 10 µg of streptomycin final concentration, GIBCO) and L-glutamine (2 mM final concentration, GIBCO). The flasks, containing cells, were incubated in 5 % CO_2 at 37 °C. Cells were removed from the flask using TrypLE™ Express (GIBCO) and passaged into fresh media when the monolayer reached 90-95 % confluence (about 3 days growth). Cells were stored in liquid nitrogen, in fetal calf serum supplemented with sterile 10 % DMSO (Sigma).

2.35 Western Blotting of Fibroblast Lysate

To measure the relative levels of full length filamin A in fibroblast cell lines, protein from each cell line was analysed by a western blot with filamin A antibodies. Cells were grown to 90 % confluence in T75 tissue culture flasks (Greiner) in 10 mL DMEM media. The growth medium was removed and the cells were washed with 2 mL PBS (50 mM potassium phosphate, 150 mM NaCl). Then the PBS was removed and 0.5 mL of lysis buffer (10 mM Tris.HCl, pH 7.4, 100 mM NaCl, 1 mM EDTA, 1 mM EGTA, 1 % Triton X-100, 10 % glycerol, 0.1 % SDS, 0.5 % deoxycholate, 1x protease inhibitor tablet (Roche)) was added to the flask. A cell scraper was then used to physically remove the cells. The cell lysate was removed centrifuged at 13 000 g for 10 min at 4 °C and the supernatant stored as 50 µL aliquots at -80 °C.

The protein concentration of the cell lysate was determined by a BCA assay (section 2.22). Each protein sample was diluted to 0.5 mg/mL, mixed 1:1 with 5X loading buffer, boiled for 5 min and 15 µL was loaded onto a 10 % SDS PAGE gel. The gel was run at 150V through the stacking gel, then the voltage was increased to 200V until the dye reached the end of the gel. The stacking gel was removed and the remaining gel

transferred to a Hybond-C nitrocellulose membrane (Amersham) in a mini Trans-Blot® tank (Biorad) overnight at 40V, in transfer buffer (25 mM glycine, 20 mM Tris.HCl, 7.6 mM SDS, 20 % methanol). The membrane was removed and stained with ponceau stain (2 % w/v ponceau S (Sigma), 30 % w/v trichloracetic acid, 30 % w/v sulfosalicylic acid) to confirm the transfer. The blot was then sectioned with a scalpel and blocked in 5 % w/v skim milk powder and TBST buffer (20 mM Tris.HCl, 150 mM NaCl, 0.05 % Tween20, pH 7.5), for 1 hour. The blot was then rinsed with TBST buffer and incubated with the primary antibody for 1.5 hours. The filamin A antibody (Chemicon MAB1678) was diluted 1/15 000 in TBST buffer, and the α-tubulin antibody (Sigma) was diluted 1/4000 in TBST buffer. The membrane was then rinsed 6 times for 5 min with TBST buffer. All blots were then incubated with secondary mouse antibody (Sigma) diluted to 1/6000 in TBST buffer. The blot was then rinsed 6 times for 5 min in TBST. The detection system was the horseradish peroxidase reaction using the SuperSignal® west pico chemiluminescent substrate solution (Pierce), according to the manufacturer's instructions. Data were captured on film (Fujifilm) and also using an intelligent dark box II (Fujifilm). The densitometry was calculated by the LAS-1000 pro software from the data collected on the intelligent dark box.

2.36 Cell Motility Assays

Motility assays were carried out as previously described (Liang *et al.,* 2007). A confluent monolayer of cells is wounded (or scratched), and the rate the cells move into the wound is followed by microscopy and the rate of cell motility can then be calculated. As a reference point, a cross was drawn on the underside of the 30 mm coated tissue culture plates (Nunc). Then, to coat the plates with the protein matrix, 1 mL of fibronectin (10µg/mL) in PBS (50 mM K_2HPO_4/KH_2PO_4, pH 8, 150 mM NaCl) was incubated in the plate overnight at 4 °C. The fibronectin solution was then removed, the plate rinsed with 2 mL of PBS and blocked with BSA (2 mg/mL) in PBS at 37 °C for 1 hour. The plate was then rinsed with 2 mL PBS. Media (1 mL) with 20 % fetal calf serum was then added to the plate, which was then inoculated with 300 µL of cells (5.0×10^4) and grown 3 days (until the cells were 90 % confluent). A scratch was then made, across the reference cross, with a p200 pipette tip. The media was removed and replaced with media containing 10 % fetal calf serum (to slow cell growth). At this point an image was captured on a Zeiss Axiophot compound light microscope as

quickly as possible – this image is time point "0". The plate was incubated at 37 °C with 5 % CO_2 and removed briefly at each time point for image collection.

The images were processed using ImageJ (author Wayne Rasband, NIH) by the method described by Liang *et al.*, (2007) using the crosses on the base of the plate as a reference point. The width of the scratch was measured at time "0", and at the 8 or 10 hour point. The difference between these two measurements was termed distance travelled, and this was calibrated by the time incubated to give the rate (mm/hr). Each assay was performed in triplicate.

2.37 Fibroblast Adhesion Assay

The adhesion assay was carried out as described by Gillies *et al.*, (1986). The amount of cells adhering to a plate is determined by a crystal violet stain. Cells were plated out at 50 µL (2 x 10^4 cells/well) into a 96 well nunclon™ coated tissue culture plate (Nunc). The plate was incubated 1 hour at 5 % CO_2 and 37 °C. The media (and any cells that had not adhered) were removed with a pipette and the plate washed with 50 µL of PBS (50 mM potassium phosphate, 150 mM NaCl). The remaining cells were then fixed with 50 µL of 95 % ethanol for 10 min, and the ethanol was removed by inverting the plate onto tissue paper. The cells were then stained with 50 µL of 0.1 % crystal violet (Sigma) solution for 30 min. The excess stain (not bound to the cells) was then removed by carefully immersing the entire plate in a 5 L beaker of RO water for 15 min. The water was then removed by inverting the plate. To lyse the cells and solubilise the stain, 50 µL of a 0.2 % TritonX solution was pipetted into each well, and the plate mixed by gentle inversion for 15 min. The absorbance at 570 nm was measured on a Powerwave XS spectrometer (Biotek). The background absorbance of a "media only" control well was removed, and these final absorbance values plotted.

2.38 Crystallographic Methods

Programmes from the CCP4 suite were used for much of the data processing (Collaborative Computational Project, 1994). All images were collected using strategy from CrystalClear (Rigaku). The diffraction intensities were then integrated with either MOSFLM (Leslie, 1992) or XDS (Kabsch, 1993). The images were scaled and averaged with SCALA (Evans *et al.*, 2006). The phases of each structure was solved by

molecular replacement using PHASER (McCoy *et al*., 2005). Model building was done in COOT (Emsley and Cowtan, 2004), and refinement was performed by REFMAC (Murshudov *et al*., 1997) and PHENIX (Adams *et al*., 2002). Data validation was performed by PROCHECK (Laskowski *et al*., 1993) and MolProbity (Davis *et al*., 2007). The graphics in this thesis were produced by PyMOL (DeLano Scientific), UCSF Chimera (Pettersen *et al*., 2004) and CCP4mg (Collaborative Computational Project, 1994).

2.39 Bioinformatics and Sequence Analysis

Sequence alignments were performed by ClustalW (Thomson *et al*., 1994), and T-Coffee (Notredame *et al*., 2000). Protein domain boundary predictions were performed by the pFAM (Finn *et al*., 2008) and SMART (Schultz *et al*., 1998) databases. The protein:protein interactions were analysed by PROTORP server (Reynolds *et al*., 2009). Vector and plasmid maps were constructed using VectorNTI software (Invitrogen). The properties of the proteins (such as the molecular weight, pI, etc.) were calculated by the ProtParam server (http://au.expasy.org/).

3 Cloning, Expression in *E. coli* and Purification

3.1 Introduction

To enable structural and biochemical studies of the actin binding domain, the DNA encoding the open reading frame of the ABD from filamin A (accession number P21333.4) was cloned in the *E. coli* expression vector pProEX™ HTb. In addition to this construct, two point mutants (with the amino acid substitutions E254K and A200S) were also cloned into pProEX™ HTb. This enabled recombinant protein expression with a Ni^{2+} affinity tag separated from the filamin A ABD by a tobacco etch virus (TEV) protease site. This recombinant expression system enabled a two step purification system, with Ni^{2+} affinity chromatography as the first step, followed by gel filtration as a polishing step.

3.2 Filamin A ABD Wildtype

3.2.1 Cloning

To determine the domain boundaries, the amino acid sequence of filamin A was analysed by the pFAM database (methods section 2.39). This analysis predicted that the CH1 domain spanned from residues 40 to 149 and the CH2 domain from 168 to 269. Therefore the open reading frame encoding amino acid residues of the actin binding domain (2-269) from filamin A were PCR amplified (details methods section 2.6) and cloned into the *Nco*I and *Hind*III sites of the vector pProEX™ HTb by Andrew Sutherland-Smith (pers. comm.) (Figure 3-1).

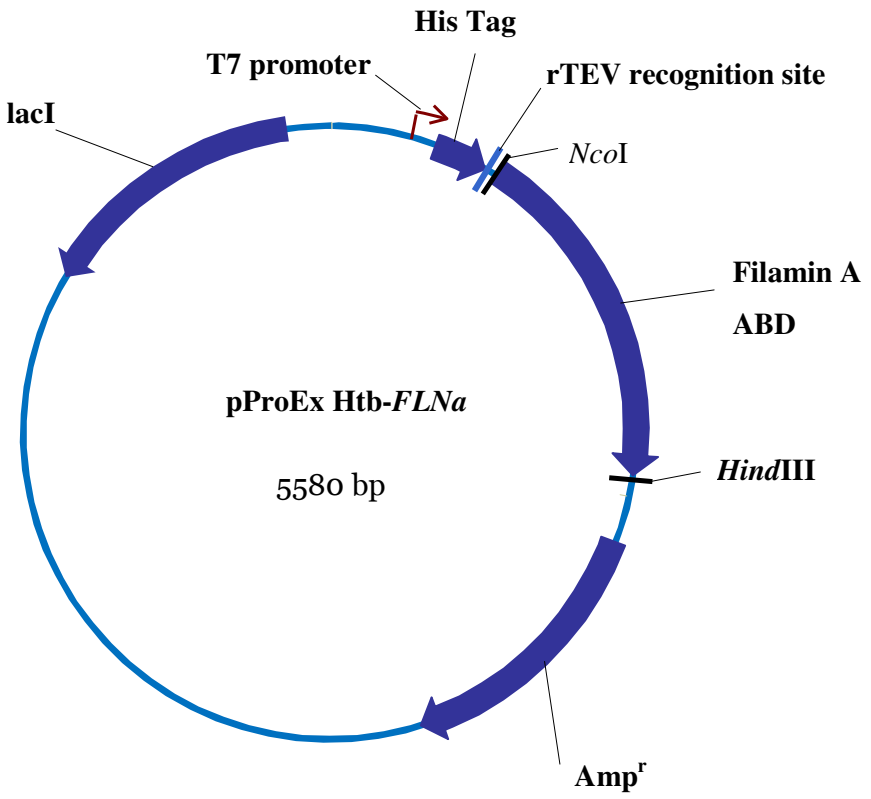

Figure 3-1. Vector Map of the Plasmid Used in this Work.
This map shows the key elements of the *E. coli* expression vector used in this work.

3.2.2 Expression and Purification

The expression plasmid containing the sequence encoding the filamin A ABD was transformed into *E. coli* BL21(DE3) and the protein expressed at 25 ˚C for 5 hr (see methods section 2.10). Following expression, the cells were lysed by French press, then sonicated to shear the nucleic acids (see methods section 2.19) and the lysate was centrifuged to remove any insoluble material.

Purification was performed using a HighTrap™ Ni^{2+}-NTA column, with a stepwise gradient of imidazole (see section 2.20). The column was washed with purification

buffer containing 10 mM, 20 mM and 50 mM imidazole. The His tagged filamin A ABD protein was eluted from the column with 100 mM and 250 mM imidazole (Figure 3-2).

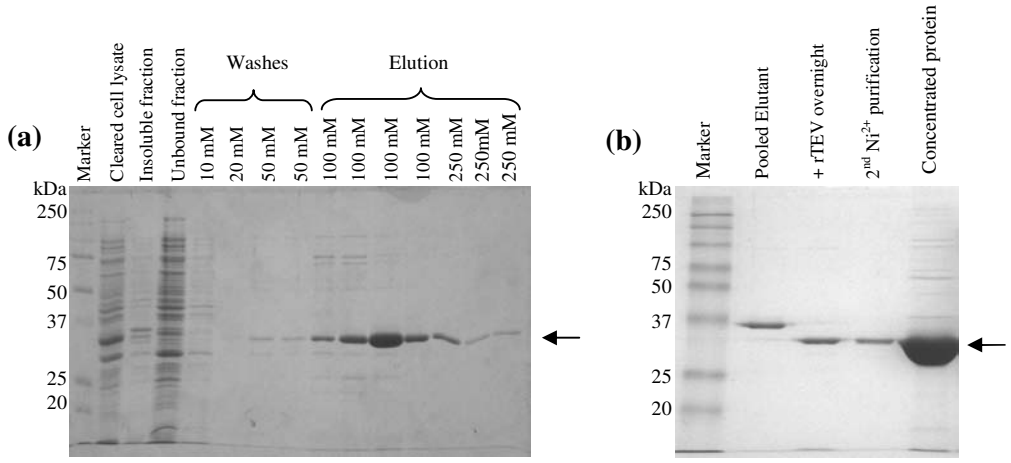

Figure 3-2. SDS PAGE Analysis of Ni^{2+} Affinity Purification and Affinity Tag Removal of the WT filamin A ABD.

Protein was purified over a HisTrap™ HP column, containing Ni -NTA resin. The purified recombinant protein was then digested with the protease rTEV to remove the Ni affinity tag.

a) The concentration of imidazole in the buffer is shown above the wash and elution fractions. The arrow indicates the 33.4 kDa filamin A ABD protein with the Ni affinity tag. The fractions labelled 'Elution' were combined for further purification.

b) The rTEV protease processing of the recombinant protein that was purified in gel (a). The arrow indicates the 30 kDa filamin A ABD protein.

The affinity tagged protein was incubated with rTEV protease (Carrington *et al.* 1988) (see methods section 2.25). The pProEX Htb plasmid encodes the recognition site for rTEV (Glu-Asn-Leu-Tyr-Phe-Gln↓Gly) between the Ni^{2+} affinity tag and target protein. The rTEV cleavage occurs between the Gln and the Gly. The affinity tag, any uncleaved protein and the rTEV protease are removed after the digestion by passing through a clean Ni^{2+} column, with the WT filamin A ABD eluting from the column. The flow through from this second Ni^{2+} affinity purification is then collected and concentrated and analysed by SDS PAGE (Figure 3-2).

The ~30 kDa filamin A ABD protein was then further purified by gel filtration on a Superdex75 column, with 0.5 mL fractions collected throughout the purification. Two filamin A species eluted at molecular masses of 52 kDa and 26 kDa on the calibrated column (methods section 2.27), consistent with the filamin A ABD being in two forms; a monomer and a dimer. When gel filtration was done under reducing conditions (1 mM DTT), the dimeric species is converted to monomer (Figure 3-3). As a result of this observation, 5 mM DTT was added to all further gel filtration buffers to insure the protein eluted as one species (the monomer). However, the oxidised protein species (dimer) from the first purification was used for the first crystal trials resulting in a structure from this preparation.

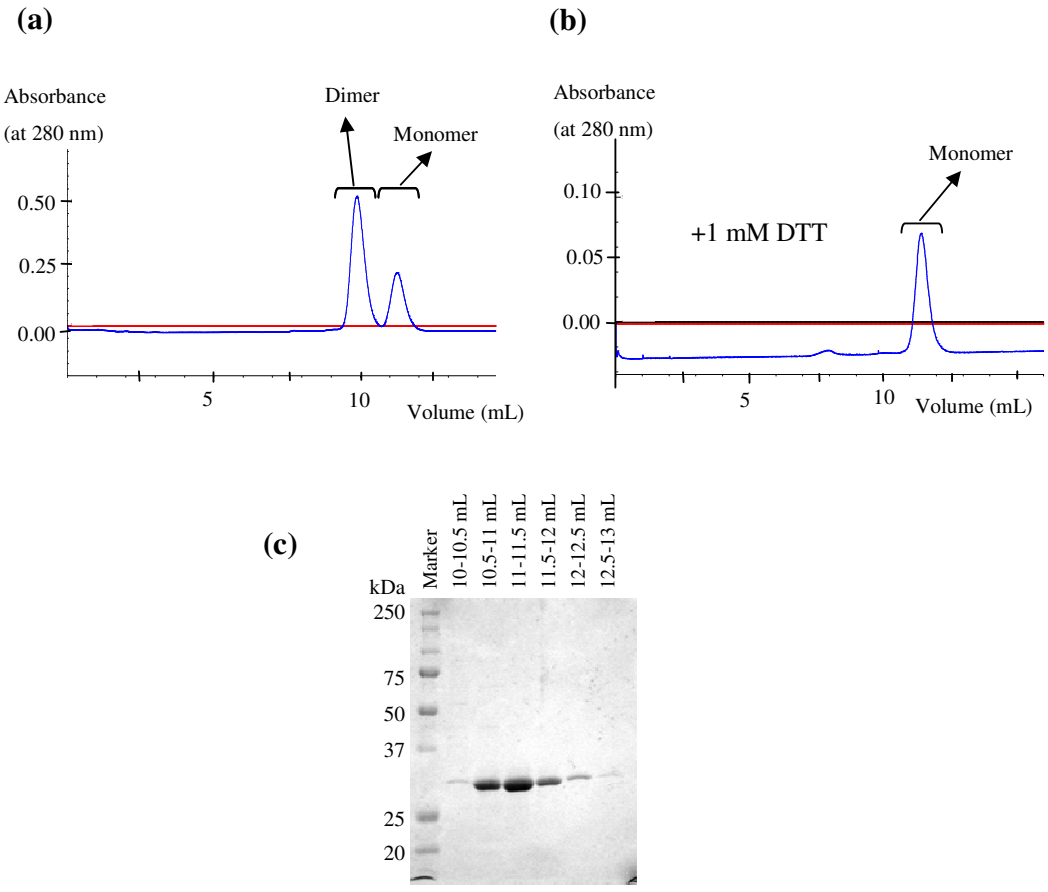

Figure 3-3. Gel Filtration Purification.

The dimeric form of the filamin A ABD is converted to monomer in reducing conditions, resulting in the monomeric species eluting between 10 and 13 mL.

a) The A_{280} traces from gel filtration of filamin A ABD. The filamin A ABD elutes as a monomer and as a dimer.

b) Upon the addition of 1 mM DTT, to both the protein solution and the running buffer of the gel filtration, the dimeric species is converted to monomer.

c) SDS PAGE analysis of the final purified product (in the presence of 1 mM DTT). Lanes are labelled with the volume that the fraction was eluted at.

The gel filtration fractions at 10-13 mL were pooled and concentrated. At this point the purified protein was either used for crystal trials or frozen at >5 mg/mL in ligand buffer with DTT (20 mM TrisHCl, 6.25 mM DTT, 120 mM NaCl, pH 8) for further studies.

Protein was tested before and after freezing in an actin binding activity assay, and no change in actin affinity was observed.

3.3 Filamin A ABD E254K

3.3.1 Introduction

The mutant E254K was chosen as it is associated with OPD2, and this mutation was predicted to break a highly conserved salt bridge between E254 and K196. The contribution of salt bridges to protein stability is not straightforward. However salt bridges are important in maintaining protein structure and play an important role in the function of proteins (Perutz, 1978). The conservation of salt bridges is low, unless the interaction is involved in a particular function (Barlow, 1983). Also, loss of this salt bridge is disease associated in both filamin A and filamin B. Taken together these observations show this salt bridge is important for the function of the ABD.

3.3.2 Cloning

A plasmid construct containing the 5' terminal 907 base pairs of filamin A gene with the mutation 760G>A, resulting in the amino acid substitution E254K, was a gift from Stephen Robertson (Otago University). The open reading frame encoding amino acid residues of the actin binding domain (2-269) from filamin A were PCR amplified (see method section 2.6). The pProEX HTb vector and PCR product were digested with the restriction enzymes *Nco*I and *Hind*III (methods section 2.7). The vector and insert were then ligated (see methods section 2.8) and transformed into *E. coli* Top10 cells (see methods section 2.10). The plasmid (from a single colony) was isolated and digested with the restriction enzymes *Nco*I and *Hind*III. The restriction digest of the vector confirmed the presence of an insert of 804 base pairs, the expected size (Figure 3-4). This plasmid was then sequenced to confirm that the DNA sequence was error free (see methods section 2.13).

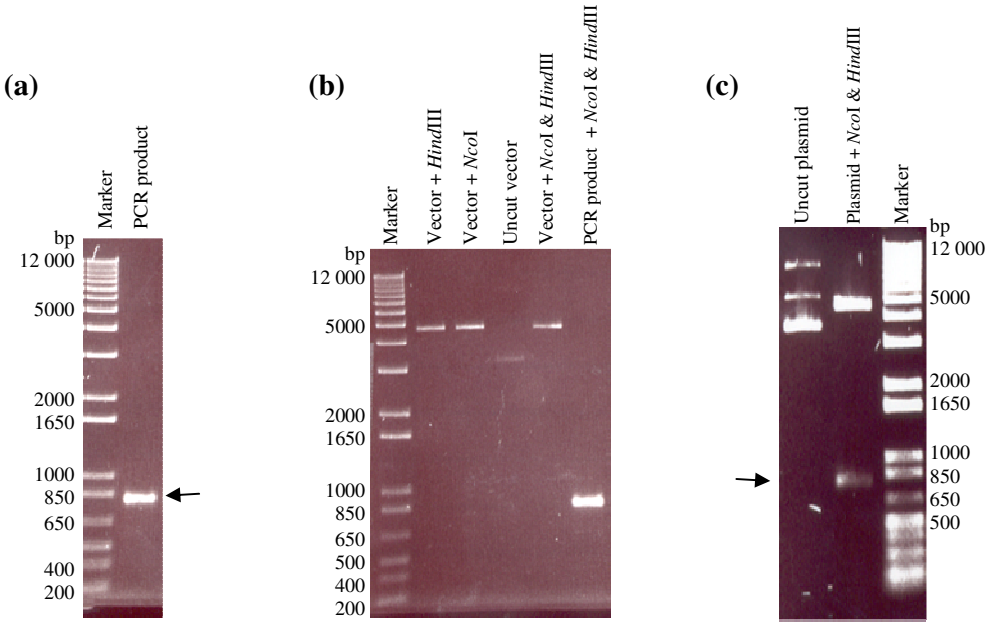

Figure 3-4. Cloning of E254K into the Vector pProEX HTb.

Agarose gels showing the DNA at each step of the cloning.

a) The PCR product of the expected size (804 bp) is indicated by the arrow.

b) Both the enzymes have cut the vector, as shown by the shift from the uncut vector.

c) The plasmid digested with enzymes that cut either side of the insert generates the fragment of the correct size (arrow), indicating that this plasmid contains the insert.

3.3.3 Recombinant Protein Expression in *E. coli*

The plasmid containing the sequence encoding the filamin A ABD E254K was transformed into *E. coli* BL21(DE3) and protein expressed at 25 ˚C for 5 hr (see methods section 2.19). Cells were then seperated from the media by centrifugation (6000*g*) for 30 min at 4 °C. The media was removed and the pellet was either stored at -80 °C or resuspended in lysis buffer (50 mM K_2HPO_4/KH_2PO_4, 0.5 M NaCl, 10 mM imidazole, 1 EDTA free protease inhibitor tablet (Roche), pH 8).

3.3.4 Purification

Following expression the cells were lysed by French press, then sonicated to shear the nucleic acids and finally the lysate was centrifuged (at 30000*g*) to remove any insoluble material. Purification was performed using a HighTrap™ Ni-NTA column, with a stepwise gradient of imidazole (see section 2.20). The column was washed with

purification buffer containing 10 mM, 20 mM, 50 mM and 50 mM imidazole. The His tagged filamin A ABD E254K protein was eluted from the column with 100 mM and 250 mM imidazole. The protein yield from the E254K mutant purification is less than that of the WT protein (compare Figure 3-5 to Figure 3-2)

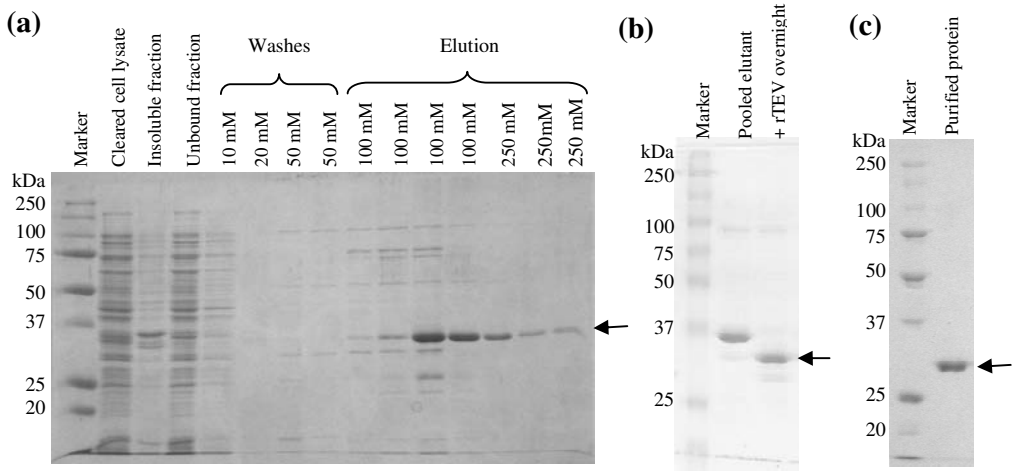

Figure 3-5. SDS PAGE Analysis of the Purification of Filamin A ABD E254K.

Protein was purified by Ni affinity chromatography, the affinity tag was then removed and finally purified by gel filtration.

a) The concentration of imidazole in the buffer is shown above the wash and elution fractions. The fractions labelled 'Elution' were combined for further purification. The arrow indicates the 33.4 kDa filamin A ABD E254K protein.

b) The rTEV protease digestion. The arrow indicates the purified filamin A ABD E254K protein without the Ni affinity tag.

c) SDS PAGE analysis of the purified filamin A ABD E254K, after the Ni^{2+} affinity chromatography and gel filtration chromatography.

Following the Ni^{2+} affinity chromatography and affinity tag removal the filamin A ABD E254K protein was then purified by gel filtration (see methods section 2.27). This protein behaved in the same way on the column as the WT and so the fractions from 10 to 13 mL were pooled and concentrated. Protein was either used for crystal trials or frozen at >5 mg/mL in ligand buffer (20 mM TrisHCl, 5 mM DTT, 120 mM NaCl, pH 8) for further studies.

3.4 A200S

A plasmid construct containing the 5' terminal 907 base pairs of filamin A gene with the mutation 598G>T, resulting in the amino acid substitution A200S, was a gift from Stephen Robertson (Otago University). This fragment was cloned in the same way as E254K, with the same primers, as the E254K ABD. The protein was then expressed and purified as described for the E254K construct.

3.5 Summary

The DNA encoding the WT, E254K and A200S filamin A ABD were each cloned into an *E. coli* vector, providing a recombinant expression system that produced soluble filamin A ABD. The protein was purified, using a two step procedure, Ni^{2+} affinity chromatography followed by gel filtration chromatography. This provides a ready source of pure recombinant filamin A ABD protein for further studies.

4 Structural Studies of the Filamin A Actin Binding Domain

4.1 Introduction

The role in bone development that filamin A, and more specifically the ABD, plays has yet to be elucidated. However, mutations in the filamin A ABD are associated with the developmental bone disorders otopalatodigital spectrum disorder (OPD1 and OPD2), frontometaphyseal dysplasia (FMD) and the neurological disorder periventricular nodular heterotopia (PVNH). The mechanism of the actin binding by this domain is also yet to be elucidated fully. Structural data may help to understand the way that the filamin A ABD binds to actin, and eventually the role of filamin A in bone development. This, in turn, will assist our understanding of the molecular basis of the OPD type associated bone diseases, and the other diseases associated with mutations in this domain.

The disease associated mutations highlight key areas of the ABD, providing a starting point for structure-function studies of this domain. Before this work there was no structural data for any of the filamin actin binding domains. Structural studies were completed for the wildtype filamin A actin binding domain (ABD) and two mutant filamin A ABD proteins associated with the disease OPD2, E254K and A200S. This was done to determine if there are structural changes that occur with these two pathogenic mutations, and, if so, can these changes explain the altered/gained function that is associated with the mutation. This chapter details the structural studies of these three proteins and presents an analysis of these structures.

4.2 The X-Ray Crystal Structure of Wildtype Filamin A ABD

4.2.1 Crystallisation of Wildtype Filamin Actin Binding Domain

The dimeric (oxidised) species from gel filtration (in the absence of DTT) was concentrated to 9.6 mg/ml in the crystallisation buffer (20 mM HEPES, pH 7.4, 100 mM NaCl). Crystals were set up using the hanging drop method, 1 μL protein solution was mixed 1:1 v/v with the well mother liquor and the trays were then incubated at 20 ˚C (see method section 2.28). Rod-like crystals were observed within 2 days. Final data

sets were collected from crystals grown from 20% polyethylene glycol 4000, 0.1 M Tris HCl (pH 8.5), 0.2 M lithium sulfate. Crystals were briefly soaked in a solution of mother liqueur containing 20% v/v glycerol as a cryoprotectant, then flash frozen in liquid nitrogen. The loop containing the frozen crystal was mounted in the beam with data collected at 120 K (see methods section 2.29).

4.2.2 WT Structure Determination

To generate a crystallographic model there are a number of prior steps to process the diffraction data. The first step is indexing the diffraction pattern. This allows the unit cell to be determined, and the space group to beassigned. Each spot is then integrated to determine the intensity. Following indexing and integration the data were, scaled, averaged and the cut off resolution assigned. The final step before a solution is to calculate the structure factor amplitudes from the merged intensity values (see methods section 2.38).

4.2.3 Diffraction Collection and Indexing

Two initial images were collected at 90°, from these the unit cell dimensions were calculated; a=58.07 Å, b=71.64 Å, c=158.91 Å, and the angles $\alpha=\beta=\gamma=90^{\circ}$, which corresponds to an orthorhombic unit cell. Data were collected by CrystalClear, using the strategy recommended for this space group, unit cell and crystal orientation. Images were collected at a crystal to detector distance of 150 mm, with an exposure time of 10 min for each image, and 400 images were collected over a total oscillation angle of 100°. The initial diffraction images from screening at 0° and 90° showed the data were quite mosaic (1.1°). Therefore each frame of data was collected over a narrow oscillation angle (0.25°). With mosaic data collection there can be overlap problems and collecting finer slices of diffraction can counteract this problem. The diffraction was anisotropic, with a noticeable difference in the diffraction quality over the total oscillation range of 100° (Figure 4-1).

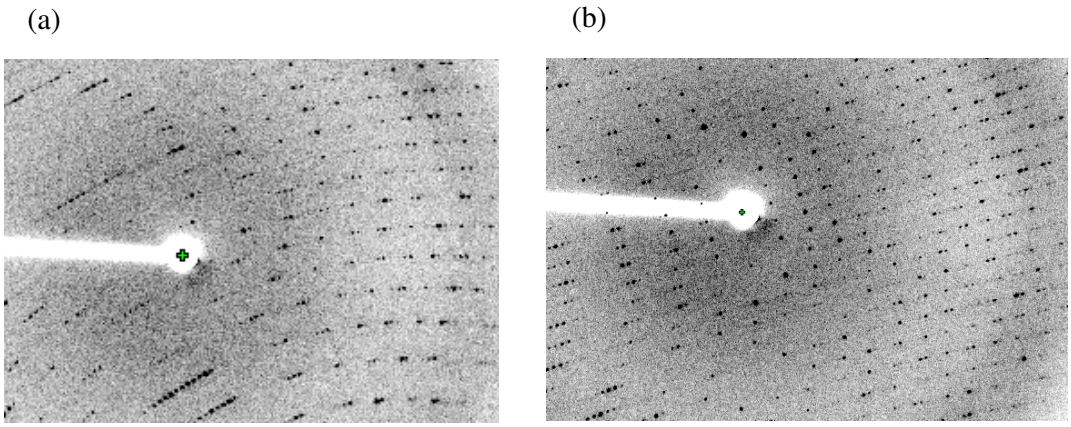

Figure 4-1. Diffraction Images from the Data Collection of the WT Crystal.

These images show the anisotropy of the crystal. These two diffraction images are taken from different angles of the same crystal. The diffraction in the second image (b) has much more clearly defined spots (and diffracts to a higher resolution) than the first image shown (a).

a) Image number 201

b) Image number 400

The clear patch in each image is the beam stop shadow.

The resulting images were then indexed and integrated by XDS (Kabsch, 1993). The space group is $P2_12_12_1$ (number 19), and was determined by analysis of the systematic absences in the reflections by CrystalClear (Rigaku), where $h00$: $h=2n$ and $0k0$: $k=2n$ and $00l$: $l=2n$, with only the even numbered reflections present along these axes. Matthew's coefficient was used to determine the number of molecules in the asymmetric unit and the unit cell (Matthews, 1968). This method is based on the assumption that protein crystals typically contain ~40-60% solvent. Using the molecular weight of the protein, the volume of the protein is determined (assuming a sphere). The volume of the unit cell is known, and therefore the number of protein molecules that gives a value around 40-60% of the volume of the unit cell is considered the most likely solution. The filamin A ABD structure contains 8 molecules in the unit cell, which gives a solvent content of 47.2% v/v. The space group $P2_12_12_1$ dictates that there are 4 copies of the asymmetric unit in the unit cell and therefore 2 molecules in the asymmetric unit. This crystal arrangement is shown in Figure 4-2 from the refined solution.

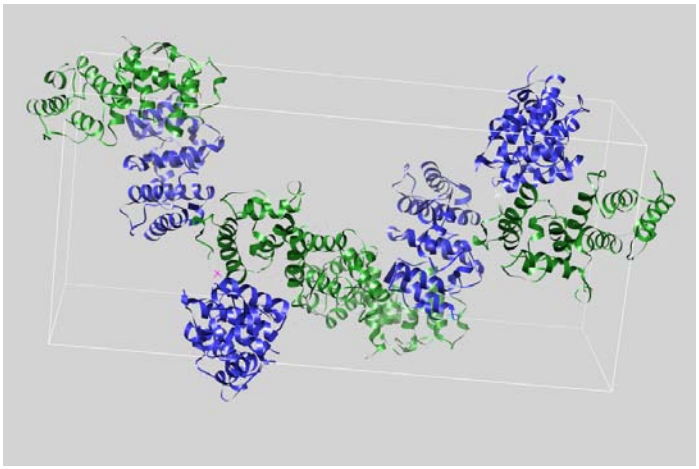

Figure 4-2. The Crystal Packing of the WT Filamin A ABD Crystal.
The crystal system is orthorhombic ($a \neq b \neq c$ and $\alpha=\beta=\gamma=90°$). The two molecules in the asymmetric unit are shown in green and blue, and the unit cell is shown as a white box. The phosphates are shown as sticks. The space group is $P2_12_12_1$.

4.2.4 Scaling and Averaging the X-Ray Diffraction Data

The diffraction images were scaled and averaged using SCALA, and the data quality and resolution range determined. Given the mosaic and anisotropic nature of this data (some angles of the crystal diffracted to a higher resolution), the resolution cut off point was not absolutely clear. To determine the resolution cut-off, the *I*/sig*I*, as a general rule the signal should be two times greater than the background. At 2.3 Å the ratio of I/sigI is 2.8. Ideally the R_{merge} of the outer shell should also be less than 0.5, and the data in this structure at 2.3 Å give an R_{merge} of 0.53 in the outer shell. Based on all this information, the data from 38.97 Å to 2.3 Å resolution were used (Table 4-1).

4.2.5 Molecular Replacement

When the reflections are collected, the location and intensity of the reflection (or spot) is measured; however, the phase is unknown. A similar structure can be used as a search model in molecular replacement to determine a starting phase (Read *et al.*, 2001). In this case a structure with high sequence identity (which is indicative of structural similarity) was available in the protein data bank. For the determination of the initial phases

molecular replacement was used with one monomer of the α-actinin-3 ABD (pdb code 1WKU) structure (Franzot *et al*., 2005) as the search model. The sequence identity between these domains was 37%, with a sequence similarity of 59%, as determined by a BLAST alignment. A PHASER rotation and translation search gave two solutions corresponding to the two molecules expected in the asymmetric unit (McCoy *et al*., 2005). The resulting model had an initial *R*-factor of 41.0%, and a correlation coefficient of 0.752, with sensible crystal packing and good quality electron density maps.

4.2.6 Refinement of the Structure

Refinement is the process where the calculated structure factors (model) are compared to the observed data and the model improved. The improvement of the model was determined by following the R_{work}/R_{free} which are a measure of how well the observed data agree with those calculated from the model. To insure that the maps were not overinterpreted the R_{work} and R_{free} were kept within approximately 5% (Brunger, 1992). The R_{free} is a set of reflections (5%) that are not refined against the model, and therefore contain no model bias. These reflections were automatically (and randomly) selected by SCALA during the data processing. Refinement was performed by REFMAC initially, with some rebuilding in COOT (Emsley and Cowtan, 2004). However, in the later stages of refinement the programme PHENIX was used, enabling refinement with simulated annealing, TLS and NCS techniques (Adams *et al*., 2002). These maps calculated from PHENIX were used to rebuild the model using rebuilding in COOT. Ordered waters (greater than 3σ peaks in the F_o-F_c map) were entered manually into chemically sensible positions in the maps using COOT.

4.2.6.1 Density Modification

The CCP4 program DM was used to calculate a mask around were the protein molecules in the unit cell. This technique is used to improve maps, by calculating structure factors with modified and potentially improved phase values (Cowtan and Zhang, 1999). New maps can then be calculated from these structure factors. This is a particularly powerful technique when there is non crystallographic symmetry (NCS), as this information can also be used to define the area/shape of the protein, which would be expected to be the same in each molecule in the asymmetric unit. There were two

molecules in the asymmetric unit with 47.2% v/v solvent, and the orientation between the two molecules was also defined. Using this information, 10 rounds of density modification refinement were performed with the DM program, and the output files containing maps in which the solvent area has been flattened. The maps generated by DM were used to build the model into in COOT, followed a round of refinement in REFMAC. Improved R_{work}/R_{free} values indicated that new information about the phases was provided by this technique.

4.2.6.2 TLS Refinement

The atomic displacement factors (*B* factors) describe the thermal motion of an atom. However, rather than the thermal motion of an atom being a sphere, the motion is often more ellipsoidal and this is described as anisotropic motion. Three tensors T, L and S describe the thermal motion of a molecule in a crystal. These TLS parameters describe the anisotropic thermal motion of the atoms, and are given as 6 parameters per atom, which define the shape of the ellipsoid - the atomic displacement parameter (ADP). This technique is referred to as TLS refinement (Schomaker and Trueblood, 1998). In small molecule crystallography it is possible to refine anisotropic *B* factors. However, in a protein structure, adding 6 further parameters to refine the B factor for each atom is not possible due to the number of atoms compared to the number of reflections. To solve this limitation the *B* factor from one atom (eg the C_α) can be assigned to a group of atoms (eg a residue), the other atoms are assigned a B factor correction based on the distance from the C_α. This group can be very large, such as a domain of a protein, or the whole protein molecule. An anisotropic *B* factor is derived for each atom in a TLS group. These *B* factors are correlated by belonging to the same "rigid body", and only 20 refinement parameters are required for each TLS group. This refinement of TLS parameters enables refinement of anisotropic displacements without using the large number of parameters that full anisotropic refinement demands (Winn *et al*., 2000). In this refinement the two peptide chains were assigned as the two TLS groups.

4.2.6.3 Non Crystallographic Symmetry Refinement

In this crystal arrangement there were two molecules of protein in the asymmetric unit (Figure 4-2) and the rms deviation between these molecules (chain A and chain B) was

0.48 Å over the 222 C_α atoms in the final crystallographic model. The relationship between the two molecules is described as non crystallographic symmetry (NCS). The two molecules are the same protein molecule but, due to crystal packing, they have slightly different structures and so can not be transposed exactly upon one another. In refinement this provides further restraints that can be applied. In this refinement the programme PHENIX automatically selected the conserved regions, and refined these with NCS restraints. Tight restraints were used on regions such as helices, and more loose restraints were applied to regions that differed slightly between the two molecules (such as loops at crystallographic interfaces).

4.2.7 Determining the Reduced WT Filamin A ABD Structure

The structure of the WT ABD in the presence of DTT was also determined. Crystals were grown from 5 mM DTT, 25% polyethylene glycol 4000, 0.1 M Tris HCl (pH 8.4), 0.2 M lithium sulfate mother liquor. Images were collected with a scan width of 0.5 °, with a range of 0 to 113° with 23 min exposure time for each image. Data were processed (using the WT oxidised structure as a model) in the same way as the oxidised WT structure, with the same R_{free} reflections (Table 4-1).

4.3 Solving the X-Ray Crystal Structure of Filamin A ABD E254K

The point mutation E254K in CH2 domain of the ABD of filamin A is associated with OPD2 highlighting the importance of this residue. This substitution would be predicted to disrupt the conserved salt bridge that between E254 (helix G) and K169 (helix A), which may also lead to further structural changes. The structure of filamin A ABD E254K was solved to study structural changes that may be associated with this pathogenic mutation.

4.3.1 E254K: Crystallisation and Data Collection

For the E254K the monomeric species was selected from gel filtration in 5 mM DTT and concentrated to 4.1 mg/mL in the same crystallisation buffer as the WT. Protein solution was mixed 1:1 with the well mother liquour containing 20% polyethylene glycol 4000, 0.1 M Tris HCl (pH 8.8), 0.2 M lithium sulfate, 5 mM DTT, and set up as hanging drops (see methods section 2.28). Crystals were obtained in two days, and were

a similar crystal form (rod shape) to the WT crystals. Crystals were mounted as described for the WT crystals. The mosaicity was 0.57°, and so data were collected with a 0.5° oscillation angle, using the strategy suggested by CrystalClear. Images were collected over 110°, with a collection time of 20 min per image and a crystal to detector distance of 100 mm. Other than these parameters, the crystal mounting, R_{free} reflections and data collection were the same as described for the wildtype protein crystals.

4.3.2 E254K: Integration, Indexing and Scaling

The diffraction images were indexed and integrated by MOSFLM. The unit cell dimensions were *a*=57.66 Å, *b*=73.94 Å, *c*=154.44 Å, with all the angles equal to 90˚ corresponding to an orthorhombic unit cell with a solvent content of 55 % v/v (corresponding to two molecules in the asymmetric unit). The crystals belonged to the space group $P2_12_12_1$. The data from 57.64 Å to 2.3 Å were scaled and averaged with SCALA. Data quality statistics are provided in Table 4-1.

4.3.3 E254K: Molecular Replacement

The phase problem was solved by molecular replacement using chain B of refined wildtype filamin A ABD structure (with residues 253, 254 and 255 omitted) as a search model in a PHASER search (McCoy *et al*., 2005). These maps resulted in an initial R_{work} of 0.30, and a correlation coefficient of 0.85.

4.3.4 E254K: Refinement

The maps were then used to rebuild the model using rebuilding in COOT and several rounds of refinement in REFMAC followed by PHENIX refinement, using the same R_{free} set as the WT structure. The same refinement method was used as described for the refinement of the WT structure.

4.4 Solving the X-Ray Crystal Structure of Filamin A ABD A200S

A200 is a highly conserved residue in helix C in the CH2 domain of the filamin A ABD (Figure 1-10). The amino acid substitution A200S is associated with OPD2, which further highlights the importance of this residue. However, no clear role for the A200 residue could be predicted from an inspection of the WT structure. This amino acid position may be restricted to a small residue. However, this alanine to serine mutation is a relatively conservative amino acid change. The two OPD2-associated residues are not co-localised; in the WT structure A200 is 19 Å away from E254. Solving the structure of this protein would allow it to be compared and contrasted to both the WT and the E254K structures. The aim of this structural study of A200S was to investigate any structural changes that may be associated with OPD2.

4.4.1 Crystallisation and Data Collection

The monomeric species was selected and concentrated to 4.0 mg/mL in the same buffer as the WT. Protein solution was mixed 1:1 with a mother liqueur containing 25% polyethylene glycol 4000, 0.1 M Tris HCl (pH 8.0), 0.2 M lithium sulfate, and set up as hanging drops (see methods section 2.28). Crystals were obtained in two days, and were a similar crystal form (rod shape) to the WT crystals. The crystals were frozen using mother liquor with 10% PEG 550 as a cryoprotectant. Data collection, equipment, R_{free} relflections and methods were the same as those used for the wildtype protein.

4.4.2 A200S: Data Collection, Structure Determination and Refinement

Data were collected in 0.5° scans using the strategy as determined by crystal clear software. Images were indexed and integrated by MOSFLM. From the systematic absences the crystals were assigned to the space group $P2_12_12_1$. The unit cell dimensions were a=57.29 Å, b=74.27 Å, c=156.19 Å, with all the angles equal to 90° corresponding to an orthorhombic unit cell. The number of molecules in the asymmetric unit was determined to be most likely two, with a solvent content of 56% v/v. The data from 37.1 Å to 3.0 Å were scaled and averaged (SCALA). The resolution was cut off at 3.0 Å, corresponding to an I/sig$I$ of 3.1, and an R_{merge} of 0.49 in the outer shell. The wildtype chain B structure was used as a search model in a PHASER molecular

replacement search (McCoy *et al*., 2005). This resulted in 2 peaks of Z-scores (of 12 and 14) corresponding to the two molecules expected in the asymmetric unit.

4.4.3 A200S: Refinement

The maps calculated with PHASER coefficients were then used to rebuild the model using the same refinement methods described for the WT structure.

4.4.4 Statistical Validation of All the Structures

There are a number of parameters that can be measured to determine the accuracy of the diffraction data and the resulting crystallographic model. Following refinement to 2.3 Å (E254K), 2.3 Å (WT), and 3.0 Å (A200S), the structures were analysed by MolProbity (Davis *et al.*, 2007). The statistics from all structures are summarised in Table 4-1.

Parameter	Wildtype (oxidised)	Wildtype (reduced)	E254K	A200S
Data Collection				
Wavelength (Å)	1.5418	1.5418	1.5418	1.5418
Space group	$P2_12_12_1$	$P2_12_12_1$	$P2_12_12_1$	$P2_12_12_1$
Cell parameters:				
a (Å)	57.85	57.67	57.66	57.29
b (Å)	71.22	72.29	73.94	74.27
c (Å)	158.28	155.32	154.44	156.19
$\alpha = \beta = \gamma$	90	90	90	90
Reflections	116 874	72 824	122 444	69 664
Unique reflections	29 893	17 832	29480	13 989
Resolution (Å)	44.9-2.30 (2.42-2.30)	42.1-2.7 (2.79-2.7)	57.6-2.3 (2.42-2.30)	37.1- 3.16 (3.16-3.0)
Redundancy	3.9 (3.9)	4.1 (3.9)	4.2 (4.1)	5.0 (5.0)
Completeness (%)	100 (100)	96.7 (94.5)	98.0 (93.9)	99.93 (100)
R_{merge}	0.10 (0.53)	0.12 (0.59)	0.088 (0.53)	0.085 (0.49)
Data Refinement				
I/sig$I$	9.4 (2.8)	11.4 (2.0)	11.7 (1.8)	15.3 (3.1)
R_{work} (%)	21.0	22.8	22.4	21.4
R_{free} (%)	26.1	29.4	26.3	27.4
Rmsd from ideal geometry:				
Rmsd bonds (Å)	0.018	0.008	0.006	0.011
Rmsd angles (°)	.65	1.2	0.9	0.91
Number of protein atoms	3623	3512	3375	3557
Number of H_2O molecules	140	31	103	0
Ramachandran plot:				
Outliers (%)	0.2	0.2	0	0.92
Allowed (%)	99.8	99.8	100	99.1
Most favoured (%)	96.4	96.8	98.8	94.2
Rotamer outliers (%)	3.5	1.8	1.53	3.25
Wilson B-value (Å^2)	45.3	60.3	38.4	78.2
Overall B-value (Å^2)	37.7	47.1	39.5	61.7

Table 4-1. Crystallographic Data.

The data collection parameters are listed, along with the refinement statistics. These statistics were analysed to determine the validity of the crystallographic model. The outer shell values are shown in parenthesis.

4.4.5 Ramachandran Plots

The Psi (between C_α-C) and Phi (between the N-C_α) angles of the peptide backbone are not restrained during the refinement process, and are useful to check of the validity of the structural model (Ramachandran *et al.*, 1963). Ramachandran plots provide a visual

check of the Psi and Phi angles (Figure 4-3). Given the alpha helical nature of all these proteins there would be a cluster expected in the lower left hand quadrant (where amino acids that are in right hand helices are found) in the Ramachandran plots.

(a) WT (oxidised) (b) E254K (c) A200S

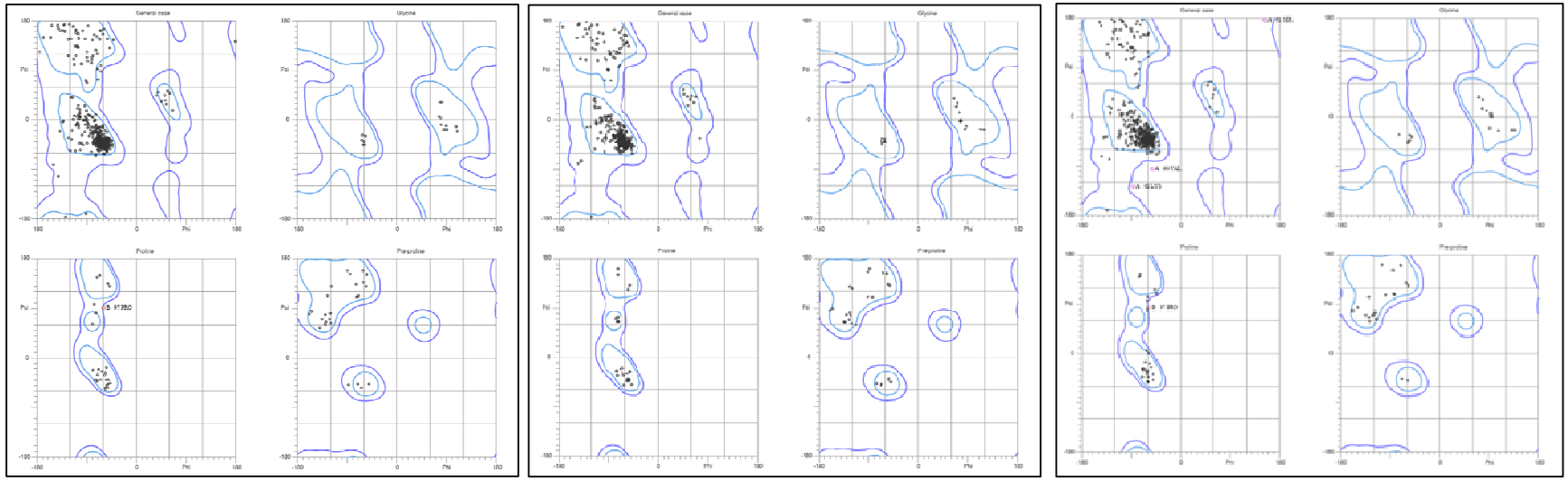

Figure 4-3. Ramachandran Plots of the WT, E254K and A200S Filamin A ABD Structures.

These maps show the Phi and Psi angles of the main chain atoms in the three crystallographic models.

a) The WT ABD has one (0.2%) outlier residue, Pro 97 in chain B.

b) The E254K ABD plot has no outliers.

c) The A200S plot has four outliers.

For each plot, the top left grid shows the general case, the top right shows the glycines, the bottom left shows the prolines and the bottom right shows the pre-proline residues. These maps were generated by the MolProbity server.

4.5 The Filamin A ABD Structure

4.5.1 The Crystallographic Dimer

The ABD protein crystallised with two molecules in the asymmetric unit. The cysteine 59 in each monomer forms a disulfide with the cystine 59 of the other monomer in the asymmetric unit. This disulfide bond is assumed to be a non native interaction formed when the protein is removed from the reducing environment of the *E. coli* cytoplasm. This prediction is supported by electron microscopy data of the ABD of full length native filamin A which shows that the two ABDs within the homodimer are located distal, and do not associate (Tyler *et al.,* 1980, Nakamura *et al*., 2007). When the interface between the molecules was analysed by PROTORP the area was 470 $Å^2$, indicative of a crystal interface rather than a native interaction (Reynolds *et al*., 2009). The interface is comprised of 18 residues that form 4 hydrogen bonds, 11 salt bridges and a disulfide between chain A and chain B. When the ABD was purified by calibrated gel filtration there are two species; the expected monomer of 29 kDa, but also a dimer of 58 kDa. The 58kDa species was converted to a 29 kDa monomer upon addition of 1 mM DTT to both the protein solution and the running buffer of the gel filtration. When the protein is crystallised in the presence of 5 mM DTT the crystals diffracted to a lower (2.7 Å) resolution than the oxidised structure (2.35 Å), indicating that the disulfide may be assisting in the crystallisation. This has been observed in other proteins, and introducing a cysteine pair on the surface of a protein can assist crystallisation (Banatao *et al*., 2006). Both oxidised and reduced structures form the same interface between the monomers of the asymmetric unit, and the same crystal packing and space group (Table 4-1). The reduced structure contains a free cysteine at residue 59; however, there is a 3σ peak in the F_o–F_c (difference) map where the disulfide would be located, indicating that less than 5% of the cystine 59 is oxidised.

(a) Oxidised Crystallographic Dimer

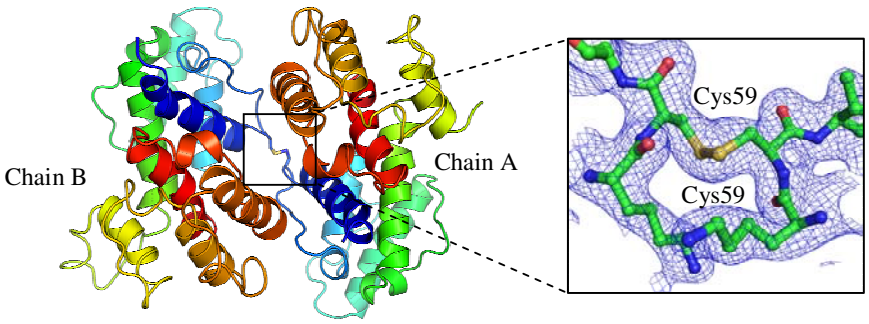

(b) Oxidised/Reduced Cystine

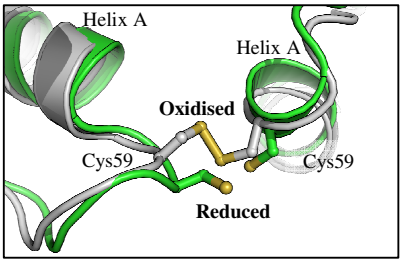

(c) C_α Chains of the Oxidised/Reduced

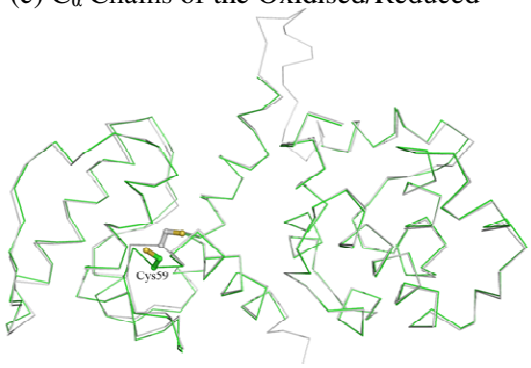

Figure 4-4. The Monomer of Oxidised Crystallographic Model Represents the Filamin A ABD Native Structure.

a) The structure of the asymmetric unit in the oxidised WT filamin A ABD structure. The monomers are both coloured blue (N - termini) to red (C - termini) and the disulfide at cystine 59. The inset shows a close up of the disulfide bond with the $2F_0$-F_c map contoured at 1σ.

b) A close up view of the disulfide in the oxidised structure (grey), compared with the reduced structure (green). This overlay was produced from superimposing the entire asymmetric unit from each structure in COOT.

c) An overlay of chain B from reduced structure (green) and the oxidised structure (grey), with the cystine 59 of each protein shown as sticks. The 222 C_α atoms of each monomer were overlaid in COOT. This shows that the changes are minimal and localised when the monomeric structures are compared.

The C_α backbone residues of the oxidised and reduced structures were overlaid (with Superpose, in the CCP4 suit). There are very few structural changes and the rms deviation between the monomers is 0.41 Å. This indicates that this disulfide formation

has not affected the structure of the ABD (Figure 4-4). This difference is equivalent to the difference seen between the chain A and chain B of the crystals in the WT oxidised filamin A ABD (rmsd is 0.42 Å). At the site of the disulfide bond the Cys59 C_α have moved apart by 2.3 Å. The 3 residues either side of the Cys59 in both chains are perturbed by 0.2–0.5 Å but this is a localised and small change. The changes seen in the overlay are mainly due to the two ABD moving relative to each other, and not to changes within the ABD structure. So given this data, the higher resolution (oxidised) structure only will be discussed further.

4.5.2 The WT Monomer Structure

The filamin A ABD monomer (residues 2 – 269) is an all helical protein domain. The first 38 residues (chain A) and 36 (chain B) do not have sufficient density present to model and are assumed to be disordered. CH1 is comprised of six alpha helices, A-G: A residues 41-58, B 70-72, C 75-85, E 100-117, F 126-131, G 134-152 (D is absent in CH1). CH2 is comprised of seven alpha helices: A' 168-176, B' 196-205, C' 213-215, D' 213-215, E' 221-236, F' 244-248, G' 254-267. Each CH domain contains four major helices, A, C, E and G, that are arranged in the typical ABD fold. Three of these helices (C, E and G) lie roughly parallel to each other, with the fourth helix (A) roughly perpendicular to the other three (Banuelos *et al*., 1998; Keep *et al*., 1999; Norwood *et al*., 2000; Borrego-Diaz *et al*., 2006). The two minor helices B and F are each comprised of one helical turn (Figure 4-5).

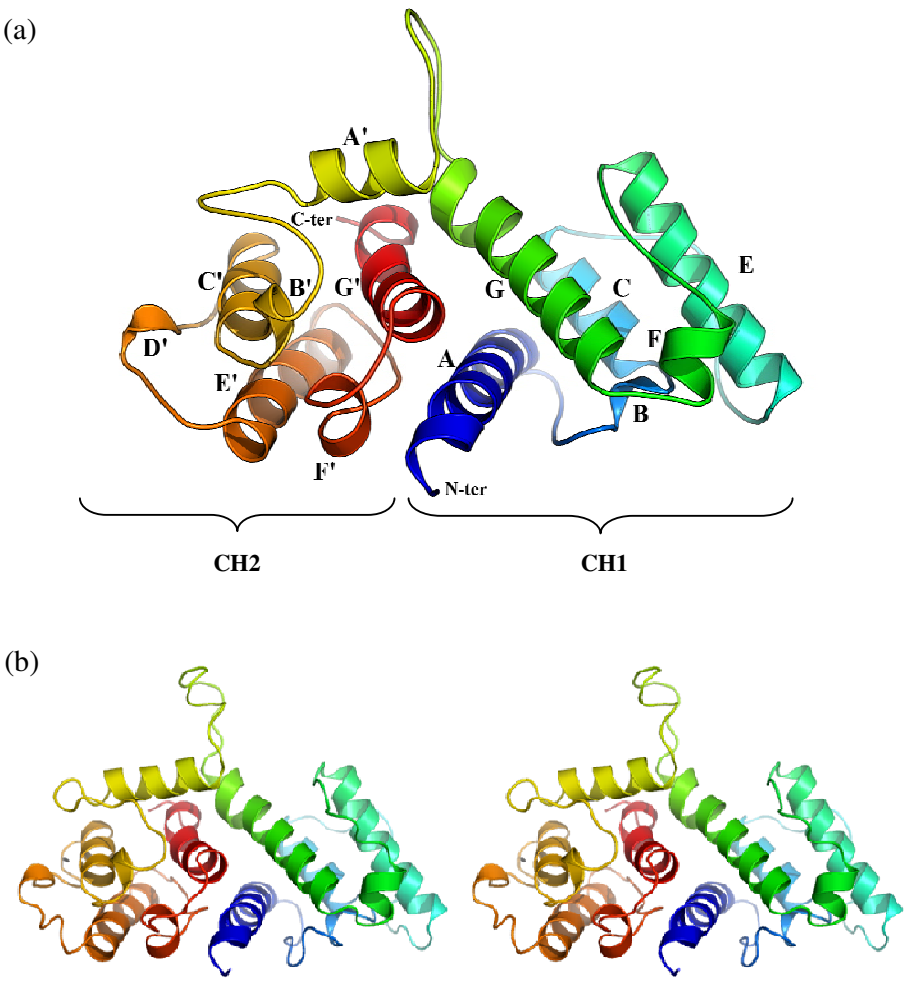

Figure 4-5. The Structure of the Filamin A ABD Monomer.

a) The filamin A ABD monomer. The polypeptide backbone is coloured blue (N-terminus) to red (C-terminus). Each CH domain is comprised of α helices designated A-G.

b) The monomer (from above) is shown in stereo.

The two calponin homology (CH) domains pack together with the A and G helices as observed in the structure of α-actinin. The CH1/CH2 interface was analysed by the Protorp server (Reynolds *et al.*, 2009), and is an extensive interface of 854 $Å^2$, containing 9 hydrogen bonds and 13 salt bridges, with solvent molecules completely excluded. In context the CH domains of utrophin and dystrophin form an extended dumbbell shape with the loop linking the two distal CH domains. However, in utrophin

and dystrophin the same CH1/CH2 interface is formed in the crystal structure, but it is formed with the CH domain of a different peptide chain (Figure 4-6).

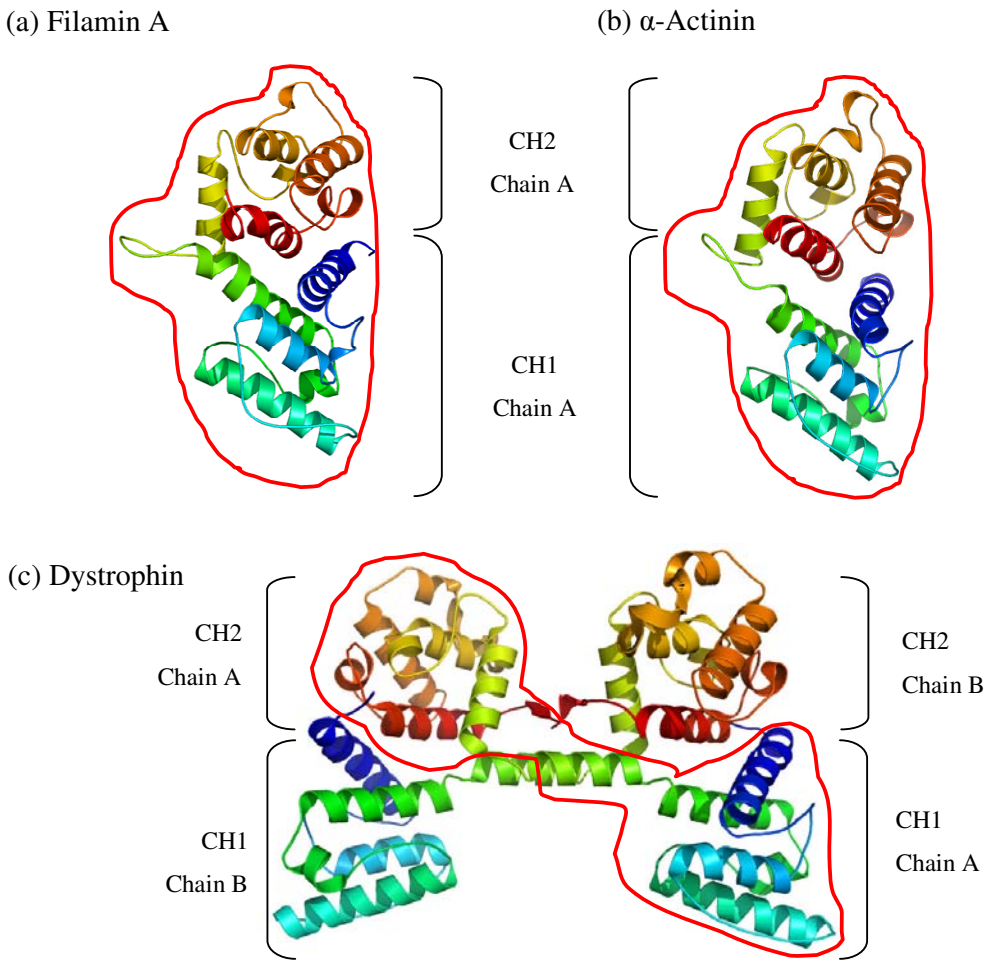

Figure 4-6. Comparing the Overall Fold of Three Actin Binding Domain Structures.

a) The filamin A ABD monomer, in the 'closed' form.

b) The α-actinin ABD monomer, in the 'closed' form (PDB 1WKU).

c) The dystrophin ABD. Showing the 'open' ABD form, with the head-to-tail dimers (PDB 1DXX).

In each structure one monomer is shown circled in red.

The filamin A ABD structure was compared to other homologous domains, and the rmsd determined for the ABD (residues 38-269), CH1 (residues 38-153) and CH2 (residues 167-269) using the DALI server (Holm *et al.*, 2008). These superposition results (and an overlay of some of these structures) are shown in Figure 4-7.

(a) Overlay of ABD

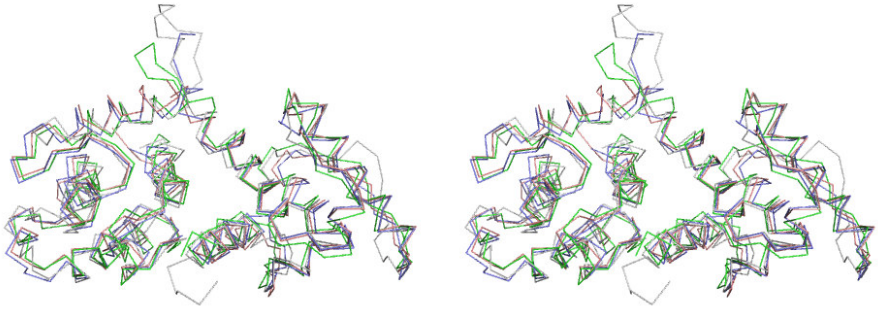

Key:

Grey: Filamin A

Green: α-Actinin-3

Purple: Dystrophin

Pink: Utrophin

(b)

	PDB code	ABD RMSD (Å)	CH1 RMSD (Å)	CH2 RMSD (Å)
Filamin B	3FER	1.0 (234 Cα)	0.7 (111 Cα)	0.9 (102 Cα)
Plectin-1	3F7P	1.6 (231 Cα)	1.4 (113 Cα)	1.5 (102 Cα)
Alpha-actinin-4	2R0O	2.1 (229 Cα)	1.6 (114 Cα)	1.8 (102 Cα)
Alpha-actinin-3	1WKU*	2.1 (227 Cα)	1.5 (112Cα)	1.8 (102 Cα)
Alpha-actinin-1	2EYI	2.1 (234 Cα)	1.6 (112 Cα)	1.8 (102 Cα)
T-Fimbrin	1AOA	2.7 (247 Cα)	2.7 (111Cα)	1.8 (93 Cα)
Utrophin	1QAG		1.3 (108 Cα)	2.0 (101 Cα)
Dystrophin	1DXX		2.8 (113Cα)	1.9 (102 Cα)

Figure 4-7. Structural Comparison with other ABDs.

a) Stereo diagram of an overlay (performed by COOT) of the Cα chains of ABD of filamin A, α-actinin-3, dystrophin and utrophin. This shows the highly conserved ABD fold.

b) When the filamin A ABD is compared to the ABD from a number of different proteins by the DALI server, the RMSD between the ABD domains is small (1-2.7 Å) showing this domain is highly structurally conserved.

When the putative actin binding sites (ABS) are mapped to the filamin A ABD structure the residues do not form a continuous surface (Figure 4-8). Also included in the ABSs are residues that are not located at the surface and therefore appear unlikely to form a direct interaction with actin in this structural arrangement of the ABD (see alignment section 1.5.2).

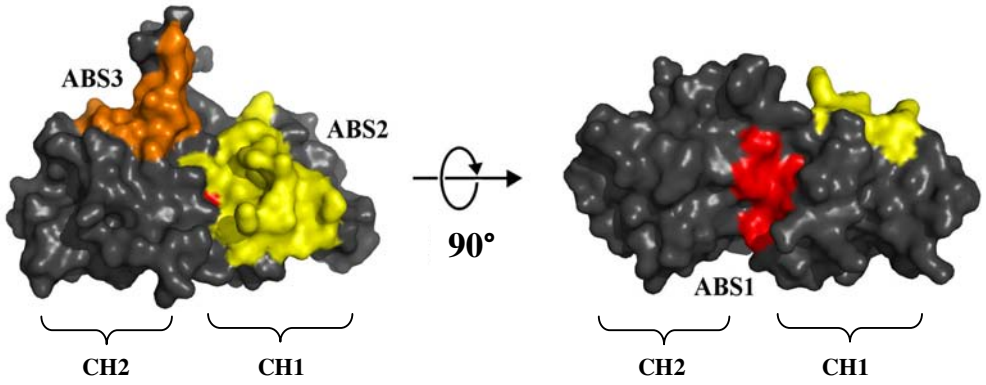

Figure 4-8. The Residues of the Putative ABS do not Form a Continuous Surface on the Filamin A ABD Structure.

The structure is shown from two angles, 90° to one another. The three actin binding surfaces (ABS) are shown in red (ABS1), yellow (ABS2) and orange (ABS3). The two CH domains are labelled.

Some of these ambiguities about the amino acids that interact with actin can be attributed to the lack of available structural data when these sequences were being characterised. A ClustalW alignment of filamin A, B & C, α-actinin, β-spectrin, utrophin and dystrophin (shown in section 1.5.2) was performed. The alignment was used to colour the residues in the structure according to sequence conservation. This analysis showed that the ABS corresponds to highly conserved regions on the surface of the protein and buried in the protein at the CH1/CH2 interface (Figure 4-9).

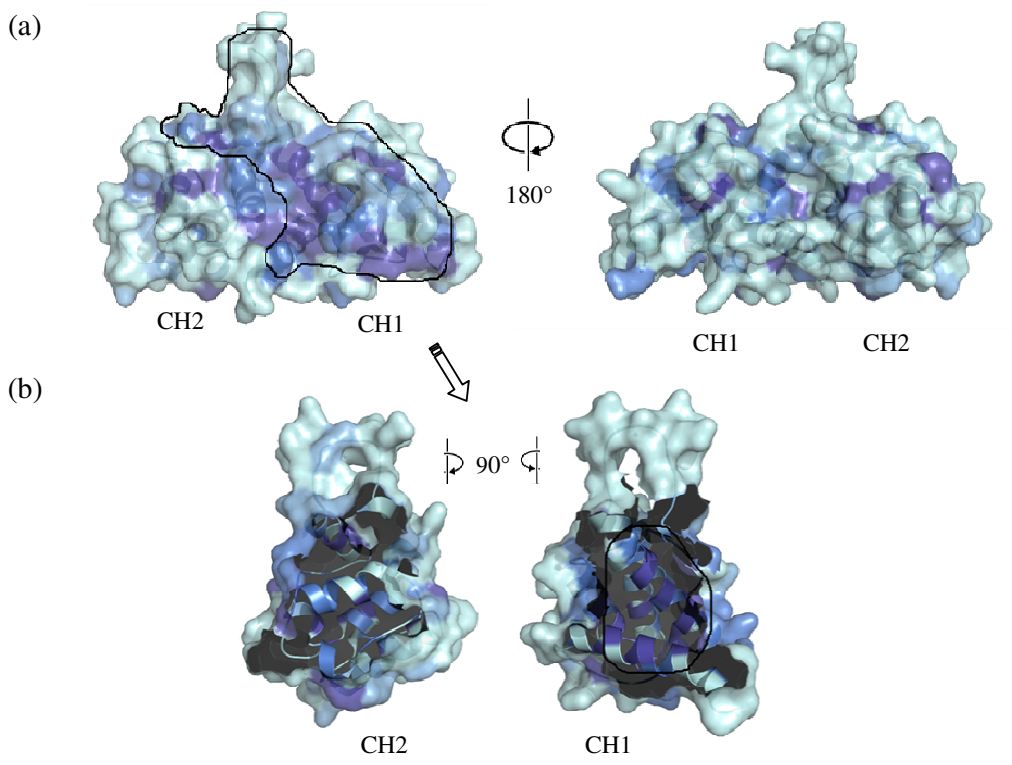

Figure 4-9. The Putative ABS of Filamin A is Comprised of Highly Conserved Residues.

a) The structure of the filamin A ABD, showing two sides of the molecular surface.

b) The interface of the CH1/CH2 domains.

Residues of the putative ABS are outlined with the black lines. Amino acids are coloured dark blue – absolutely conserved to light blue – not conserved.

The acidic loop connecting the CH1 and CH2 sub-domains, residues 155-164 (DEEEDE EAKK), is assumed to be disordered in the "A" monomer of the asymmetric unit, as there is insufficient density to model these residues. The acidic loop, which is ordered in monomer B (Figure 4-5), lies out from away from the core structure of the protein and there is sufficient density for the peptide backbone to be modelled; however, the side chain positions were not clear. As a result the backbone has been modelled, with the side chain occupancy set to zero.

The acidic loop connecting the CH1 and CH2 sub-domains was predicted by Nakamura *et al.* (2005) to lie over the putative CaM binding site (residues 50-60), binding in a basic pocket nearby (Figure 4-10). The basic pocket that was also described can be

identified in the electrostatic potential surface; however, the acidic loop does not lie over this basic pocket, and it would take a considerable structural rearrangement for this to take place.

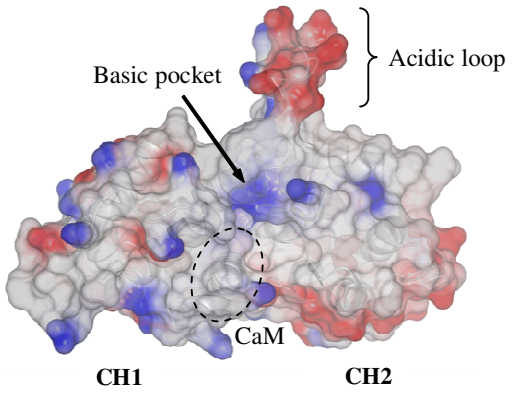

Figure 4-10. The Acidic Loop Does Not Block Access to the Putative Calmodulin Binding Site. The filamin A ABD is shown with the surface coloured by electrostatic potential. The putative CaM binding site (residues 50-60) is shown as a black oval, and located just above this is the pocket of basic residues predicted (Nakamura *et al*., 2005) and at the top is the acidic loop. The surface is coloured according to electrostatic potential, using a linear colour ramp with −0.5 V (red) to 0.5 V (blue).

Density equivalent to a phosphate or sulfate is present in both molecules in the asymmetric unit, and is located at the base of helix E' of CH2 near Thr223 and the N-H groups of Pro221 and Val222. Given this chemical environment and the observation that protein was purified and crystallised in buffers containing phosphate, this was determined to be the most likely molecule. However, it is possible that this is a SO_4 molecule which was present in the crystallisation mother liquor. These two molecules are indistinguishable by the electron density maps, or by chemical environment. Therefore this molecule will be referred to as a phosphate; however, it equally may be a sulphate.

Flanking these phosphate molecules are two highly acidic patches on the surface of the protein (Figure 4-11). This PO_4 binding site was inspected for suitability as a phosphotidylinositol 4,5-bisphosphate (PIP_2) binding site, as the PO_4 may mimic the

phosphates on the head of PIP_2. PIP_2 is an inositol lipid that binds to a variety of proteins and has a regulatory role in a number of signalling pathways. The primary PIP_2 binding site is thought to generally be a arginine/lysine-rich basic region (reviewed in Bella, 2005). Therefore this site where the PO_4 is bound is not a suitable PIP_2 binding site, given its highly acidic electrostatic potential (Figure 4-11).

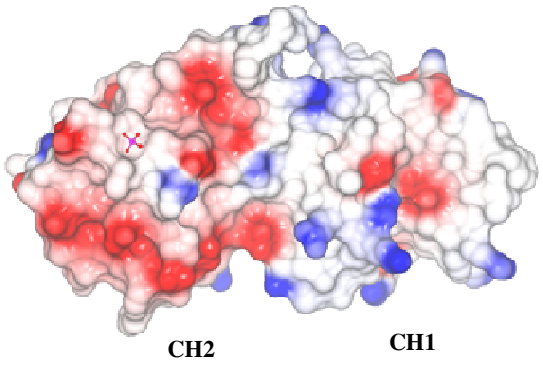

Figure 4-11. The Phosphate Binding Site on the Filamin A ABD Structure.
The surface coloured by electrostatic charge. Showing the phosphate binding site is flanked by two acid regions on the surface. The CH1 and CH2 domains are labelled. The phosphate molecule is shown as sticks bound in the CH2 domain. The surface is coloured according to charge, using a linear colour ramp with −0.5 V (red) to 0.5 V (blue).

In the dystrophin and α-actinin-3 ABD, PIP_2 binds near the ABS3 (Mejean *et al*. 1995; Fukami *et al*., 1996; Franzot *et al*., 2005). In α-actinin the site was predicted to be formed by a triad of arginine residues on the surface on the ABD; however, these residues are not conserved in the filamin A sequence (Figure 4-12). Upon further inspection of the surface no suitable PIP_2 binding sites were found.

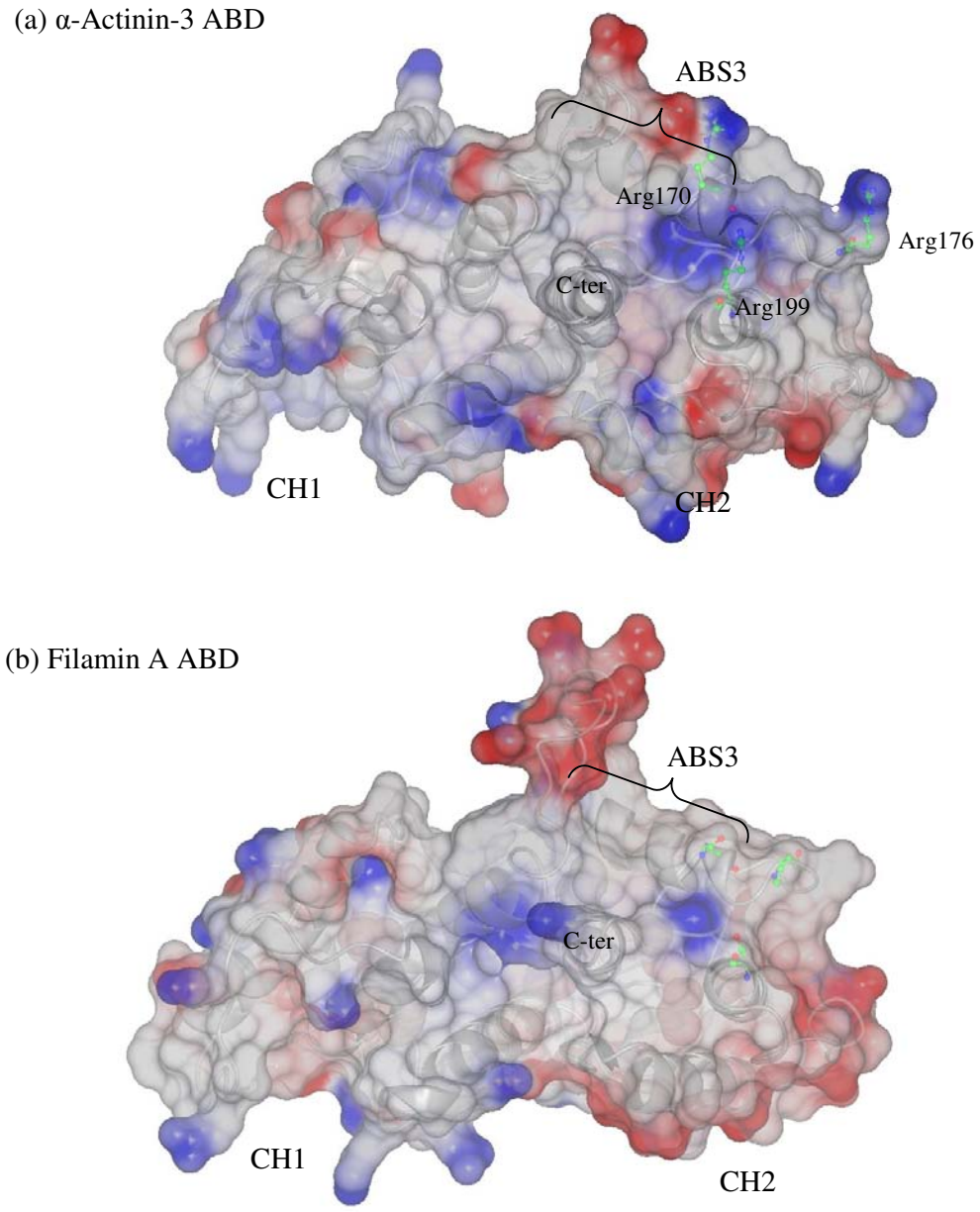

Figure 4-12. PIP_2 Binding Site Showing the Basic Triad of Arginines on the α-Actinin-3 Structure.
These putative PIP_2 binding arginine residues are not conserved in the filamin A sequence, and are also not conserved in the structure.

a) The α-actinin-3 ABD structure (1WKU). The putative PIP_2 binding site formed by residues Arg 170, 176 and 199, shown as green ball and sticks.
b) The filamin A ABD structure. The filamin A residues that are in equivalent positions (178, 181 and 204) to the three arginine in α-actinin, also shown as green ball and sticks.

The surface is coloured according to charge, using a linear colour ramp spanning −0.5 V (red) to 0.5 V (blue). The carboxyl terminus (C-ter) is shown and the helix of ABS3 is also labelled.

4.6 The Structure of E254K

To confirm that an amino acid change has occurred in a structure, an omit map was constructed. An omit map removes the potential model bias. If the density for the residue is observed in the difference map (F_o-F_c) after simulated annealing refinement, the density is real and unbiased (Bhat 1988). The omit map of the E254K of structure shows the amino acid substitution, from a Glu to a Lys (Figure 4-13). This was an important experiment, to confirm that this structure was not also the WT structure.

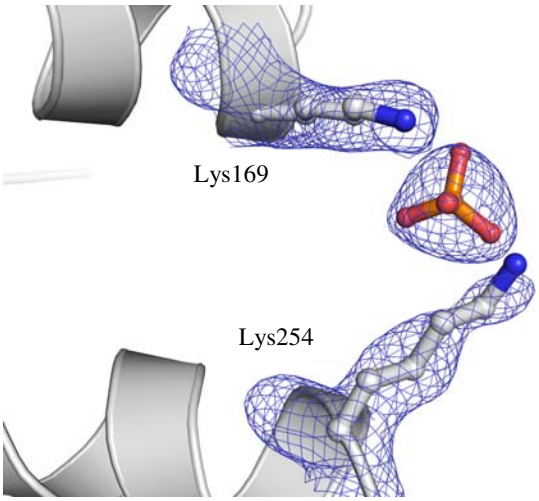

Figure 4-13. Omit Map of the Residue 254 to Confirm the Substitution E254K.
The maps were generated by simulated annealing and refinement (in PHENIX) against the initial model (from PHASER) with residues 253, 254 and 255 absent from the model. Residues are shown modelled into the density for clarity, and the phosphate is also shown (depicted in orange). The map shown is the $2F_o$-F_c map is contoured at 1.0σ.

4.7 A Comparison of the WT and E254K Structures

The salt bridge between E254 and K169 links ABS3 (residue 169) in helix A and helix G on the surface of the CH2 domain. The WT and E254K structures have an RMSD of 0.41 Å (over 222 Cα), showing very few structural changes occur to the overall structure.

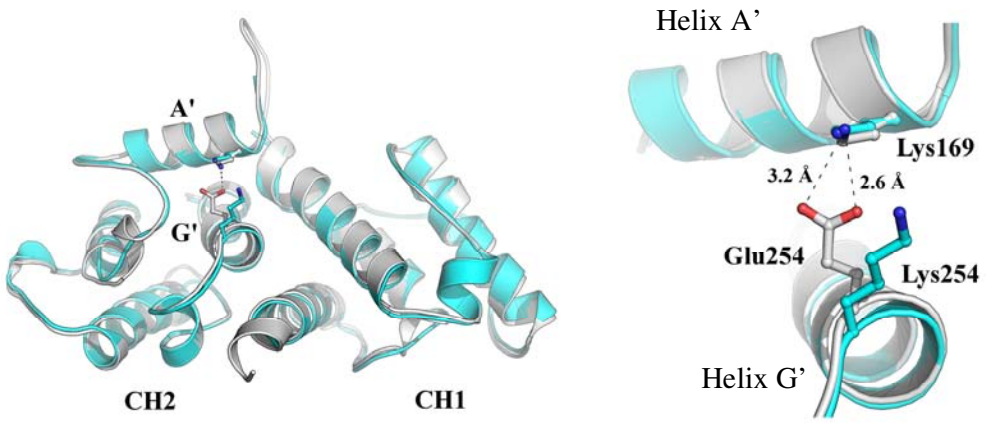

Figure 4-14. A Comparison of the WT Structure to the E254K.
The 222 C_α atoms were overlaid in COOT, the WT structure is shown in grey and the E254K structure in cyan. The salt bridge between E254 (in helix G') and K169 (in helix A') in the WT structure is shown with a dashed line. An insert (right) shows a close up view of the salt bridge.

When the structures are overlaid the C_α of residue 254 moves 0.96 Å, between the structures, and the C_α of the Lys169 moves 0.17 Å. The loop between the CH1 and CH2 domains (acidic loop) is disordered in both molecules of the asymmetric unit. However, despite these minor changes, there are no significant structural changes to the amino acids surrounding this region, and the two helices A and G (that this salt bridge links) remain the same. There is a phosphate/sulfate at the site of the amino acid change for one of the two molecules, perhaps to compensate the two adjacent positive charges from the lysine side chains (Figure 4-13). The region surrounding the site of the substitution changes chemically, becoming much more neutrally changed in the mutant structure (Figure 4-15). This is also seen in an α-actinin-4 structure (2R0O), with a pathogenic mutation, that is in the adjacent residue in filamin A (Lee *et al*., 2008).

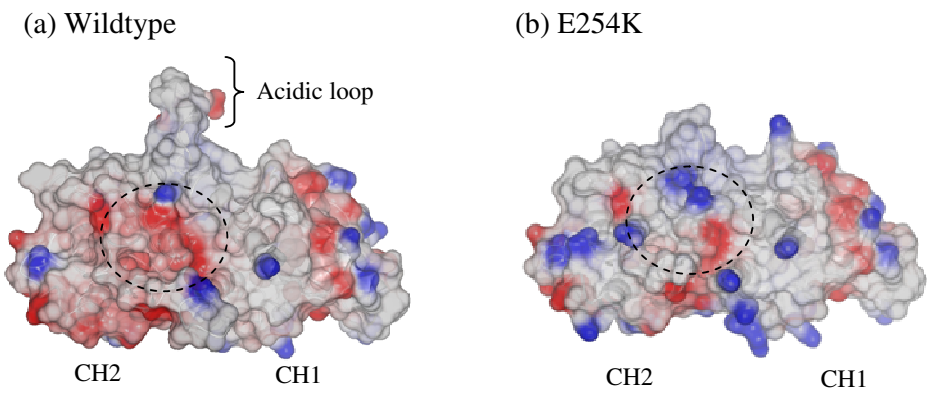

Figure 4-15. Electrostatic Potential Surface Analysis.
The mutation E254K changes the electrostatic potential of the surface of the protein, with the loss of an acidic patch (circled). The surface is coloured according to charge, using a linear colour ramp with -0.5 V (red) to 0.5 V (blue).

4.7.1 The Importance of the Salt Bridge between E254 and K169

Salt bridges do not tend to be conserved unless they are important for a particular function (Barlow and Thornton, 1983), and this salt bridge is conserved across the ABD (Figure 1-10). In filamin B E227K (the equivalent mutation to filamin A E254K) results in Larsen syndrome (Krakow *et al.*, 2004; Bicknell *et al.*, 2007). Given that the polarity of this interaction is reversed in both utrophin and dystrophin, it seems more likely that this is a structural element rather than a binding surface (Borrego-Diaz *et al.*, 2006). There is no equivalent interaction between helix A and helix G for CH1.

(a) A Conserved salt bridge

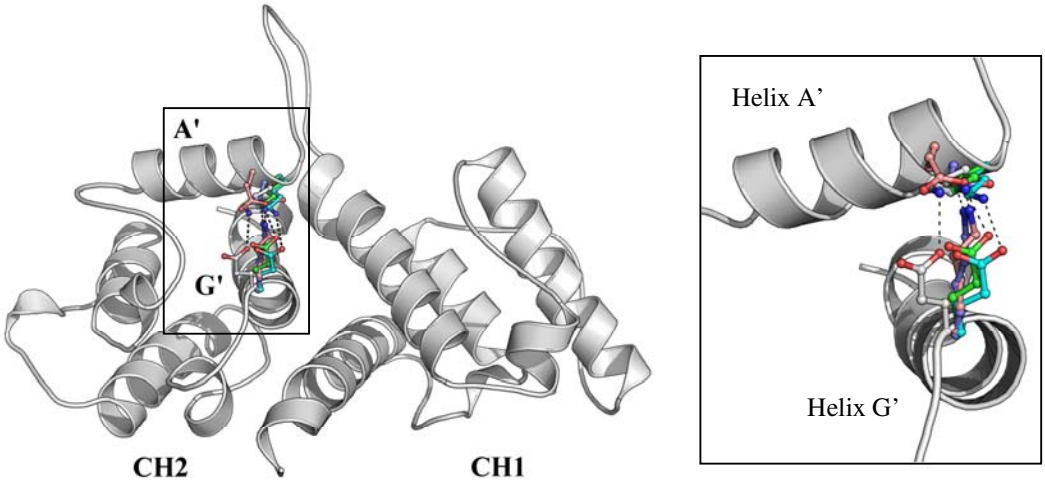

(b) Conservation

(c) The ABS

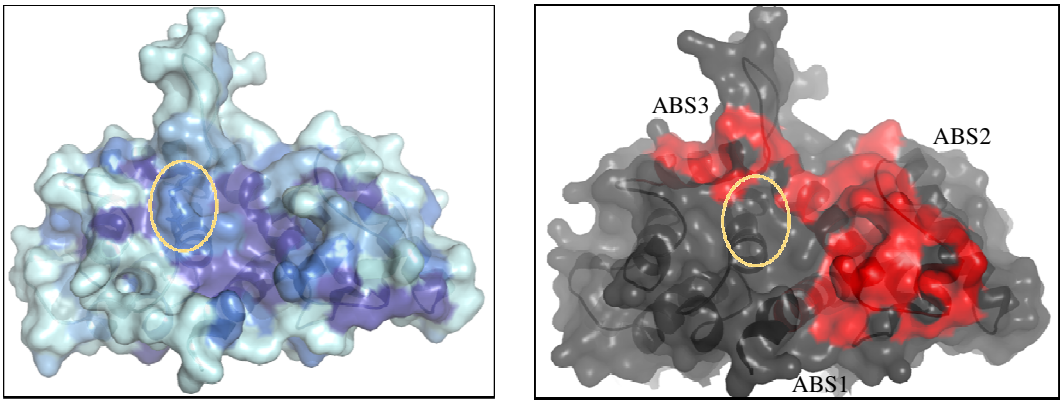

Figure 4-16. A Conserved Salt Bridge Shown on the WT Filamin A ABD Structure.

This salt bridge is a conserved feature in the ABD, and lies in a pocket of conserved residues near the ABS. All structures are shown in approximately the same orientation.

a) An overlay of the entire ABD from a number of human actin binding proteins; the filamin ABD structure is shown. This shows the conservation of the salt bridge. The residues of the saltbridge are shown as sticks. Grey: Filamin A. Cyan: Spectrin. Green: Actinin. Purple: Dystrophin. Pink: Utrophin. The two helices linked by the salt bridge are labelled A' and G'.

b) The WT filamin A ABD, coloured by amino acid conservation: Least conserved residues are coloured light blue, with the most conserved residues coloured dark blue. The location of the salt bridge is indicated by a yellow circle.

c) The WT filamin A ABD with the putative actin binding surfaces coloured red. The location of the salt bridge is indicated by a yellow circle.

4.8 The Filamin A ABD A200S Structure

The omit map was essential to confirm that the amino acid change had taken place, given the similar size of these two amino acids. Also contributing to the uncertainty was the resolution of the structure – as 3 Å makes it difficult to distinguish the difference between a Ser and an Ala in the $2F_o$-F_c map. This omit map of the filamin A ABD A200S confirms the amino acid substitution has occurred (Figure 4-17).

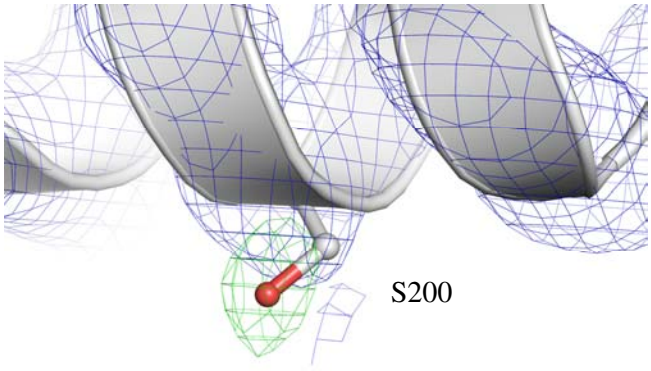

Figure 4-17. Omit Map of Residue 200, Confirming the A200S Substitution.
The maps were generated following simulated annealing refinement (in PHENIX) against the initial model generated from PHASER, A200S with an Ala modelled at position 200. The $2F_o$-F_c map contoured to 1.5σ and the F_o-F_c (difference map) is scaled to 3.5σ. The peak in the difference map shown here is a 5σ peak.

When the 215 C_α atoms of the WT and A200S structures are overlaid the overall rmsd is 0.3 Å. There are no observable structural changes, and within the helix in which the A200 is located there are only some very minor changes in the position of the C_α atoms (Figure 4-18a-b). However, given the low resolution of this structure (3.0 Å) these changes are within the error range of the resolution. The more significant changes occur in the surrounding residues sidechains of Leu180 and Leu183 to accommodate the larger Ser residue (Figure 4-18c). However, from a purely structural point of view it is unclear why these subtle structural changes are causing disease.

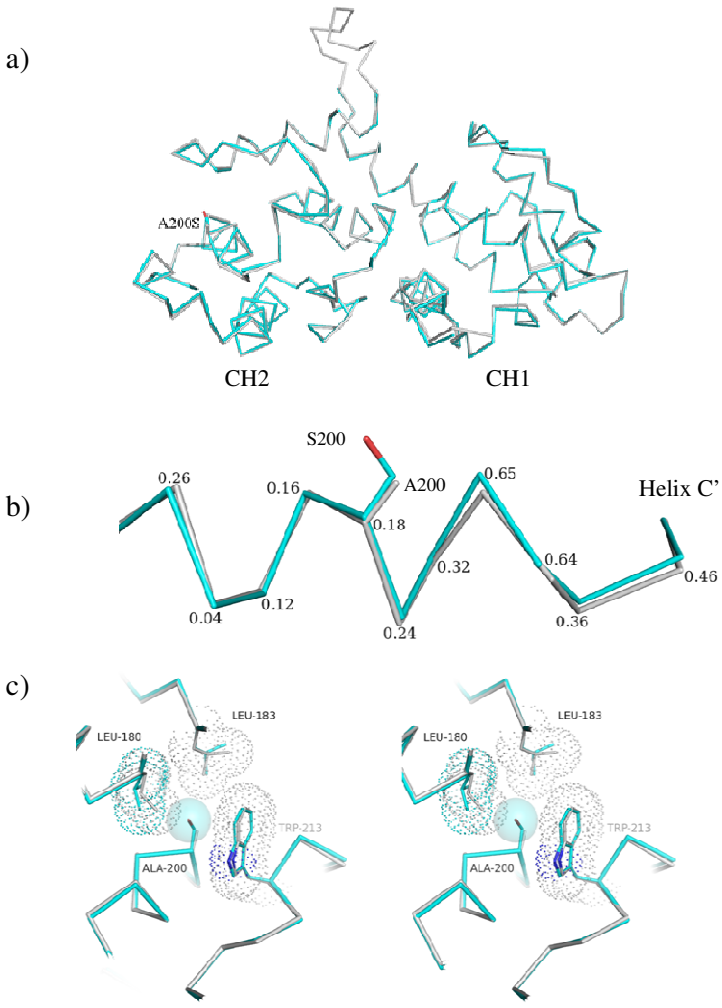

Figure 4-18. An Overlay of the WT and A200S Filamin A ABD Structures.

The 221 Cα atoms of the backbone of the two structures were overlaid in COOT; the resulting overlaid structures are shown in a-c. The WT structure is shown in grey and the A200S is shown in cyan.

a) The C_α trace of the overall structure is shown here. A200 and S200 are represented as sticks.

b) A close up of the C' helix (CH2) from the overlay shown in 'a'. The amino acid substitution A200S is depicted, and the change in position of the C_α atoms is listed (in Å) alongside the C_α atoms.

c) The site of the substitution in shown in stereo. The van der Walls radii of the surrounding residues are shown as dots, of the same colour as the sticks of the residue. The VDW radius of the serine OHγ side chain is shown as a cyan sphere. The changes in the surrounding amino-acid side-chain positions are shown.

4.9 The WT Filamin A ABD Structure – Insights into Disease Associated Mutations

Solving the structure of the WT ABD of filamin A has provided us with some insight into the disease associated mutations that cluster in the ABD. The residues that are associated with pathogenic mutations are mapped to the WT ABD structure (Figure 4-19). The mutations associated with PVNH all map to the CH1 domain, with mutations associated with the OPD and FMD disorders mapping to CH2 (Figure 4-19).

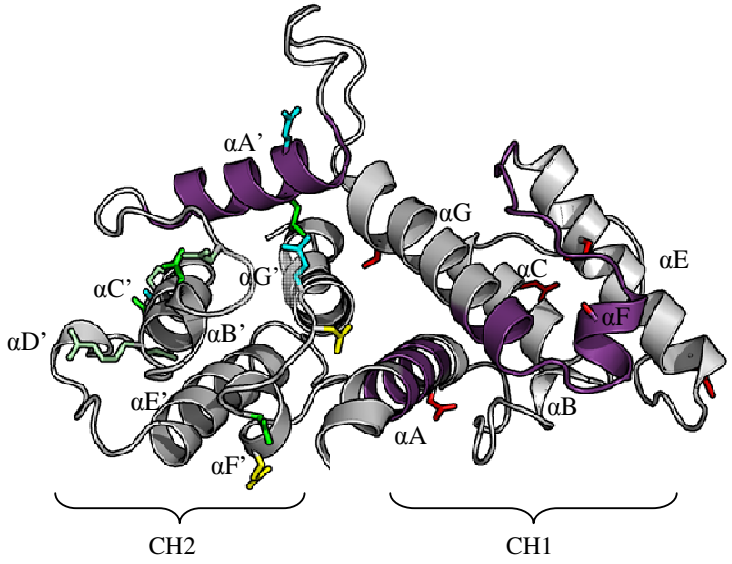

Figure 4-19. The Structure of the WT Filamin A ABD with Pathogenic Mutations Mapped onto it. Residues are coloured by the associated disease. Cyan is OPD2, green is OPD1, yellow is FMD and red is PVNH. The two calponin homology (CH) domains and the helices are labelled. The ABS residues are coloured purple.

4.9.1 PVNH Associated Amino Acid Substitutions

The PVNH disorder is the loss of function phenotype, typically associated with a complete absence of filamin A. The PVNH associated mutations in the CH1 domain of the ABD highlight the importance of the function of this domain. The substitution M28K (unpublished results – Robertson pers. Comm.) is in the N terminal residues that are presumed to be disordered, so predictions about the basis of the disease associated mutation are not possible. The substitutions N54I and N54Y (unpublished results – Robertson pers. Comm.) would both break two hydrogen bond interactions between the

N54 side chain and the backbone of residues I64 and R63 in the helix A of ABS1 and the following loop that connects helix A and B (Figure 4-20a).

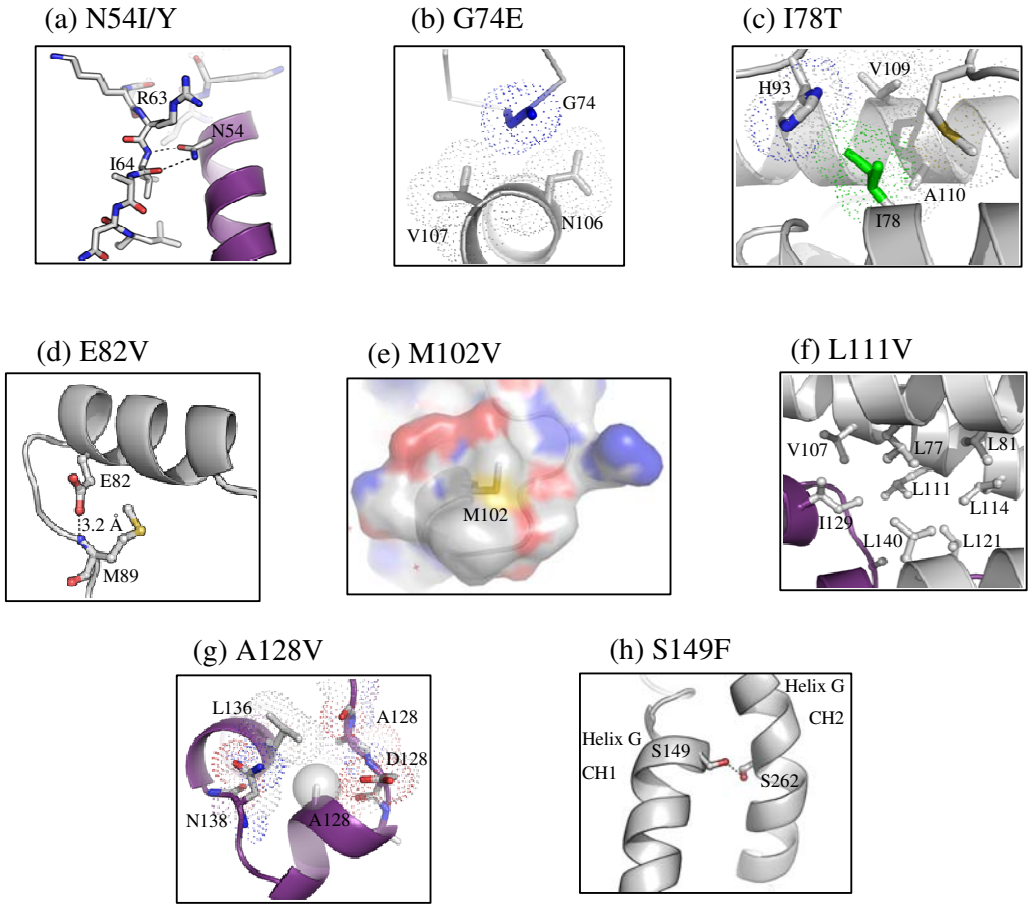

Figure 4-20. The WT Structure Showing the Sites of PVNH Associated Mutations.

The images a) to h) are labelled with the pathogenic mutation associated with the residue.

Dots or transparent spheres, where shown, indicate the VDW radii of the atoms. The C_α backbone of the ABS residues is coloured purple. Salt bridges and H-bonds are shown as black dashes.

The mutation G74E is in a loop between helices B and C. This mutation would be expected to disrupt the packing, as this loop lies adjacent to V107 and N106 in helix E. The substitution of Gly by the bulkier Glu would result in a steric clash, disrupting the packing of this loop (Figure 4-20b). The mutation I78T results in the slightly smaller and polar residue, Thr (Figure 4-20c), introducing a cavity that may disrupt this hydrophobic pocket. The E82V mutation (Moro *et al.*, 2002) would result in the loss of

a hydrogen bond between the side chain of E82 and the backbone nitrogen of M89 (Figure 4-20d). The residue E82 is absolutely conserved across the ABDs (Figure 1-10). It is interesting to note that the E82V mutant was cloned and expressed in this work, however it was largely insoluble when expressed in *E.coli.* The mutation M102V results in a change to a surface residue; however, it is not clear why this is pathogenic (Figure 4-20e). The mutation L111V is a conservative amino acid change. This residue lies in a hydrophobic pocket formed, in part, by residues from ABS2 (Figure 4-20f). The Val is one CH_2 shorter, and it seems most likely that the substitution introduces a cavity in this large hydrophobic pocket, which may destabilise the structure. The amino acid substitution A128V (Gomez-Garre *et al*., 2006) occurs in helix F within ABS2. The Val could result in a steric clash, as the A128 sits in a small pocket in close proximity to helix G (Figure 4-20g). This mutation is associated with the Ehlers-Danlos variant of PVNH; however, it is not known if the Ehlers-Danlos phenotype is due to an additional mutation in an unknown gene. The mutation S149F disrupts a hydrogen bond between helix G of CH1 (Ser149) and helix G' of CH2 (Ser262). The substitution A39G (Sheen *et al*., 2005) is also associated with the Ehlers-Danlos variant of PVNH. The residues from residue 2 – 39 are assumed to be disordered in the WT filamin A ABD structure and so a structural analysis is not possible. It is, however, interesting to note that both these residues (A128 and A39) that are associated with this Ehlers-Danlos variant of PVNH are conserved within the filamins but not in the ABD of other proteins. These observations are summarised in Table 4-2.

Mutation	Disease	Location	Reference	Putative structural consequences	Conservation
A39G	PVNH/EDS	N termini	Sheen, 2005		Only in filamins
N54I/Y	PVNH	Helix A	Robertson, pers. com.	Loss of two hydrogen bonds	Absolutely
G74E	PVNH	Loop B-C	Robertson, pers. com.	Steric clash	Absolutely
I78T	PVNH	Helix C	Robertson, pers. com.	Introduction of a cavity	Non polar
E82V	PVNH	Helix C	Moro, 2002	Loss of a hydrogen bond	Absolutely
M102V	PVNH	Helix E	Guerrini, 2004	Surface residue - unclear	Only in filamins
L111V	PVNH	Helix E	Robertson, pers. com.	Introduction of a cavity	Leu/Ile
A128V	PVNH/EDS	Helix F	Gomez-Garre, 2006	Steric clash	Only in filamins
S149F	PVNH	Helix G	Guerrini, 2004	Loss of a hydrogen bond	Only in filamins

Table 4-2. A Summary of PVNH Mutations.

The putative structural consequences are shown and the amino acid conservation across ABDs from α-actinin, β-spectrin, utrophin, and dystrophin is listed. The associated disease is listed for each pathogenic mutation; periventricular heterotopia (PVNH) and Ehlers-Danlos syndrome (EDS). A number of these pathogenic mutations were provided by a collaborator Stephen Robertson (University of Otago), and the data are yet to be published.

A point mutation, L54R, in the CH1 domain of the dystrophin ABD results in lower levels of dystrophin *in vivo*, resulting in the Duchenne muscular dystrophy (DMD) (Prior *et al*., 1993). DMD disease is, like PVNH, associated with the complete loss of functional protein. A similar underlying mechanism may occur in filamin A and PVNH, particularly with respect to the three filamin A mutations (G74E, I78T and E82V) in close proximity to the equivalent residue in filamin A (L81). At least three of these mutations would be predicted to affect the actin binding regions of the protein, suggesting an alternative basis behind these PVNH mutations, although these are not conflicting hypothesises. The CH1 domain is known to be critical in the actin binding activity of the ABD (Way *et al*., 1992). Studies of the CH domains in the dystrophin ABD showed that the CH1 domain (containing ABS1 and 2) binds to actin, but the CH2 (containing ABS3) does not, indicating that CH1 is the major contributor to the actin binding surface (Winder *et al*., 1997).

4.9.2 OPD Associated Amino Acid Substitutions in the X-linked Filamin A ABD

4.9.2.1 The CH2 Structure and OPD Disorders

OPD-spectrum disorders are split into the more severe disorder OPD2 and the less severe OPD1. All the ABD mutations associated with OPD disease are in the CH2 domain, but are distributed throughout the CH2 domain, and are both surface and buried residues. There is no clear pattern that could be discerned from simply the amino acid position in the CH2 domain. The mutations R196W and P207L can result in either OPD1 or OPD2 in patients. This suggests that they may also be additional factors contributing to the severity of the disease, and therefore the clinical diagnosis of either OPD1 or OPD2. The disease is less severe in heterozygous females. Skewing of X-inactivation that favours the expression of the non-mutant allele is strongly correlated with the severity of the diagnosis (Robertson *et al*., 2003).

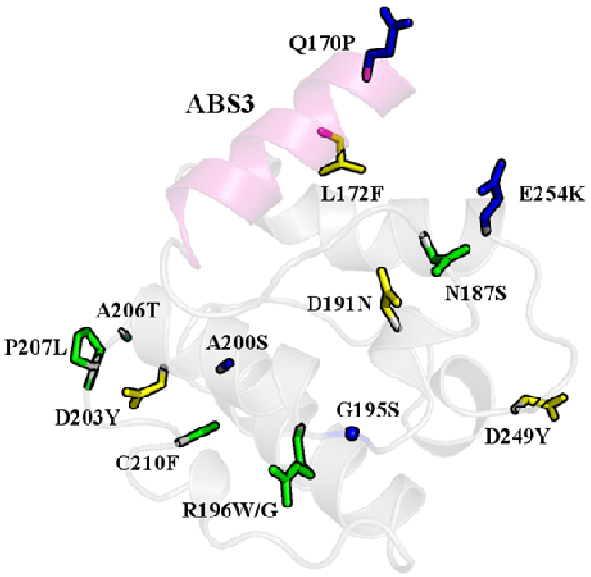

Figure 4-21. The CH2 Domain of the Filamin A WT ABD Showing the Residues that are Associated with Pathogenic OPD Mutations.

The residues are shown as sticks are coloured by the associated disease. Yellow denotes OPD1 and blue denotes OPD2. Green denotes that either the OPD type was not specified by the clinician, or the mutations can be associated with either OPD1 or OPD2. The ABS3 residues are shown in pink.

4.9.2.2 OPD2 Associated Amino Acid Substitutions

The Arg 196 is not absolutely conserved (see alignment Figure 1-10); however, at this position there is a large basic residue in all filamins, Arg in filamin A and Lys in filamin B and C. At residue R196 two different amino acid changes are each associated with two different disease phenotypes. The R196 makes a hydrogen bond with the backbone carbonyl group of Trp216 (Figure 4-22a). When the Arg is replaced by a Gly the disease associated is OPD2; however, when the Arg is substituted for Trp this is, in some patients, associated with the milder phenotype OPD1. This suggests that the Trp is, in part, able to recover some function that is lost when the substitution is Gly. This also illustrates an interesting relationship between OPD1 and OPD2. These diseases are most likely resulting from a disruption of the same cellular/molecular function – and are simply a milder (OPD1) and more severe (OPD2) form of the same phenotype. OPD1 in boys results in some mild skeletal anomalies, but often goes undiagnosed in females. Boys with OPD2 have disabling skeletal anomalies, and are often unable to survive past infancy (reviewed in Robertson *et al*., 2005).

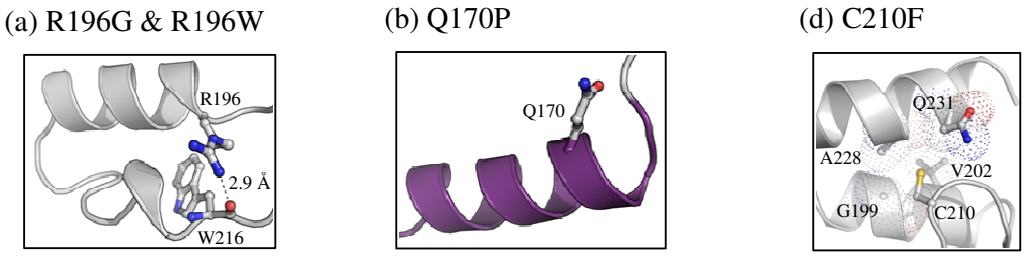

Figure 4-22. The WT Structure Showing Three Mutations Associated with OPD2.
The images a) to c) are labelled with the pathogenic mutation associated with the residue shown. In a) the residue at position 196 has two different reported disease associated mutations.
Dots, where shown, indicate the VDW radii of the atoms. The ABS residues are coloured purple and H-bonds are indicated by black dashes.

The mutation Q170P introduces a proline into a helix in the putative ABS, this amino acid change could disrupt or bend the helix causing it to terminate prematurely (Figure 4-22b). The amino acid proline cannot form a regular α-helix structure due to the steric

hindrance from its side chain and also the cyclic side chain also blocks the main chain N atom preventing it forming a hydrogen bond. The Q170 is conserved in the filamin family, however it is not conserved in other ABDs (see alignment page 31). The mutation C210F would be expected to cause a steric clash with residues surrounding the 210 position (Figure 4-22c). The residue C210 is only conserved in filamins, and there is no conservation in the other ABDs.

The residue G195 is in a tight turn between helices B and C (Figure 4-23). Gly has the largest conformational flexibility of all the amino acids and the Phi and Psi angles of G195 in this structure are 90°/-1° (in chain A) and 81°/-9° (in chain B). These angles can not be formed by Ser. The role of this Gly is absolutely conserved across the ABDs.

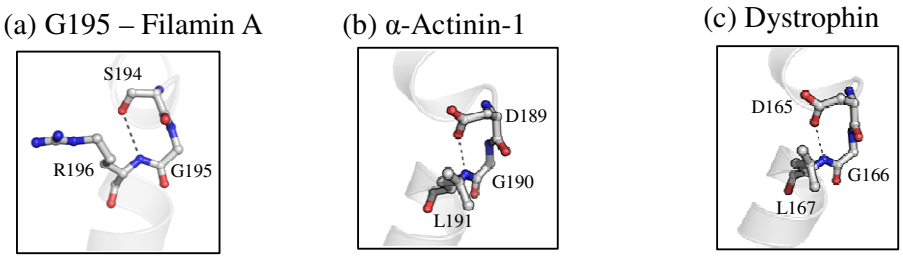

Figure 4-23. G195 Forms a Conserved Turn.

The mutation G195S Associated with OPD2. The images a) to c) are labelled with the ABD that the structure is from. The hydrogen bonds are indicated by black dashes.

4.9.2.3 OPD1 Associated Amino Acid Substitutions

The L172F mutation would result in a steric clash, as there is not enough room for the bulky Phe sidechain (Figure 4-24a). The substitution D191N disrupts a turn in the backbone (Figure 4-24b). D191 makes two H-bonds with the side chain and the backbone nitrogens of N187, with lengths of 2.9 Å and 2.8 Å respectively. To create a tight turn that loops back to ABS3. The D203 substitution also disrupts a turn (Figure 4-24c). D203 also forms turn by forming an H-bond (3.2 Å long) with the backbone nitrogen of L209. P207 forms a tight turn to end a helix, and the Leu may not provide

the rigidity required (Figure 4-24d). This mutation also introduces a surface exposed Leu.

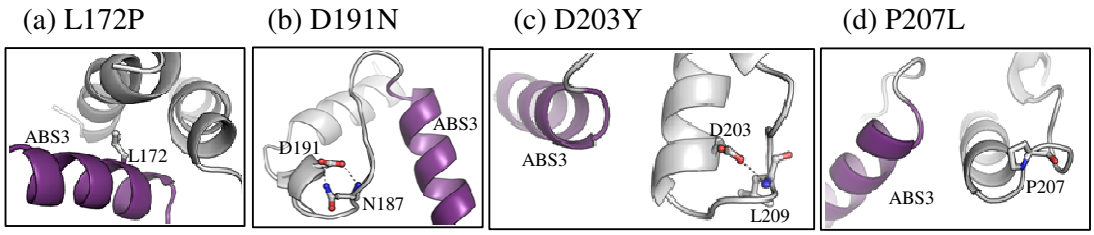

Figure 4-24. The WT Structure Showing the Mutations Associated with OPD1.

The images a) to d) are labelled with the pathogenic mutation associated with the residue shown.

The ABS residues are coloured purple, with hydrogen bonds and salt bridges are indicated by black dashes.

4.9.2.4 FMD Associated Amino Acid Substitutions

There are two reported mutations D253E and E245K (Robertson pers. Comm.) that are associated with FMD; these both involve highly conserved residues located in CH2 near the CH1/CH2 interface (Figure 4-25).

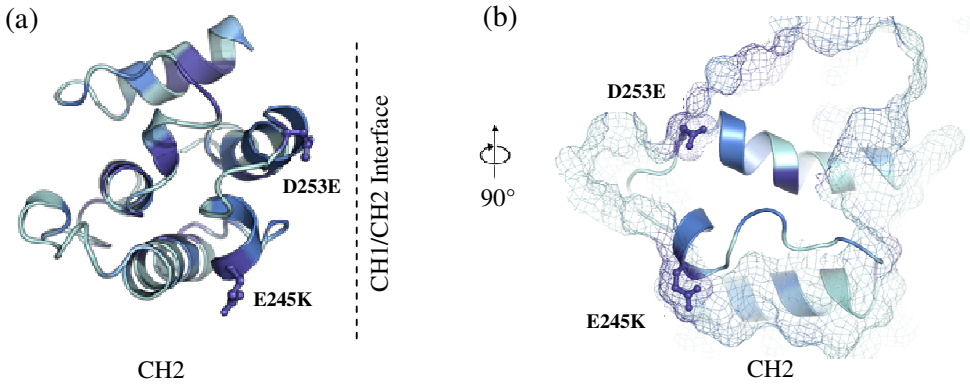

Figure 4-25. FMD Associated Mutations are Located at the CH1/CH2 Interface.

This figure shows location of the two surface residues which, when mutated (D253E and E245K), are associated with FMD.

a) Both these highly conserved residues are on the surface of the ABD, but also near the CH1/CH2 interface.

b) These residues are shown in a view (rotated 90° from a) looking from the CH1 domain – down the interface at CH2.

Residues are coloured by amino acid conservation with light blue = not conserved to dark blue = absolutely conserved. In b) the surface is shown as a mesh.

The D253E is a relatively conservative amino acid substitution, as both amino acids are negatively charged. The D253 forms a hydrogen bond to Q45 linking the CH1 and CH2 domains. The Glu sidechain is only one carbon longer than the Asp; however, the length of this residue is important, presumably to form the hydrogen bond that links two helices from CH1 and CH2 (Figure 4-26a). This residue is on the surface of the ABD, and so the larger residue would not be expected to interrupt the internal packing – which may be expected with residues within the protein. The E245K swaps a negatively charged residue (Glu) for a positively charged residue Lys. Both these residues are conserved and on the surface of the ABD. The E245 residue is absolutely conserved across all ABDs, and it links helix F with helix E in CH2; however, the salt bridge it forms in filamin A is not conserved.

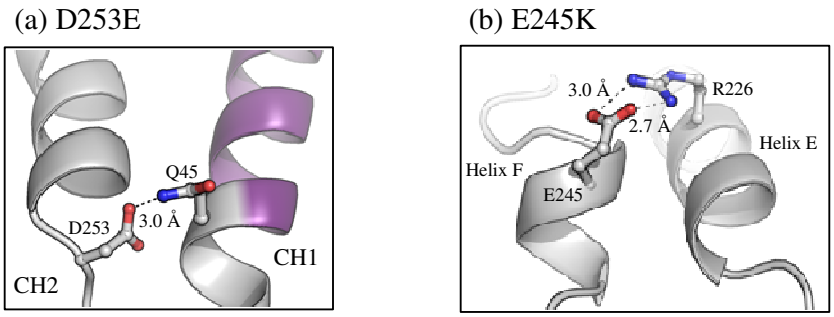

Figure 4-26. The WT Structure Showing Two Mutations Associated with FMD.
The images a) and b) are labelled with the pathogenic mutation associated with the residue shown. The ABS residues are coloured purple, and hydrogen bonds and salt bridges are indicated by black dashes.

In α-actinin a pathogenic mutation (K255E) results in kidney disease. This residue is located in the CH1/CH2 interface, and structural studies of the mutant protein revealed that it retains the compact ABD structure (Weins *et al.*, 2007; Lee *et al.*, 2008). However, the mutation in α-actinin is accompanied by an increase in actin affinity. It is conceivable that these filamin A mutations D253E and E245K result in similar molecular consequences to this α-actinin mutation.

4.10 Comparing and Contrasting the Three Structures

The E254K and A200S are both associated with OPD2, so an analysis of these structures may provide insight into structural changes, found in both mutant structures, which may be associated with OPD2. When the 222 Cα atoms are overlaid there are very few structural differences that are common to both mutations (Figure 4-27).

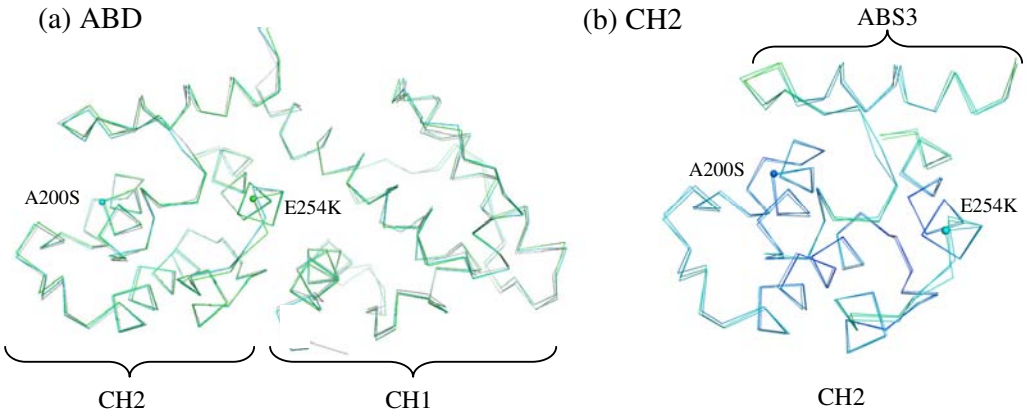

Figure 4-27. Overlay of Three Structures.

Comparing the WT structure to the E254K and A200S, mutations both associated with OPD2.

a) An overlay of the 222 C_α of the three structures. WT is shown in grey, A200S in cyan and the E254K in green.

b) A close up of the overlay, showing the CH2 domain coloured by *B*-factor. From dark blue = low *B*-factor to yellow = higher *B*-factor.

The two pathogenic mutation sites are shown as spheres.

4.11 Summary

This chapter described the crystallographic studies of WT filamin A ABD and two mutant forms of this domain associated with the disease OPD2. The WT filamin A ABD has the typical ABD fold, with two CH domains arranged in a compact monomeric globular fold. The WT ABD structure is a resource for studies to understand the actin binding mechanism and disease associated point mutations that cluster in this domain.

The two mutant forms of the ABD associated with OPD2 (E254K and A200S), reveal largely unchanged structures, with only subtle and localised structural changes. As predicted, the E254K breaks a conserved salt bridge; however, there were very little other structural changes in the protein. The A200S causes a steric clash, displacing the side chains of the surrounding amino acids; however, the C_α chain of the surrounding helices remains unaffected. The reason these two amino acid changes are associated with a severe disease like OPD2 remains unclear from these structural studies.

The OPD2, FMD and OPD1 associated mutations cluster in the CH2 domain of the wildtype structure. The OPD1 associated mutations localise to amino acids 172-207, which is near ABS3. The FMD associated mutations are two conserved surface residues located at the CH1/CH2 interface, one of which forms a link between the CH1 and CH2 domains.

The PVNH associated mutations cluster in the CH1 domain. This is a loss of function disease associated with the absence of filamin A. A number of these mutations are in or near the ABS residues. However, these PVNH associated residues are also in a similar region of the domain to a mutation in dystrophin which causes instability and the loss of dystrophin protein in cells. Therefore, given these two observations, it seems likely that these mutations typically reduce or abolish either the activity of the actin binding domain or the filamin A protein level in cells.

5 *In Vitro* Studies of the Recombinant Actin Binding Domain from Filamin A

5.1 Introduction

This chapter details biochemical studies to characterise the WT filamin A ABD. The mutation E254K is associated with the disease OPD2, which is a gain/altered function phenotype and these biochemical studies were aimed at improving our understanding of the ABD and the molecular basis of OPD2. In order to study the ABD activity, actin co-sedimentation assays were performed. Changes in actin affinity of filamin A may alter the function of this cytoskeletal protein. Studies of the secondary structure of the WT and disease associated mutant proteins was determined by circular dichroism. A comparison of the stability of the WT and E254K was done using both differential scanning fluorimetry and circular dichroism. These two techniques measure the thermostability of the proteins in two slightly different ways. The differential scanning fluorescence followed the loss of structure, by the exposure of hydrophobic regions of the proteins. The circular dichroism follows the changes in secondary structure.

5.2 Actin Binding Assays

The F-actin affinity was determined by an actin co-sedimentation assay. The polymerised actin is mixed with the actin binding protein of interest and the polymeric actin is pelleted (with any associated protein) by high speed centrifugation. The pellet and supernatant fractions are then separated and run on a SDS PAGE, and the bands quantified by densitometry (see methods section 2.30). Thus the K_d of proteins can be determined by determining the percentage of actin binding protein in the pellet fraction when different concentrations of actin binding protein are added to the assay (Figure 5-1). A standard curve was constructed to confirm the linearity of the Coomassie stain with the WT filamin A ABD within the range used in the assay (see appendix 9.2).

Protein	K_d (μM)	ABD (Residues)	Stoichiometry (mol/mol)	Reference
Filamin A	48	2-269	1:1	This work
Filamin A	17.3	2-278	1:1	Nakamura *et al*., 2005
Filamin B	7.0	2-242	1:1	Sawyer *et al*., 2009
α-Actinin	31.7	1-271	1:1	Weins *et al*., 2007
Dystrophin	44	1-246	1:1	Way *et al*., 1992
Utrophin	67	1-261	1:1	Keep *et al*., 1999
Plectin	22.3	59-293	1:1	Garcia-Alvarez *et al*., 2003

Table 5-1. The Actin Affinity of the ABD of Human Actin Binding Proteins.

The binding stoichiometry between actin:ABD mol/mol is shown. The actin affinity of the filamin A ABD residues 2-269 is consistent with other ABDs.

The wildtype ABD bound to F-actin with a dissociation constant (K_d) of 48 ± 11 μM and the E254K ABD bound with a K_d of 13 ± 5 μM, under the conditions of this assay. The data were fitted to a single binding site saturation curve: $Y = B_{max}$ x $X \div (K_d + X)$. The R^2 for each of the data sets was 0.95 for the WT and 0.81 for the E254K, indicating that these are both statistically valid fits. There is some variability seen in the F-actin:ABD stoichiometry, it is expected to be 1:1 (mol/mol) for the WT. The calculated F-actin:ABD (mol/mol) stoichiometry was 1:1.6 for WT and 1:1.3 for E254K. This variability is consistent with assays with other ABD binding domains (such as dystrophin) – and can be largely attributed to the limitations/errors of the assay, and non specific interactions at higher protein concentrations (Sutherland-Smith *et al*., 2003). At the higher ABD protein concentrations (60-100 μM) more may be pelleting non-specifically. The WT would be more susceptible to this due to the higher protein concentrations required for binding saturation. This K_d also differs from the filamin A ABD literature value reported in 2005; 17.3 μM (Nakamura *et al.,* 2005) (Table 5-1). The construct used in this work was 268 amino acids (residues 2-269) and the construct used by Nakamura *et al*., (2005) was 9 residues longer (residues 2-278). This was due to different predictions of the boundaries of the ABD. In this work pSMART predicted the ABD includes amino acids up to 264 and pFAM predicts the ABD ends at 269. Both these constructs of the ABD were separately cloned into the expression vector (pers. com. Andrew Sutherland-Smith); however, the 2-269 construct expressed more soluble recombinant protein in *E. coli* which is the reason that this construct (2-269) was chosen to study in this work.

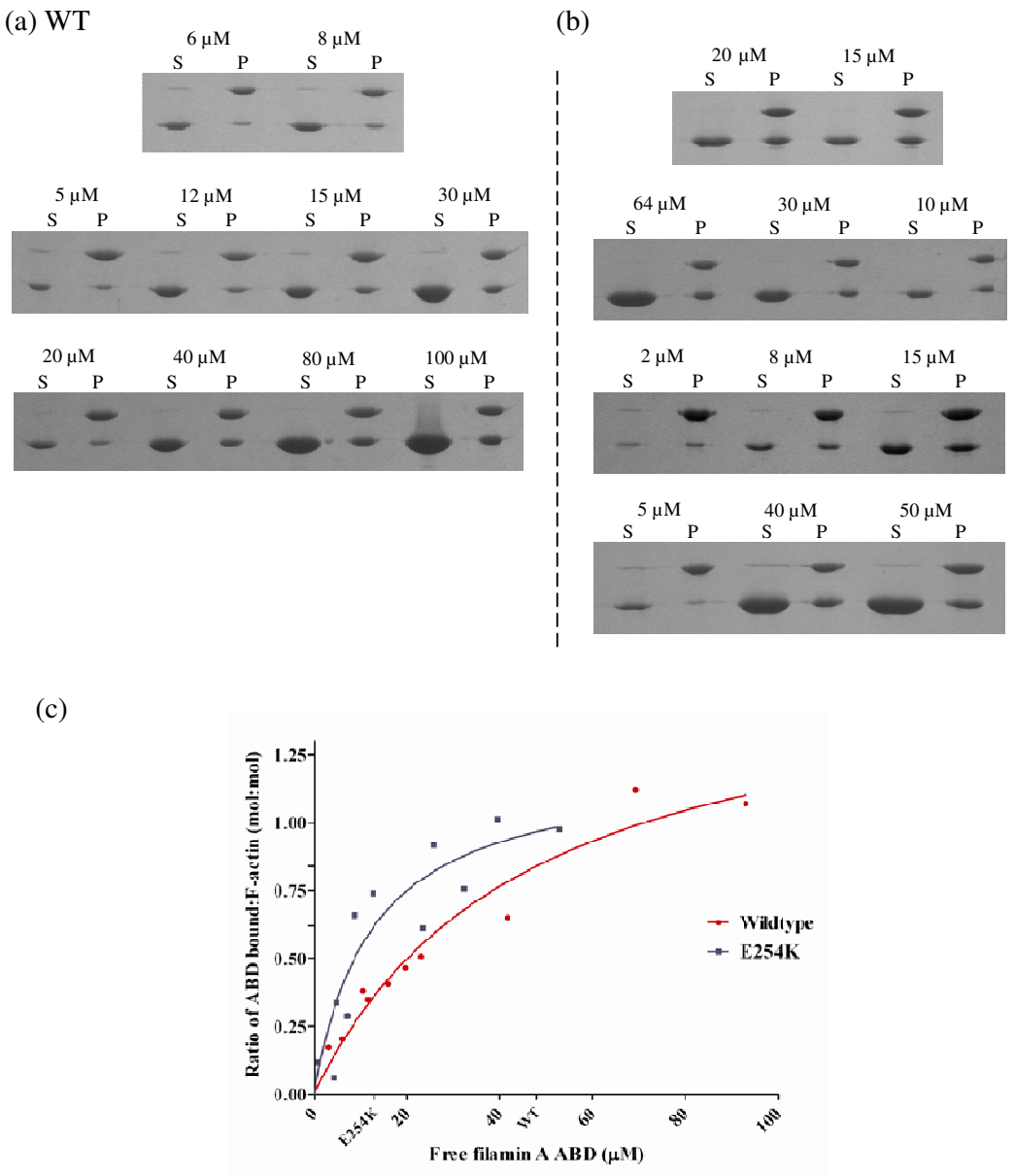

Figure 5-1. Actin Co-Sedimentation Assays.

a) The WT raw data. SDS PAGE gels*

b) The E254K data. SDS PAGE gels*

c) Densitometry of SDS PAGE (above) was graphed; the K_d of each protein is indicated on the *x* axis; WT= 48 µM and the E254K=13 µM.

*The soluble fraction (S), and and pellet fraction (P), the total ABD concentration is shown. In each SDS PAGE the top band is actin (42 kDa) and the lower band is the filamin A ABD (30 kDa).

Each curve on the graph was fitted by GraphPad using non linear regression.

The E254K ABD (2-269) bound to F-actin with a significantly higher affinity (K_d of 13 ± 5 µM) under the same assay conditions; this is a 3.6 fold increase when compared to

the wildtype affinity. The disease associated with this mutation is consistent with a gain in or altered function. These results also agree with studies on filamin B and α-actinin-4, where the disease associated gain of function mutations also result in an increased affinity for actin (Sawyer *et al*., 2009; Lee *et al*., 2008).

5.3 The Effect of PIP_2 on the Actin Affinity of the Filamin A ABD

Phosphatidylinositol 4,5-bisphosphate (PIP_2) is an inositol lipid that binds to a variety of proteins and has a regulatory role in a number of signalling pathways (reviewed in Bella, 2005) (also see structural studies in Figure 4-12). PIP_2 inhibits the actin-filamin interaction in both actin gels formed by native smooth muscle filamin crosslinking and in co-sedimentation assays (Furuhashi *et al*., 1992). Mejean *et al*. (1995) investigated PIP_2 interaction with dystrophin, and showed that the PIP_2 site was in the ABD. The ABD of α-actinin also contains a putative PIP_2 binding site (Fukami *et al*., 1996; Franzot *et al*., 2005). Therefore it seemed possible that filamin A may also be regulated through an interaction with PIP_2 at the N-terminal ABD. In this work the actin co-sedimentation assays of Furuhashi *et al*. (1992) were repeated with PIP_2 at concentrations that had shown significant inhibition (with the full length protein), but with recombinant ABD in place of the native full length protein. These experiments aimed to determine the difference between WT and E254K with respect to PIP_2 inhibition. These actin binding assays with filamin A ABD and PIP_2 showed no change in the actin affinity (Figure 5-2).

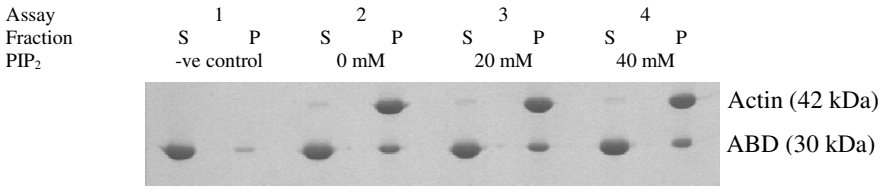

Figure 5-2. PIP_2 Does not Inhibit the Actin:ABD Interaction.

Four assays are shown on this SDS PAGE. The soluble fraction (S) and the pellet fraction (P) are loaded for each assay. In assay one (negative control) the filamin A ABD is assayed in the absence of actin, assays 2, 3 and 4 all contain 8.8 µM actin. Assays with 0 mM, 20 mM and 40 mM PIP_2 show no change in the filamin A ABD co-sedimentation. All assays contain 10 µM filamin A ABD.

The recombinant filamin A ABD:actin interaction, under the conditions in this assay, is not inhibited by PIP_2. There are a number of possible reasons for this result. The PIP_2 inhibition may only occur with native and/or full length filamin A. However, this does not rule out the PIP_2 binding site being in the ABD. It is possible that the PIP_2 interacts with the ABD of filamin A but requires the protein to be full length for inhibition. In vinculin PIP_2 binds and activates the actin binding activity; however, the PIP_2 must then be hydrolysed to promote actin binding (Fukami *et al*., 1994). Given that filamin A co-localises with SHIP-2, a phosphatidylinositol 3 kinase, processing of the PIP_2 may be required to inhibit filamin A (Dyson *et al*., 2001). As the assays showing inhibition were with native protein it is possible that this protein was either co-purified with an additional factor (such as a SHIP-2) or that the native ABD is modified is some way that the recombinant ABD is not. However, it can be concluded that, under the conditions in this assay, PIP_2 does not significantly inhibit the actin:filamin A ABD interaction.

5.4 The Effect of Calmodulin on the Actin Affinity of the Filamin A ABD

In 2005 Nakamura *et al*. showed that the filamin:actin interaction was disrupted by the presence of holo-calmodulin. The authors proposed that, like actinin and dystrophin, the camodulin (CaM) binding site of filamin may be in the ABD. There is no strict consensus amino acid sequence for CaM binding; however, several different binding motifs have been recognised based on factors such as alpha-helical propensity, residue weight, residue charge, hydrophobic residue content, helical class and the occurrence of certain residues (Afshar *et al*., 1994). Proteins may also have more than one CaM-binding domain. These criteria mean that determining a CaM binding site is not straight forward from sequence anaylsis. When the filamin A sequence is submitted to the CaM binding database (http://calcium.uhnres.utoronto.ca/ctdb/ctdb/home.html) a binding site in the C-terminal region, within the dimerisation domain is predicted comprised of residues: SRLYSVSYLLKDKGEY. A less likely binding site is predicted in the ABD (LEFLDRESIK LVSIDSKAIV DGNLKLI); however, this is not the hypothesised binding site described by Nakamura *et al.* (2005).

In this work actin co-sedimentation assays were performed with the addition of apo and holo human and bovine CaM (see methods 2.31) to investigate whether the E254K mutation affected CaM regulation of filamin A binding (Nakamura *et al*., 2005). Due to the low levels of filamin (0.1 µM), and the vast excess of CaM required to see an effect (800 fold excess), a western blot was used to visualise the filamin A. The blot was then analysed by densitometry using Quantity One® software (Biorad). In the work of Nakamura *et al.* (2005) filamin A ABD was tagged with GST and detected by antibodies to GST. No antibodies to the filamin A ABD were available. Therefore, the His tag was not removed and anti-His antibodies were used to detect the ABD. The His tag is a much smaller immunodetection tag than GST and would be expected to interfere less with any protein-protein interactions.

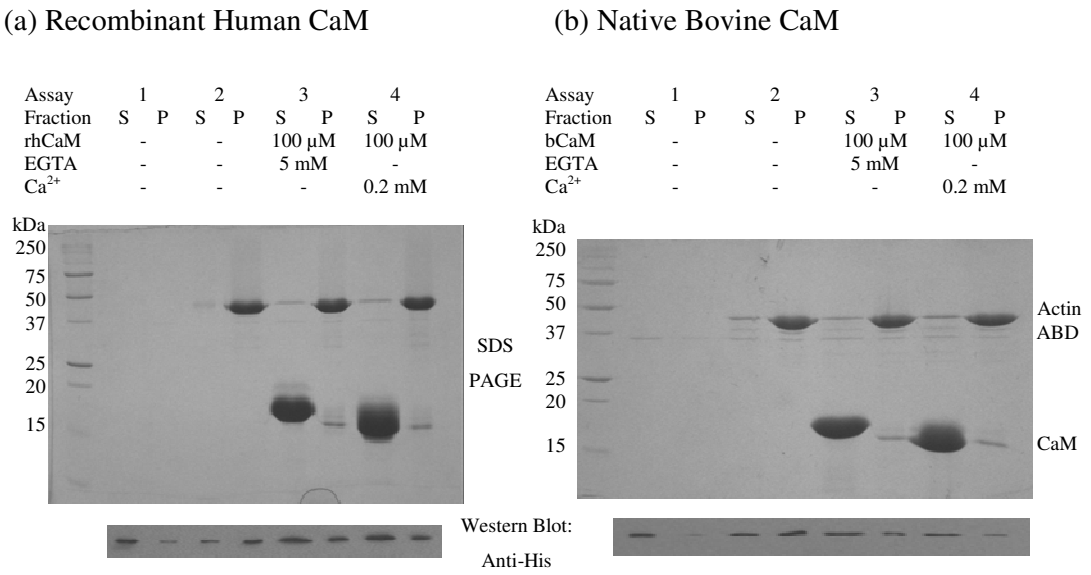

Figure 5-3. Calmodulin as an Inhibitor of the Filamin Actin Interaction.

The contents of the assay are shown in the table with the corresponding SDS PAGE below and the subsequent western blot of the SDS PAGE is shown at the bottom of this figure.

a) In this assay recombinant human calmodulin was used.

b) In this assay native bovine calmodulin was used.

0.1 µM of His tagged ABD (30 kDa) was added to all assays and detected by a western blot with anti-His antibodies; this blot is shown below each gel. Assays are shown as the soluble (S) and pellet (P) fraction. To all assays except assay one (the negative control) 8.8 µM actin (42 kDa) was added. The assay and subsequent blot was done in triplicate for each calmodulin (11 kDa) source, human/bovine, and typical results are shown.

The assay was visualised on SDS PAGE to confirm that the actin in the pellet of each assay was consistent, and the actin was evenly pelleted in each assay (Figure 5-3). The SDS PAGE also showed the typical shift of CaM in the presence/absence of Ca^{2+} (Burgess *et al*., 1980). The activity of the recombinant CaM was confirmed as active by testing the Ca^{2+} specific affinity of the CaM for a known CaM binding peptide immobilised on resin (Greg Sawyer, pers. Com.). The even transfer of the proteins from the SDS PAGE onto the membrane was confirmed using Ponceau stain of the membrane, to visualise the actin bands (other proteins were not visible). No difference in the percentage of filamin A ABD was detected in the pellet of the assay with Ca^{2+} as was observed in previous work (Nakamura *et al.,* 2005). However on inspection of the western blot the bands of filamin A ABD appear much broader in the assays containing CaM. This is most likely due to the high concentration of protein in these lanes on the SDS PAGE. To negate any errors caused by this difference, the assay with CaM and EGTA can be compared with the assay containing CaM and Ca^{2+}, and there is no difference in the filamin A ABD pellet. This assay was repeated in triplicate with constant results each time. The assay was also repeated with bovine CaM (Sigma), with the same results (Figure 5-3).

This indicates that, under the conditions of this assay, holocalmodulin does not inhibit the actin:filamin A ABD interaction. Given these results, this work was not continued with the filamin A ABD E254K mutant. These results were also consistent with results seen with the filamin B ABD (Sawyer *et al*., 2009).

5.5 Stability Studies

One obvious difference between the WT and E254K is removal of a conserved salt bridge between two helices (A' and G') in CH2. As this salt bridge may contribute to the structural stability of the protein, therefore it seemed logical to compare and contrast the stability of these proteins. Two techniques were utilised, differential scanning fluorometry and circular dichroism, to investigate the stability in two slightly different ways.

5.5.1 Differential Scanning Fluorometry

The sypro orange dye is a dye that specifically fluoresces when in a hydrophobic environment, such as the interior of proteins (Yeh *et al*., 2006; Niesen *et al.,* 2007). The protein of interest in buffer and dye is heated in a thermocycler while measuring the fluorescence, and as the protein unfolds the hydrophobic interior is exposed causing an increase in fluorescence (see methods 2.32). This technique enabled a comparison of the WT filamin A ABD with the E254K filamin A ABD. The melts were performed in triplicate, and the T_m (point of inflection of the curve) of each protein was determined by the Rotogene600 software (Figure 5-4). A cut off value of 1.1 for the first derivative of the fluorescence signal eliminated background peaks and gave a melting point for each protein. Lysozyme (at 10 mg/mL) was used as a standard as it is expected to melt at 74.8 °C, as determined by CD and sypro orange melts (Knubovets *et al*., 1999). The results shown here agree well with this value (Figure 5-4).

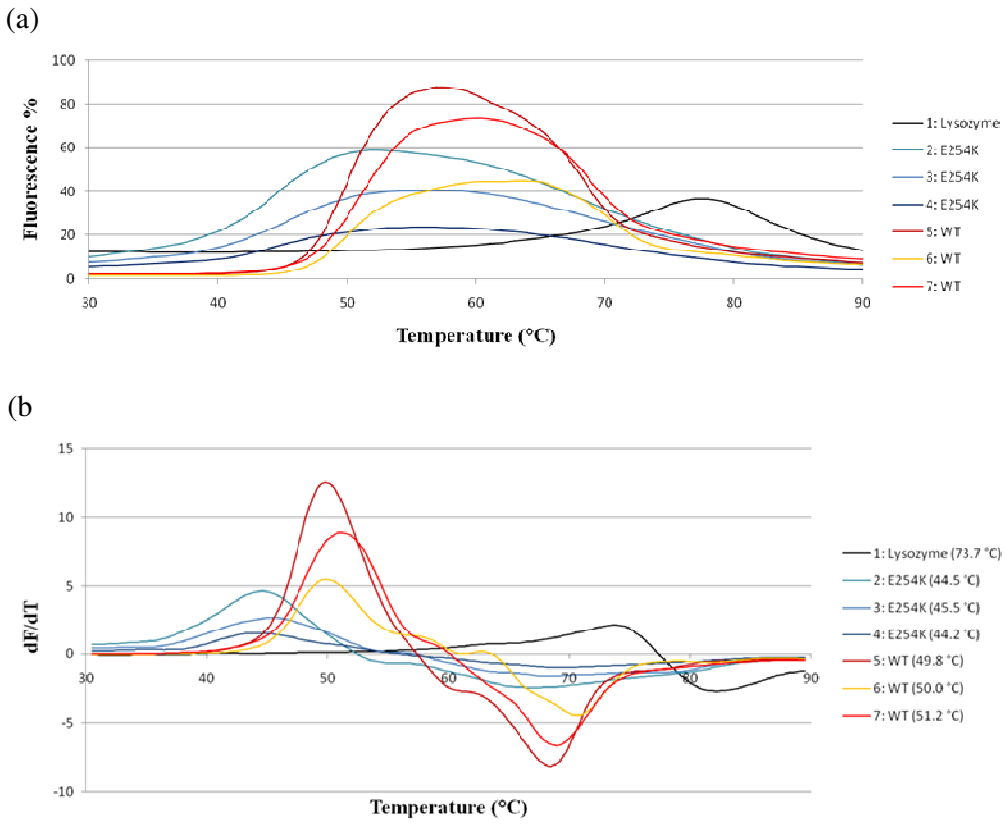

Figure 5-4. Differential Scanning Fluorometry Studies of the Filamin A ABD.

a) Graph of the fluorescence signal with respect to temperature. The fluorescence is expressed relative to the fluorescence value set as 100%.

b) Graph of the first derivative of the florescence melting curves. The calculated T_m of each protein is shown in the key in parenthesis.

The WT ABD T_m is 50.3 ± 0.8 °C (± standard deviation) is a more thermostable protein than the E254K with a T_m = 45.7 ± 0.7 °C. The melting curve shows that the E254K fluorescence peak starts earlier (37-39 °C) than the WT (43-45 °C) (Figure 5-4a) and the florescence lasts for a longer temperature range reaching a plateau at approximately the same temperature as the WT (75-80 °C). This also corresponds to (on average) a lower fluorescence maxima, although there is considerable florescence maximum signal variability, even between samples of the same protein at the same concentration. The signal variability in this assay is consistent with previous literature (Lavinder *et al.*, 2009). Despite this variation in the signal intensity the T_m of each protein is very reproducible, resulting in a clear distinction between the melting curves of these two proteins (Figure 5-4). The structural difference between these two proteins is one salt

bridge between helix A' and G'. The difference between the WT (50.3 °C) and the E254K (44.7 °C) T_m is 5.6 °C. However, due to irreversibility of the melts, the free energy change can not be determined, but this value is consistent with literature reports of changes in stability of proteins upon the loss of a salt bridge (reviewed in Bosshard *et al*., 2004). The energy of a salt bridge depends largely on the environment in which it is found. Those on the interior of proteins have a different energy of formation to those on the exterior, where they are exposed to the solvent. The energy contribution that a salt bridge has to a protein structure is not possible to predict, it is determined by changes in both entropy and enthalpy (Barlow and Thornton, 1983). As a rough estimate the range of the energy is about 5-10 kcal.mol^{-1} (Fersht, 1972; Perutz and Raidt, 1975).

5.5.2 Circular Dichroism

Circular dichroism spectroscopy measures the difference in the absorption of left-handed circularly polarised light and right-handed circularly polarised light (Johnson, 1990). Proteins contain different chiral chromophores (light-absorbing groups), with the most prevalent chiral chromophore being the peptide bond. Changes in light absorption, due to the orientation of the peptide bond, provides information about the secondary structure of the protein in solution. The recombinant ABD from filamin A was studied by circular dichroism to analyse the solution structure of the WT compared to the E254K, and also to compare the temperature stability followed by changes in secondary structure (Kelly *et al*., 2005).

5.5.2.1 Structural Studies by Circular Dichroism Spectroscopy

Each spectrum was measured from 180 nm to 260 nm, with proteins at a concentration of 1.7 mg/mL in CD buffer (20 mM K_2HPO_4/KH_2PO_4, 20 mM NaCl, 1 mM DTT). To determine the secondary structure of the WT and E254K, spectra were recorded with a 1 nm bandwidth and a 2.5 sec per time point (see methods section 2.33). Each spectra was collected 10 times, blanked against the buffer, and the blanked traces averaged and smoothed using the Chirascan software (AppliedPhotophysics). The resulting traces from the WT and E254K measured at 4 °C and were compared and contrasted (Figure 5-5).

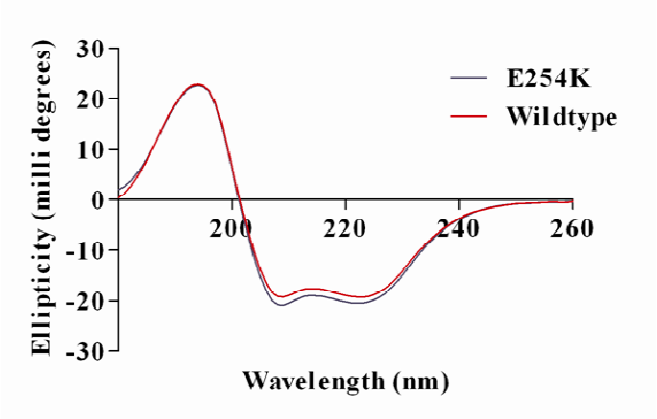

Figure 5-5. Circular Dichroism Spectra Comparing the WT and E254K ABD.
The ellipticity of the signal is plotted against the wavelength at which it was measured. The spectra of both samples were taken at 4 °C.

The cdnn software was used to predict the secondary structure of each protein (Bohm *et al*., 1994). This software compares the spectra of the test protein to the spectra of proteins where the structure is known (Andrade *et al*., 1993). The data from the CD structural analysis was compared to the structure determined by x-ray crystallography (Table 5-2). There is a small difference between the predicted helices for CD and the helices in the X-ray structures; however, CD structural predictions are rudimentary and this difference is within the error range expected (Kelly *et al*., 2005). These data also show that there is no significant difference in the CD spectra between the wildtype and E254K proteins (Table 5-2). When the sample is heated to 90 °C the helical content is reduced, and this is reduction is accompanied by an increase in the percentage of random coil.

Technique	Helical content		Random coil	
	WT (%)	**E254K (%)**	**WT (%)**	**E254K (%)**
X-ray	47	47		
Circular Dichroism (4 °C)	37 (97)	38 (95)	29	27
Circular Dichroism (90 °C)	23 (114)	24 (112)	36	35

Table 5-2. A Structural Analysis of the WT and E254K by Circular Dichroism Spectroscopy.
A comparison of the X-ray and circular dichroism data. The CD spectra were measured over 180 – 260 nm at 4 °C and 90 °C and the predicted secondary structure (helical and random coil) determined by cdnn software. Shown in parenthesis is the total of all secondary structural features predicted by cdnn.

5.5.2.2 Circular Dichroism Thermostability Studies

The temperature stability (T_m) was determined for each protein by scanning the protein over a range of increasing temperatures. As with the 4 °C experiments, the data was also collected with a 1 nm bandwidth and a 2.5 sec per time point. The curvette was heated from 5 °C to 90 °C in 5° steps with a 1 min equilibration before each spectra was recorded (Figure 5-7). After the melt, the temperature was dropped back to 4 °C and the spectrum was remeasured. This spectrum was the same as the spectrum at the end of the melt (taken at 90 °C), indicating the melting process was irreversible. Therefore the energy difference between the two states, was not able to be calculated (Johnson, 1990).

The thermostability of the WT compared to the E254K was measured by following the loss in secondary structure (at 222 nm) with increasing temperature. This wavelength is plotted against the temperature, showing the loss of secondary structure as the protein is denatured (Figure 5-7). The 222 nm wavelength chosen is a strong α-helical signal, with no buffer interference. While the protein is largely denatured at 90 °C, some secondary structure remains (see Table 5-2).

(a) WT

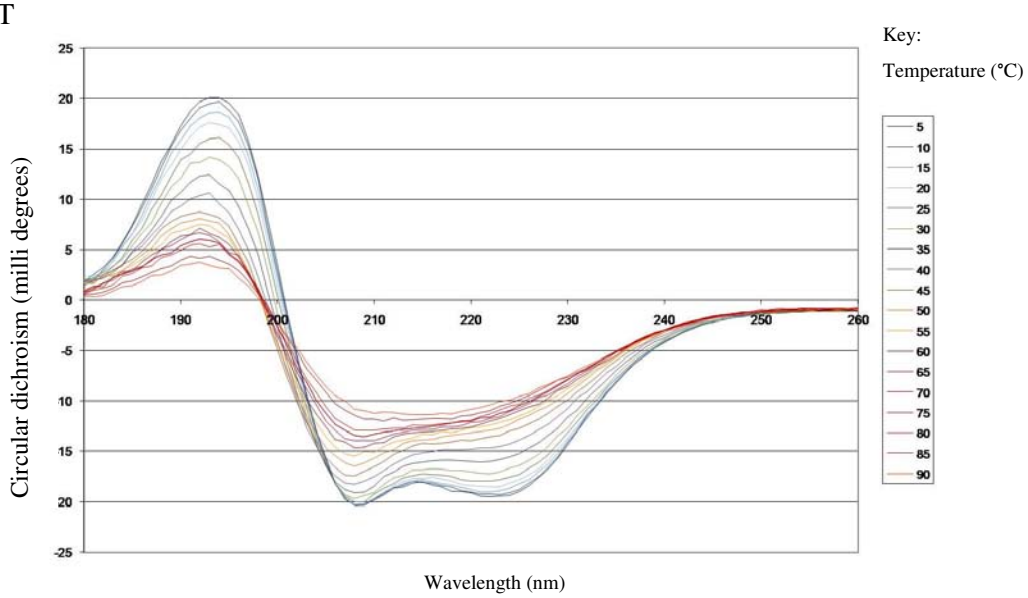

(b) E254K

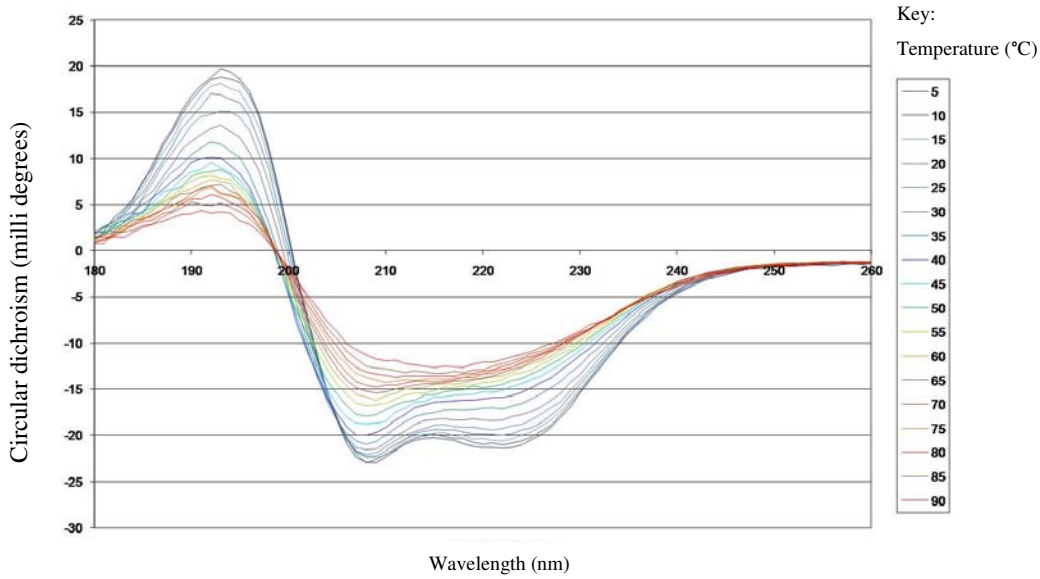

Figure 5-6. Thermostability as Measured by Circular Dichroism.

The spectra between 180 and 240 nm of protein at 5 - 90 °C, showing changes in the secondary structure signal (circular dichroism).

a) Spectra from WT protein

b) Specta from E254K protein

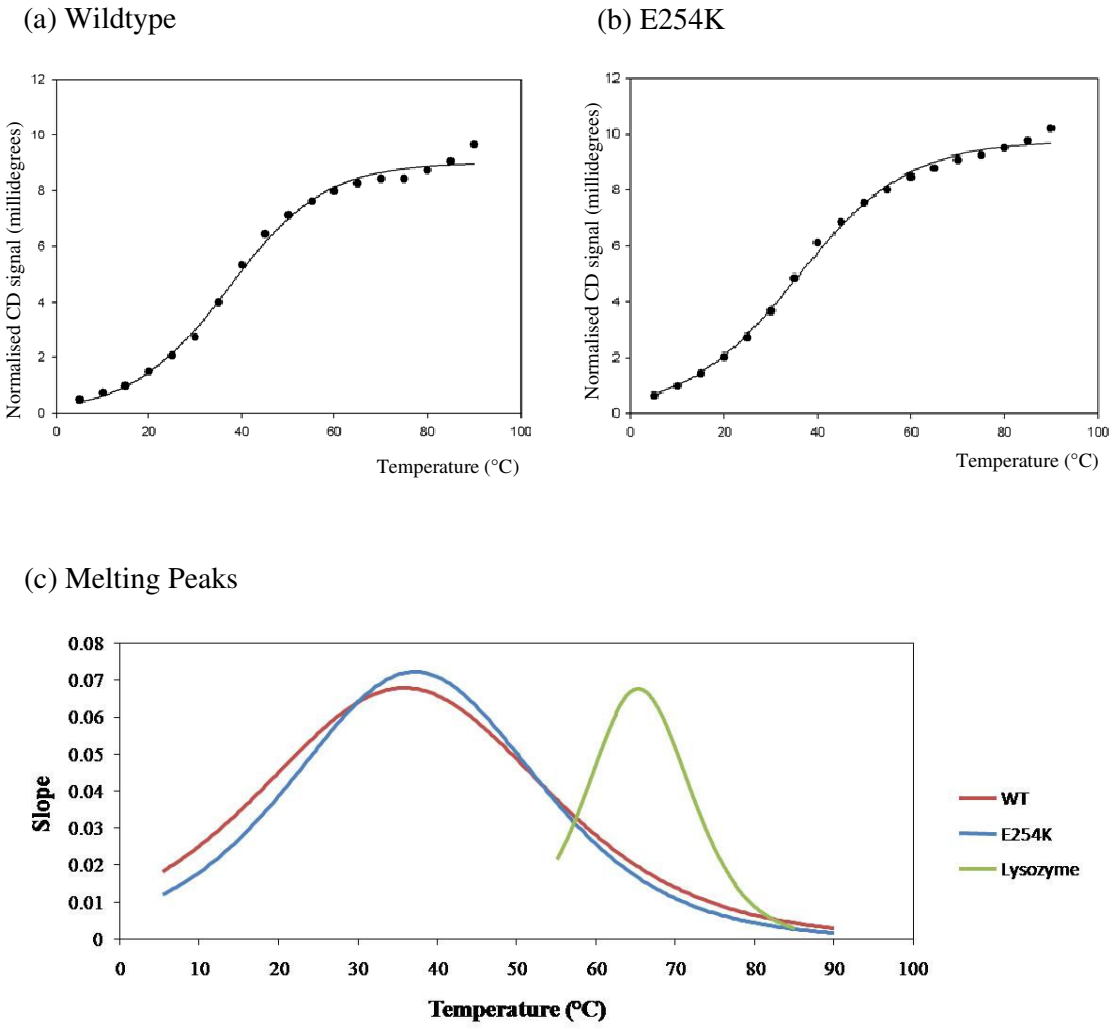

Figure 5-7. The Thermostability of the WT and E254K Proteins Measured by Circular Dichroism.
The loss of secondary structure measured at 222 nm.

a) WT CD signal graphed against temperature*.
b) E254K CD signal graphed against temperature*.
c) Graph of the first derivative of the CD melting curves. The wild type T_m is 36.2 °C and the E254K T_m is 37.2 °C. Lysozyme is shown as a positive control and has a T_m of 65.3 °C.

*The data were collected at 222 nm in 5 °C steps from 5 - 90 °C. The data were fitted to the sigmoid model by SigmaPlot (SYSTAT). The first derivative of the line of best fit is shown in (c).

The T_m is determined as the half way point between the folded and unfolded protein transition, assuming a two state transition (Gupta *et al.*, 1999). The wild type T_m is 36 °C and the E254K T_m is 37 °C, shown by graphing the slope of the melting curve (Figure 5-7). The T_m values that were determined by CD and fluorescence for each

protein are different (including the lysozyme standard). In contrast to the differential scanning fluorometry, there is no significant difference in the melting points of the wildtype and the E254K proteins in the CD temperature analysis.

5.5.2.3 Comparing the Differential Scanning Fluorometry and Circular Dichroism Data

Both these techniques were used to investigate the thermostability of the proteins; allowing us to compare the WT to the E254K mutant stability. However, when the results from these two techniques are compared, we get slightly different information. For the wildtype the differential scanning fluorometry gave a melting point of 45.5 °C and the T_m as determined by CD was 36 °C. This has two possible explanations. 1. There are different buffers used in these two experiments. 2. By measuring different properties in these two techniques we are following a slightly different process.

In the differential scanning fluorometry the salt concentration was 120 mM, which was lowered to 20 mM in the CD experiments to reduce buffer signal. The buffer system was different as the Tris group (used in differential scanning fluorometry) interferes with the CD signal, so a phosphate buffer was used. These two techniques measure different properties during protein unfolding. CD measures the change of secondary structure and the differential scanning fluorometry measures the exposure of hydrophobic surfaces. In addition to these changes the total time of the CD melt was different to the fluorescence melts. This is due to the time taken at each step to equilibrate the CD curvette and take the scan. So while the fluorescence melts took 15 min, the CD melts occurred over 2 hours. What is most concerning is the difference in the standard control protein lysozyme. This inconsistency in the CD melts needs further investigation. Therefore, for all of the reasons listed above, each melting temperature stability study must be analysed separately – rather than treating these two studies as complementary results.

The loss of this salt bridge between Lys169 and Glu254 does affect the stability of the ADB, as observed with the differential scanning fluorometry. This is consistent with the X-ray structural studies that showed this salt bridge is a tertiary structure element, linking helix A' and G'. The loss of this tertiary structural element (in E254K) exposes

a hydrophobic surface at a lower temperature than WT. The exact nature of this hydrophobic surface is not able to be predicted. The secondary structure stability of these helices (A' and G') is not affected when the WT and E254K are compared by CD. In addition to these studies, following the thermal denaturation by tryptophan signal may provide useful information about the tertiary structure.

5.6 Summary

The protein structures, as determined by X-ray crystallography and CD spectroscopy, show very little difference between the WT and the E254K mutant proteins, in crystals and in solution. However, a limitation of both these techniques is that very little information on the protein dynamics is provided. The crystallographic B-factors were analysed and regions absent from the crystallographic model provide some information about dynamics. A comparison of these proteins by NMR would provide more information about the structural flexibility/mobility of domains and regions of the protein. However, at 30 kDa this protein is on the edge of the NMR size limit, and in initial spectra of unlabelled protein we were only able to identify 30 out of the 268 amino acids (data not shown); therefore further studies were not pursued.

The WT and E254K proteins differ in the biochemical properties that were investigated in this work – actin affinity and thermostability. The actin affinity is 3.6 times higher for the E254K protein – consistent with the gain of function phenotype associated with this mutation. The actin affinity of the recombinant WT filamin A ABD was not inhibited by calmodulin or PIP_2 under the assay conditions tested in this work. Therefore studies with the E254K protein were not carried out.

There was a difference in the thermostability of the WT and E254K proteins. When the proteins were melted the E254K has a T_m that is 5.6 °C lower than the WT protein by differential scanning fluorometry. The thermostability was also investigated by CD spectroscopy with the signal at 222 nm followed as the sample was heated and there was no significant difference in the thermostability between the WT and the E254K. This indicates that the loss of this salt bridge does not significantly influence the stability of the secondary structure of the filamin A ABD. This is not surprising as the

salt bridge is part of the tertiary structure of the ABD linking the G and A helices of the CH2 domain.

6 *Ex vivo* Studies in Fibroblast Cells

6.1 Introduction

To further understand the effects of filamin A disease associated mutations, the phenotype of primary human fibroblast cells from OPD2, FMD and PVNH patients was compared to control wildtype cells. The cell lines were a kind gift from Professor Stephen Robertson at the University of Otago, and are all from male patients, to ensure that only one gene product of filamin A is present throughout each cell line. The "OPD2" cell line is from a patient with OPD2 that was described by Robertson *et al.* (2003). This point mutation (E254K) is in the ABD of filamin A, and the structure and actin affinity have been described in chapters four and five of this thesis. The "FMD" and "PVNH" cell lines are from patients identified with FMD and PVNH (respectively) by Professor Robertson's group. The mutation associated with PVNH is found in repeat 24 (G2593E), and the mutation associated with FMD is in the ABD (D253E) (Robertson, pers. Comm.).

PVNH is generally associated with a loss or reduction of filamin A in cells, and it is unknown whether any changes in filamin A levels are found in OPD2 or FMD patient cells. Therefore in these studies the level of full length filamin A was measured by western blotting in cells from OPD2, FMD and PVNH patients. Given that cell mobility is dysfunctional in at least one filamin A associated disease, the adhesion and motility of the OPD2 and PVNH patient cells were also investigated.

6.2 Western Analysis: Filamin A Levels in PVNH, OPD2 and FMD Patient Cells

To study if full length filamin A is expressed to wildtype levels in fibroblasts from PVNH, OPD2 and FMD patients western blots were carried out (see methods 2.22 and 2.35). The western blots of cell lysate were done in triplicate and the chemi-luminescence from the blot was measured and quantified and α-tubulin was used as a loading control. The filamin A levels calculated relative to the α-tubulin and the wildtype protein level were normalised to one and the other cell lines expressed relative

to the wildtype. There is no significant change in the filamin A levels in all cell lines tested (Figure 6-1).

(a)

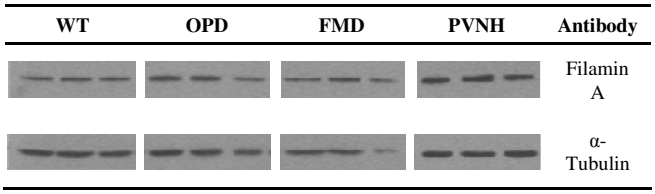

(b)

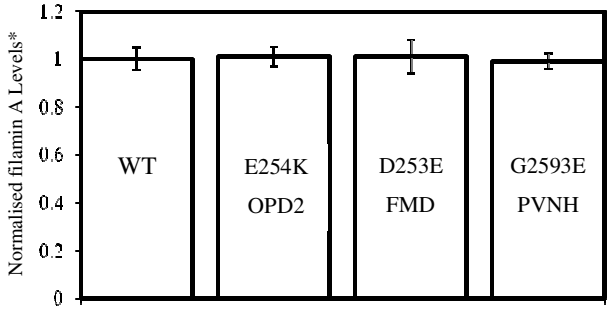

Figure 6-1. The Levels of Filamin A in Fibroblast Cells from Patients with Disease Associated with Filamin A Mutations.

a) Western blots of fibroblast lysate showing the 280 kDa filamin A and the 50 kDa α-tubulin.

b) Normalised filamin A levels from western blots of filamin A from fibroblast cell lysate, bars are labelled with the filamin A mutation (top) with the associated disease listed below.

Each blot was done in triplicate (as shown in the blots) and the error bars shown are one standard deviation. Three different "WT" control cell lines were used.

***** Expression is shown relative to the α-tubulin. The wildtype filamin A level is normalised to one and the other cell lines are shown relative to this wildtype level.

While it is not surprising that the level of filamin A in the OPD2 and FMD patients was the same as wildtype, the PVNH filamin A level was somewhat unexpected. PVNH is typically associated with a reduction in filamin A expression and is often found in patients with mutations that result in frameshifts or stop codons in filamin A. This analysis measured the total protein; however, additional factors to consider are turnover rate ($T_{1/2}$) in the cell, post-translational modifications and the cellular location. These factors may also contribute to the disease phenotype. This PVNH patient is a very mild phenotype (Robertson pers. comm.) whereas male PVNH is typically embryonic lethal but not in this instance.

6.3 Adhesion Assays of Fibroblast Cells to a Fibronectin Matrix

In α-actinin null mice podocyte cells there is a reduction in the cell-matrix interaction mediated by integrin (Dandapani *et al*., 2007). Filamin A also interacts with integrin, which is an important protein in the interaction between cells and the extracellular fibronectin matrix (Calderwood *et al*., 2001; Loo *et al*., 1998; Engler *et al*., 2009). Therefore, the adhesion of the disease associated cell lines was compared, relative to the wildtype control cell lines. The cells and media were passaged into a fibronectin coated plate, and the amount of cells that adhere was measured after one hour (see method 2.37). This time frame was chosen because after one hour about 90% of the wildtype cells are have adhered to the fibronectin matrix on the plate. To determine the amount cells that have adhered, the media and free cells are removed and the remaining cells are rinsed. These cells are stained with crystal violet, the excess stain rinsed off, the cells lysed and the absorbance measured at 570 nm (Figure 6-2). The stained and rinsed cells were also inspected under the microscope before lysis – and no difference in the number of cells could be detected. The background absorbance from a negative control (without cells) was subtracted from the absorbance of each well.

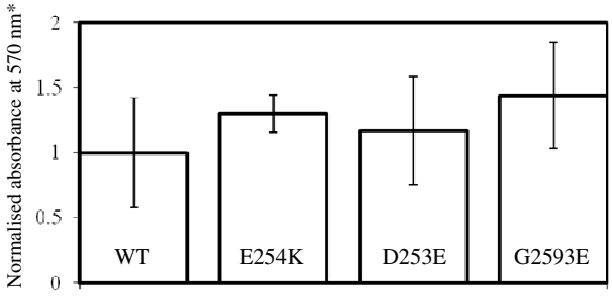

Figure 6-2. Adhesion Assay of Fibroblast Cells.

The average absorbance readings at 570 nm from an adhesion assay. Each bar (on the graph) is labelled with the mutation and associated disease, error bars show one standard deviation and each experiment was repeated at least 3 times. *Data are normalised, with the absorbance shown relative to the wildtype.

The 5 cell lines tested (2 wildtype and 3 mutants) showed no significant difference, under the conditions tested, in adhesion to tissue culture 96 well plates. There are a number of different ways that this assay could be set up. A time course of adhesion could be conducted; however, in this experiment only one time point (at 1 hr) during the adhesion process was measured. In addition, increasing force may be used to disrupt the cell-matrix interaction, allowing a comparison between patient and control cells

(Dandapani, *et al*., 2007). However, further experiments were outside the scope of this work, and therefore this is described as preliminary data.

6.4 Migration of Cells from PVNH and OPD2 Patients

Cell migration is made of three stages a) protrusion of the leading edge, b) contraction of the cell body and finally c) detachment of the trailing edge of the cell. As the leading edge contacts the substrate, adhesion receptors (such as integrins) form focal contact leading to stress fibre formation. These steps depend on a number of dynamic cytoskeleton rearrangements (reviewed by Friedl and Brocker, 2000). The level of functional filamin A in M2 cells correlated with the motility of cells, with decreasing filamin A cells migrating more slowly and cells null for filamin A being unable to migrate (Cunningham *et al*., 1992; Klaile *et al*., 2005). This phenotype may be explained by the filamin A:integrin interaction, as increased affinity of β-integrin for filamin A inhibits cell migration (Calderwood *et al*., 2001). The interaction between filamin A and the carcinoembryonic antigen-related cell adhesion molecule has also been proposed as a molecular mechanism behind the loss of mobility (Klaile *et al*., 2005). However, in contrast to these studies, mouse embryonic fibroblasts (MEF) null for filamin A are able to migrate, equivalent to WT levels (Hart *et al*., 2006).

Integrins provide a physical link between the actin cytoskeleton and the extracellular fibronectin matrix, also playing essential roles in integrating the biochemical and physical signals during cellular migration. Large cells, such as fibroblasts, have well documented integrin dependent migration (Friedl and Brocker, 2000). Therefore, this work looked at whether human fibroblasts expressing filamin A with these point mutations (that do not change the level of filamin A in the cells) were able to migrate at the same rate as wildtype fibroblasts. Patient cells from both gain of function (OPD2) and loss of function (PVNH) diseases were used in these experiments. Fibroblast cells were cultured on a fibronectin matrix, the cell monolayer was wounded with a pipet tip, and the plate followed by time course microscopy to determine if the cell lines were able to migrate into the wound (see method 2.36). Images were analysed and the distance that the cells moved calculated using ImageJ software (Liang *et al*., 2007). The cell lines from patients were compared to the wildtype control fibroblast cells (Figure 6-3).

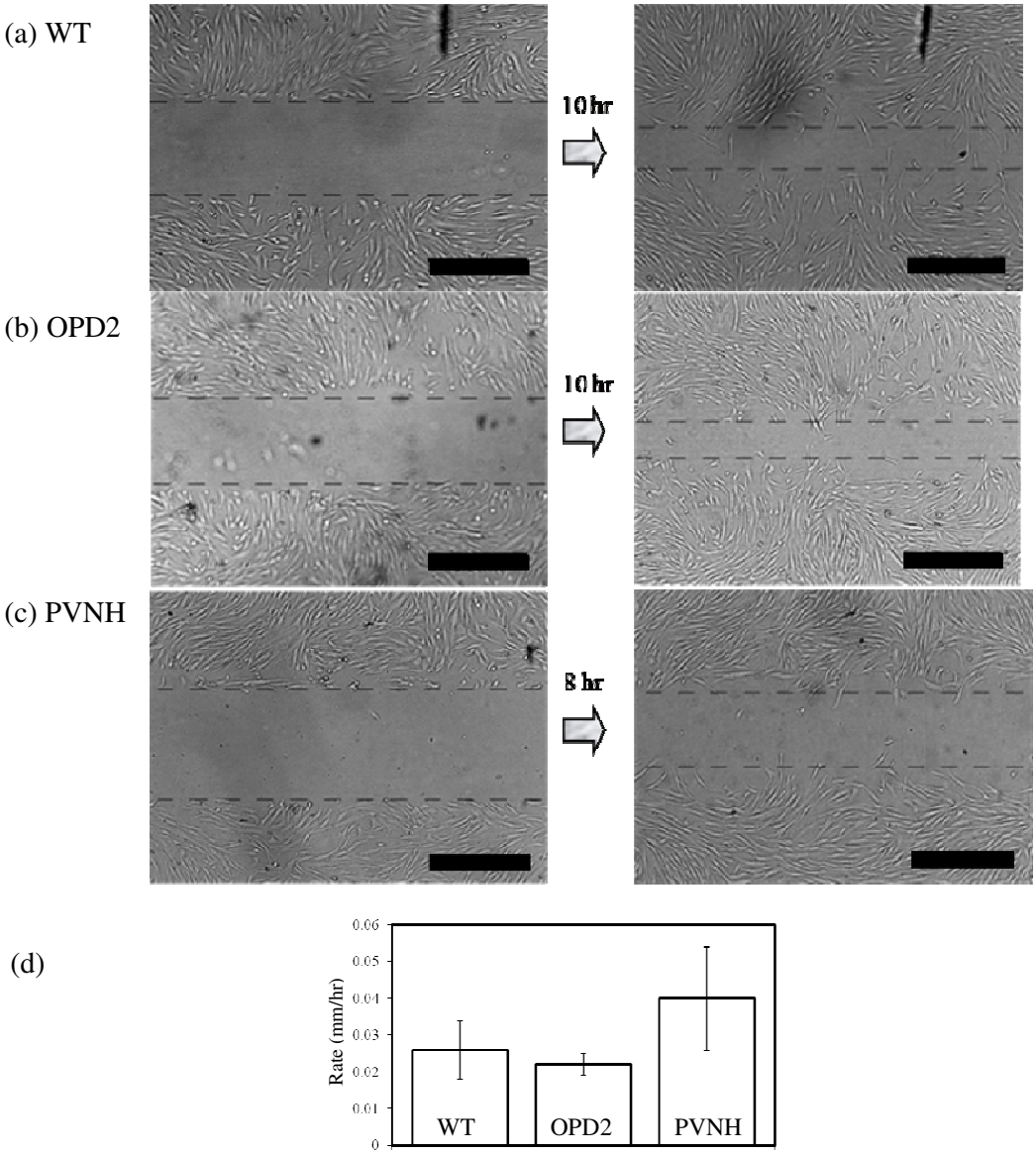

Figure 6-3. Cell Migration Assays.

Images show the monolayer of live fibroblast cells growing in DMEM media on the surface of the 30 mm plate. On the left are the images captured at time =0 after the wound was made, and on the right is the same area of the plate, after incubation for 8 or 10 hours.

a) Control cells. WT fibroblast cells at 0 and 10 hours.
b) Fibroblast cells from an OPD2 patient containing the E254K mutation at 0 and 10 hours.
c) Fibroblast cells from a PVNH patient containing the G2593E mutation at 0 and 8 hours.
d) A summary graph showing the movement rate of each cell line in the migration assays from triplicate experiments, with error bars of one standard deviation.

The images shown are typical, and all scale bars shown are 0.5 mm in length.

The wildtype cells moved at a rate of 0.026 mm/hr (± 0.008). This is not significantly different to the rate of the E254K cells, 0.022 mm/hr (± 0.003). However, the filamin A G2593E cells with moved at a greater rate, 0.040 mm/hr (± 0.014), but at a more inconsistent rate. This rate was not significantly different to that of the wildtype control cells (with a P-value of 0.16, where less than 0.1 is statistically significant). This confirms that each cell line tested could migrate across the fibronectin matrix, at least at that same rate as the wildtype lines tested.

6.5 Summary

This chapter described a number of studies that were done with the aim of comparing and contrasting the phenotypes of patient and control fibroblast cells. To confirm that full length filamin A was expressed, western blots were performed on fibroblast lysate from OPD2, FMD and PVNH patients. The cell lines tested in this work all had wildtype levels of full length filamin A protein. The adhesion of these fibroblast cells was also investigated because a) filamin A interacts with integrin (which is involved in adhesion) and b) cell motility, which filamin A is involved in, requires cell adhesion. There was no significant difference in the adherence to a fibronectin matrix between wildtype, PVNH, FMD and OPD2 cells. The ability of these fibroblast cell lines to migrate across a fibronectin matrix was also investigated. Cells from PVNH and OPD2 patients were able to migrate with comparable rates to wildtype cells.

The PVNH associated mutation (G2593E) is in the dimerisation domain of filamin A, and results in the disruption of the dimer interface (Andrew Sutherland-Smith, pers. Comm.). Fibroblasts from this PVNH patient have wildtype levels of filamin A and are able to migrate with comparable rates to wildtype control cells. This demonstrates that, although filamin A is required for M2 cell migration (Cunningham *et al*., 1992), filamin A does not need to be dimeric for fibroblast migration. This is consistent with results from mouse embryonic fibroblasts null for filamin A, which are able to migrate, at an equivalent rate to WT cells (Hart *et al*., 2006). However, for correct neuron migration, filamin A dimerisation is required. This provides further support for the idea that these disease phenotypes are due to specific CNS signalling pathways being interrupted by the mutations in filamin A, rather than a general physical disruption of cellular migration (Robertson *et al*., 2005). The fibroblast cells from the gain of function mutation (E254K) associated with OPD2 have no significant change in the filamin A level, adhesion to fibronectin and are able to migrate at wildtype rates, despite an increased actin affinity. In summary, no phenotypic differences in the fibroblast cells from OPD2, FMD and PVNH patients could be detected when compared to wildtype control cell lines in the experiments performed.

7 Discussion

7.1 Introduction

The work described in this thesis takes a three pronged approach to teasing out the role of the filamin A ABD in the cell, and understanding how disease results when this domain is mutated. Structural studies were completed, the biochemical properties of the domain were analysed and the phenotype of fibroblast cells were characterised. Here the results are compiled for each associated disease and discussed with respect to each other.

7.2 Understanding the Actin Bound Structure

When the ABSs on the ABD are mapped onto the crystal structure they do not form a continuous surface, and there are conflicting arguments about how the ABD interacts with F-actin. There are likely to be structural rearrangements, but the extent and nature of these rearrangements are not well understood. There must be a structural rearrangement for ABS1 to contact the actin at the same time as ABS2 and ABS3. The electron microscopy structure of utrophin bound to actin indicated the domains move apart and bind F-actin with a separate monomer (Moores *et al.,* 2000; Galkin *et al*., 2002) (Figure 7-1). The higher resolution structure of the fimbrin actin binding domain bound to actin also shows the domains moving apart (Galkin *et al.,* 2008). However, there is a second hypothesis, where a small structural rearrangement occurs upon actin binding that allowing all of the ABS to contact actin (Sutherland-Smith *et al.,* 2003) (Figure 7-1). A third possibility is that ABS1, which is largely buried in the ABD structures, is a region of the protein that is important for actin affinity, but does not directly contact actin.

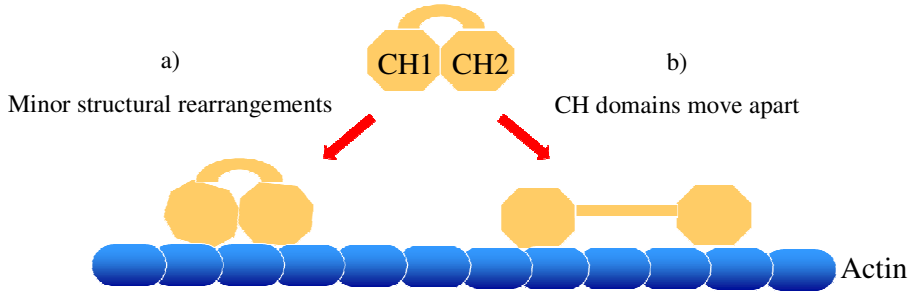

Figure 7-1. A Schematic Showing How the ABD may Interact with Actin.
Either:

a) There are some minor structural rearrangements.
b) There is a large structure rearrangement in which the CH domains move apart allowing the ABS to contact actin.

The uncertainty surrounding the actin bound structure of the ABD makes understanding the disease mutations, and how they may affect actin binding, difficult. In this thesis a reduction in stability of the E254K mutant accompanies an increase in F-actin affinity. This is consistent with a structural rearrangement of the ABD upon actin binding, but this rearrangement does not have to be the CH domains moving apart. A disease associated α-actinin mutation at the CH1/CH2 interface binds to actin with a higher affinity (Weins *et al.,* 2007). This is interesting, and the authors propose that the increase in actin affinity was due to the CH domains being able to move apart more easily. The filamin A E254K mutation may also allow the domains to separate more easily, however it is less clear how this may occur. Filamin B also has disease associated mutations that result in an increase in actin affinity, and these mutations are not located at the CH1/CH2 interface (Sawyer *et al.,* 2009). Therefore the CH1/CH2 interface location of this α-actinin mutation may not be as significant as first thought.

The ABD only binds to F-actin, and not monomeric actin, which makes studying this interaction difficult. Co-crystallisation studies are not possible and even a high resolution structure of F-actin is not available for modelling. Therefore, the models we have are low resolution and based largely on electron microscopy data, fibre diffraction

and the monomeric actin structure. The structures presented in this thesis provide us with some information about how the disease associated mutations may cause disease; however, what is required to really understand how mutations in the ABD cause disease is a high resolution actin bound structure of this protein.

7.3 Mutations in the Filamin A CH1 Domain: Understanding PVNH

Point mutations in the CH1 domain are associated with the disease PVNH, typically associated with complete loss of filamin A protein (Figure 4-19). Two likely disease mechanisms for the CH1 point mutations are the loss of stability of the ABD, leading to the reduction of the filamin A protein level, or the loss of actin binding and crosslinking activity. These are not mutually exclusive, and a substantial loss of ABD stability would likely result in loss of actin binding as well.

7.3.1 Do Mutations in CH1 Result in a Reduction in the Filamin A Level?

A point mutation, L54R, in CH1 of the dystrophin ABD results in lower levels of dystrophin *in vivo*, resulting in Duchenne muscular dystrophy (DMD) (Prior *et al*., 1993). DMD is, like PVNH, associated with the complete loss of functional protein. A similar mechanism in filamin A and PVNH, particularly with respect to the three filamin A mutations (G74E, I78T and E82V) in close proximity to the equivalent residue in dystrophin (L81) is likely (Figure 7-2). Expression of the E82V ABD in *E. coli* resulted in expression of insoluble protein (results not shown), indicating that this mutation may substantially disrupt the structure of the ABD.

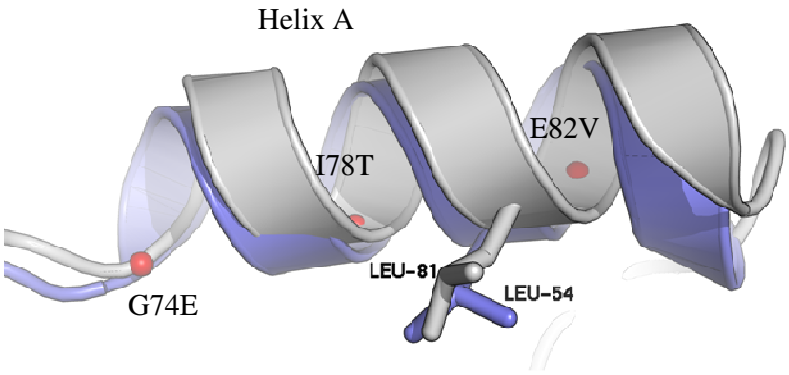

Figure 7-2. Mutations in Close Proximity to Leu81.

This overlay of the dystrophin (purple) and filamin A (grey) ABD shows the conserved Leu which is associated with DMD disease in dystrophin. The PVNH associated residues (in filamin A) are shown as red spheres.

7.3.2 Actin Crosslinking and PVNH: Studies of Filamin A G2593

Two putative ABSs are located in this sub-domain and although these mutations do not cluster in these regions the mutations could disrupt the structure or stability of the CH1 domain affecting the domains F-actin binding surface. Results from this work show that PVNH associated mutations (E.g. G2593E) can have WT levels of filamin A, but still be associated with PVNH (Figure 6-1). The G2593E mutation disrupts the dimer interface of filamin A (Andrew Sutherland-Smith, pers. comm.). This shows that the (presumably) monomeric filamin A is not degraded. Therefore this mutation would be predicted to abolish the actin cross linking activity of filamin A. Fibroblasts from this PVNH patient are able to adhere and migrate with comparable rates to WT control cells (Figure 6-2; Figure 6-3). This is consistent with the rat and mouse models where filamin A null mouse embryonic fibroblasts are able to migrate with comparable rates to WT control cells (Hart *et al* 2006). This evidence supports a specialised role of filamin A in neuronal migration (explaining why these cells are specifically affected in PVNH) and not a purely general structural role in migration. Robertson *et al*., (2005) predicted a signalling role for filamin A – based on the disease phenotype. Even in the complete absence of filamin A (in some PVNH patients) neurons are able to migrate, and it is incorrect migration, not a lack of migration that is observed. The likely mechanism for

the signalling role of filamin A in migration is through integrin, as migration is inhibited with increased integrin affinity for filamin A (Calderwood *et al*., 2001). Based on this hypothesis, it can also be concluded that dimerisation is not required for migration in fibroblasts; despite being required for the correct migration in neurons.

7.3.3 PVNH: Why Does LOF/Null Mutation Affect Neuronal Migration?

Why there are such localised phenotypic effects (in the brain/heart/joints/gut) with a ubiquitously expressed protein remains unclear. It is proposed that there is an additional role of filamin A in neurones, or that the role is different to that in other cells in the body (Robertson *et al*., 2005; Sarkisian *et al*., 2008). It is this role that is affected by mutations in the CH1 (PVNH). There may be a functional compensation by another protein (such as filamin B) in other cell types not affected to the same extent. Filamin B is expressed in a similar distribution as filamin A (Xu *et al*., 1998) and would function as an actin cross linking protein in a similar way to filamin A. However it is unlikely to compensate for a specific (putative) signalling role of filamin A in neurones. This role is also particularly sensitive to the filamin A level, with increases and decreases in filamin A levels at the periventricular zone leading to incorrect neuron migration, and to changes in the polarity and orientation of neurons (Nagano *et al*., 2004). However, we can conclude that increases in actin affinity (such as E254K) do not affect this unknown role because the OPD2 patients do not share the brain abnormalities seen in the PVNH patients.

7.4 The OPD Spectrum Diseases

7.4.1 Structural Studies

The WT filamin A ABD has the typical ABD fold, and provides a valuable resource for improving our understanding of the actin binding mechanism and disease associated point mutations that cluster in the CH2 domain (Figure 4-19). The x-ray crystal structure of two OPD2 associated (E254K and A200S) ABDs, and the solution structure of E254K (determined by circular dichroism) were essentially unchanged from the WT structure (Table 5-2). The pathogenic mutation E254K breaks a conserved salt bridge; and the electrostatic surface charge is changed (Figure 4-15). The A200S mutation

causes a steric clash, causing localised and small side chains rearrangements (Figure 4-18). However, the reason these two amino acid changes are associated with a severe disease like OPD2 remained unclear from these structural studies.

7.4.2 Protein Thermal Stability and a Conserved Salt Bridge

The circular dichroism showed no change in thermal stability between the WT and E254K. However, the differential scanning fluorimetry (which followed unfolding in a different way) showed the E254K has a T_m 5.6 °C lower than WT. Helices A' and G' in the CH2 domain are linked by the salt bridge between E254 and K169 (Figure 4-16) The E254K structure shows that the tertiary structure (link between two helices) is disrupted with E254K, and not the secondary structure. Circular dichroism measures secondary structural changes and not tertiary structure.

The loss of a salt bridge is often accompanied by a reduction in thermostability (Bae and Phillips, 2005). This salt bridge was predicted to have an important structural role for two reasons. 1. It is highly conserved and causes disease when mutated – indicating that it has a role in either structure/function and 2. In dystrophin and utrophin the polarity of the side chains is reversed – indicating that it is a structural role rather than a recognition site at the surface (Figure 4-16). The importance of this interaction was also highlighted by Borrego-Diaz *et al*. (2006) who postulated that this salt bridge in α-actinin is surrounded by two conserved areas that are connected by a salt bridge between Lys147 (in ABS3) and the Glu235. It links the helix A to helix G of CH2, which contains ABS2. It was hypothesised that this highly conserved salt bridge could be part of a continuous binding surface in ABDs. In filamin B the mutation in the equivalent residue (E227K) is associated with Larsens disease, indicating that the salt bridge in filamin B is also critical for function (Krakow *et al*., 2004). Larsens disease is a bone disorder like OPD2; however, it results in a clinically separate disease. This is consistent with the different cellular distribution of filamin A and filamin B (Krakow *et al*., 2004).

Together these observations highlight an interesting point: Filamin B has a slightly different role in the body to filamin A, however this particular residue is important for the function of both filamin A and filamin B.

The decreased domain stability (in section 5.5.1) of E254K is not accompanied by a decrease in the total filamin A protein levels (Figure 6-1). While western blotting does not tell us about turnover rate, this result is consistent with the gain-of-function hypothesis for the OPD spectrum disorders, as the absence or reduction of filamin A level results in PVNH. A decrease in protein stability can be accompanied by an increase in activity (Shoichet *et al.*, 1995). This could be explained by the structural rearrangement of the ABD that may be required upon actin binding.

7.4.3 An Increase in Actin Affinity: The Underlying Disease Mechanism?

This increase in actin affinity is consistent with the gain of function phenotype of OPD2. It is interesting to note that mutations in the repeat domains (14 and 15) are also associated with OPD2, and repeats 9-15 have been implicated in actin binding (Nakamura *et al.*, 2007). In addition, increased actin affinity is emmerging as a common theme in disease associated with point mutations in the ABD of actin cross linking proteins. Pathogenic mutations in filamin B (Sawyer *et al.*, 2009) and α-actinin-4 (Kaplan *et al.*, 2000; Weins *et al.*, 2007) result in an increased actin affinity.

Mutations in the CH2 domain of filamin B are associated with the bone dysplasia atelosteogenesis disease. Two disease associated mutations studied recently, W148R and M202V, result in a 3.5 fold and a 12 fold increase in actin affinity (respectively) when compared to the WT filamin B ABD (Sawyer *et al.*, 2009). In α-actinin-4 the point mutation K255E (adjacent to filamin A residue Glu254) results in the kidney disease focal segmental glomerulosclerosis and results in a increase in affinity for actin from 31 μM to 5.3 μM (5.8 fold) (Weins *et al.*, 2007) (Figure 7-3). These increases in affinity are similar to that seen in this work with filamin A where the mutation results in an increase from 48 μM to 13 μM (3.7 fold).

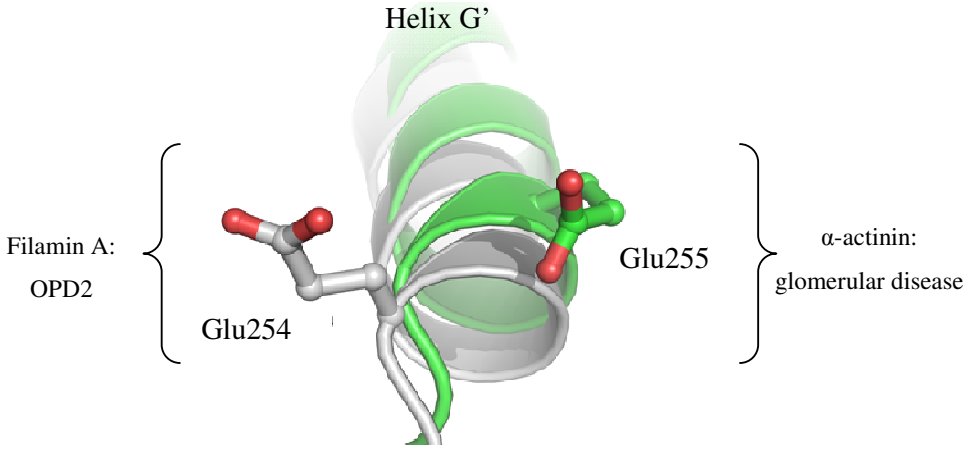

Figure 7-3. Overlay of the ABD of WT Filamin A (grey) and α-Actinin-4 K255E (green).
Both residues are pathogenic when mutated and both result in an increase in actin affinity. In filamin A the pathogenic mutation E254K results in a bone disorder and in α- actinin K255E it results in kidney disease. The α-actinin structure shown is pdb 2RO0.

Other mutations in α-actinin-4 are associated with glomerular disease and also show a higher affinity for actin than WT (Kaplan *et al*., 2000). How this increase in actin affinity with the filamin A pathogenic mutation may result in dysfunction in the cell is unknown (see future directions). However, this question has been extensively studied in α-actinin-4. The structural and bio-mechanical properties of actin filaments that were crosslinked by the mutant α-actinin were different when compared to WT α-actinin cross linking, particularly stress fibres and focal adhesion formation. The cellular localisation of the mutant α-actinin was also disrupted (Weins *et al*., 2007; Kaplan *et al*., 2000). Filamin A has cellular roles in the cytoskeleton, cytoplasm and the nucleus (Krakow *et* al., 2004; Loy *et al*., 2003). Therefore, like α-actinin, a complex disease mechanism would be predicted for an increase in actin affinity for filamin A (some are discussed in section 7.4.5).

So while the increased actin affinity may not be the only cause of disease, it is likely to contribute to the phenotype. However, it is possible that a number of mutations have different immediate molecular consequences, but lead to the same cellular/physiological consequences, and the same disease. Therefore, there may be more than one molecular mechanism underlying the OPD spectrum disorders.

7.4.4 The FMD Associated Mutations

The filamin A mutations, D253E and E245K, are both associated with FMD, an OPD spectrum disorder. Currently the molecular basis of FMD is unknown. Both these point mutations are located at the surface of the ABD, but are also near the CH1/CH2 interface, with D253E forming a salt bridge between CH1 and CH2 (Figure 4-25). These mutations highlight the importance of the CH domain interface function, previously brought to our attention in α-actinin (K255E), in which there is an increase in actin affinity, with a mutation in a residue at the CH1/CH2 interface (Weins *et al*., 2007). Based on the disease phenotype and the location of the mutations (near the CH1/CH2 interface) an increase in actin affinity would be predicted with these mutations. However, the mutations are located close together at the surface of the ABD and could also conceivably disrupt an interaction with binding partners other than actin.

7.4.5 How Does an Increase in Actin Affinity Affect Primarily Bone Development?

OPD spectrum disorder mutations in the ABD of filamin A, a ubiquitously expressed protein, primarily affect bone development and not other organs/tissues where filamin A is also expressed. Therefore either bone development is more sensitive to filamin A actin affinity changes or there is an additional role of filamin A in bone cells (as predicted for neurons and PVNH) that is disrupted by mutations associated with the OPD spectrum disorders.

Assuming that the increase in actin affinity underlies the disease, there a two ways that this may disrupt bone development. 1) The increased affinity may change the ratio of cytoskeletal/cytoplasmic filamin A, which may have far reaching effects within the cell. 2) The rate of filamin A association/dissociation from actin may be more critical during bone development, to physically allow the dynamic actin rearrangements that are required (Figure 1-14).

There are a number of proteins involved in bone development that filamin A interacts with that may require filamin A to be located correctly with the cell. This includes

signalling proteins in the MAP kinase pathway (Sarkisian *et al.*, 2006), Wnt-c-Jun N-terminal kinase pathway (Nomachi *et al.,* 2008). In osteoclast cells Rho A plays a regulatory role in the mobility of cells mediating the formation of actin stress fibers and podosomes, and it is also involved in integrin-mediated signalling events (Chellaiah *et al*., 2000). Both RhoA and integrin are filamin A binding partners (Calderwood *et al*., 2001; Ohta *et al*., 1999) (Figure 1-8). Integrins play a role in intramembranous ossification by mediating cellular adhesion of migrating cells. The repeat 21 domain of filamin A binds to integrin and inhibits integrin-dependent cell migration by preventing membrane protrusion and cellular polarisation required for migration (Calderwood *et al*., 2001). Migfilin associates with filamin A at cell matrix adhesions to modulate actin assembly, cell spreading and cellular shape (Tu *et al*., 2003; Nagano *et al*., 2004). Calcitonin (a filamin A binding partner) regulates osteoclast adhesion mechanisms during bone development (Seck *et al*., 2003). There may be a specifically bone expressed protein (yet to be found) that interacts with filamin A, and it is this interaction is disrupted with the pathogenic mutations.

Therefore, it would be expected that cellular location of filamin A is important for the filamin A interaction with one or more of these proteins. The change in actin affinity may change the cellular location of filamin A, which would affect the interactions with these binding partners. This could results in the protein:protein interaction occurring at the incorrect time, at the incorrect cellular location or not at all. This would have far reaching cellular consequences, which could result in the cell differentiation or mobility being affected, resulting in bone development disruption.

7.5 Summary

The structure of the ABD of filamin A is a typical ABD fold, similar to the ABD of other proteins, and mutations associated with OPD2 (A200S and E254K) do not significantly perturb the ABD structure. The filamin A protein level, mobility and adhesion in OPD and PVNH patient fibroblast cells is indistinguishable from that of wildtype cells. However, in at least one OPD2 associated mutation (E254K) the ABD stability is decreased, accompanied by an increase in actin affinity. These results are consistent with the gain of function phenotype of OPD2 and also with disease associated mutations in other ABD such as filamin B (Sawyer *et al*., 2009) and α-actinin-4 (Kaplan *et al*., 2000; Weins *et al*., 2007).

In summary, while it remains unclear exactly how point mutations in the ABD of human filamin A may disrupt development, these studies have shown some of the biochemical and cellular consequences of these mutations.

7.6 Future Directions

- ***In Vivo* Studies**

Study the actin cytoskeleton of fibroblasts (or osteocytes) to see the actin and filamin A localisation – particularly in migrating cells. It would be useful to compare cells from OPD spectrum disorder and PVNH patient to WT cells. Confocal microscopy would be a useful method to use, with fluorescently labelled antibodies to actin and filamin A.

- **Actin Binding Assays**

Determine the actin affinity of the ABD with point mutations in CH1 associated with PVNH with the actin co-sedimentation assay – if enough soluble protein can be obtained. Also studies of the other OPD spectrum associated mutants – to determine if increased actin affinity is a general trend.

- **Actin Crosslinking Studies**

Microscopy studies of the actin networks cross linked by full length filamin A disease associated mutants, compared to WT filamin A to determine if the way that the actin is cross linked changes due to the disease associated mutations.

- **Westerns of Filamin B in Patient Cells**

Western blots of cells from patients with OPD spectrum disorder or PVNH. This is to determine if filamin B is being up regulated to compensate for the filamin A misfunction.

- **NMR Studies**

NMR studies to investigate the flexibility/mobility of helix A' and helix G' of the E254K mutations compared to WT. Preliminary studies of the WT ABD revealed that the spectrum was not suitable for amino acid assignment, which was not surprising as the ABD (30 kDa) is on the edge of NMR size limit. However NMR studies of the smaller CH2 fragment may provide more useful spectral data.

- **Cryo-Electron Microscopy**

Microscopy of actin decorated filaments to determine the "actin bound" structure of the filamin A ABD. The crystal structure of the filamin A ABD could be modelled into the lower resolution microscopy data. A better model of the actin bound structure would allow a better understanding of how the disease associated mutations may cause disease.

- **Further Stability and CD Spectroscopy Studies**

Three additional studies that may be useful are a) look at tertiary structure by CD spectroscopy; b) reversible chemical denaturation; c) differential scanning calorimetry. Following the Trp signal in the near UV and the protein is heated would allow studies of the tertiary structure. Reversible chemical denaturation would allow an energy changes to be determined and quantified. Differential scanning calorimetry would allow a very accurate determination of the energy required for denaturation.

8 References

Adams, P., Grosse-Kunstleve, R., Hung, L., Ioerger, T., McCoy, A., Moriarty, N., Read, R., Sacchettini, J., Sauter N., Terwilliger, T. (2002). PHENIX: building new software for automated crystallographic structure determination. *Acta Crystallographica D.* **58**, 1948-1954.

Afshar M, Caves L., Guimard L., Hubbard R., Calas B., Grassy G., Haiech J. (1994). Investigating the high affinity and low sequence specificity of calmodulin binding to its targets. *Journal of Molecular Biology*. **244**, 554-571.

Agre, P., Asimos, A., Casella, J., McMillan, C. (1986). Inheritance pattern and clinical-response to splenectomy as a reflection of erythrocyte spectrin deficiency in hereditary spherocytosis. *New England Journal of Medicine*. **315**, 1579-1583.

Andrade, M., Chacon, P., Merelo, J., Moran, F. (1993). Evaluation of secondary structure of proteins from UV circular dichroism spectra using an unsupervised learning neural network. *Protein Engineering*. **6**, 383-390.

Bae, E. and Phillips, G. (2005). Identifying and Engineering Ion Pairs in Adenylate Kinases. Insights from molecular dynamics simulations of thermophilic and mesophilic homologues. *The Journal of Biological Chemistry*. 280, 30943–30948.

Banatao, D., Cascio, D., Crowley, C., Fleissner, M., Tienson, H., Yeates, T. (2006). An approach to crystallizing proteins by synthetic symmetrisation. *Proceedings of the National Academy of Sciences of the United States of America*. **103**, 16230-16235.

Banuelos, S., Saraste, M., Djinovic, C. K. (1998). Structural comparisons of calponin homology domains: Implications for actin binding. *Structure.* **6**, 1419-1431.

Barlow, D., Thornton, J. (1983). Ion-pairs in proteins. *Journal of Molecular Biology*. **168**, 867-885.

Bella, T. (2005). Inositol-lipid binding motifs: signal integrators through protein-lipid and protein-protein interactions. *Journal of Cell Science.* **118**, 2093-2104.

Bellanger, J. M., Astier, C. S., Ohta, Y., Stossel, T. P. Debant, A. (2000). The Rac1-and RhoG-specific GEF domain of Trio targets filamin to remodel cytoskeletal actin. *Nature Cell Biology.* **2**, 888-892.

Bennett, M. J., Choe, S., Eisenber, G. D. (1994). Domain swapping - entangling alliances between proteins. *Proceedings of the National Academy of Sciences of the United States of America*. **91**, 3127-3131.

Bhat, T. (1988). Calculation of an omit map. *Journal of Applied Crystallography*. **21**, 279-281.

Bicknell, L., Farrington-Rock, C., Shafeghati, Y., Rump, P., Alanay, Y., Alembik, Y., Al-Madani, N., Firth, H., Karimi-Nejad, M., Kim, C., Leask, K., Maisenbacher, M., Moran, E., Pappas, J., Prontera, P., de Ravel, T., Fryns, J., Sweeney, E., Fryer, A., Unger, S., Wilson, L., Lachman, R., Rimoin, D., Cohn, D., Krakow, D., Robertson, S. *Journal Medical Genetics*. **44**, 89-98.

Bohm, G., Muhr, R., Jaenicke, R. (1992). Quantitative-analysis of protein far UV circular-dichroism spectra by neural networks. *Protein Engineering*. 5, 191-195.

Bork, P., Holm, L., Sander, C. (1994). The Immunoglobulin Fold - Structural Classification, Sequence Patterns and Common Core. *Journal of Molecular Biology.* **242**, 309-320.

Borrego-Diaz, E., Kerff, F., Lee, S., Ferron, F., Li, Y., Dominguez, R. Crystal structure of the actin-binding domain of α-actinin 1: Evaluating two competing actin-binding models. (2006). *Journal of Structural Biology*. **155**, 230–238.

Bosshard, H., Marti, D., Jelesarov, I. (2004). Protein stabilization by salt bridges: concepts, experimental approaches and clarification of some misunderstandings. *Journal of Molecular Recognition.* **17**: 1–16.

Bresnick, A. R., Janmey, P. A., Condeelis, J. (1991). Evidence That a 27-Residue Sequence Is the Actin-Binding Site of Abp-120. *Journal of Biological Chemistry.* **266**, 12989-12993.

Brotschi, E. A., Hartwig, J. H., Stossel, T. P. (1978). Gelation of Actin by Actin-Binding Protein. *Journal of Biological Chemistry.* **253**, 8988-8993.

Browne, K. A., Johnstone, R. W., Jans, David. A., Trapani, J. A. (2000). Filamin (280-kDa actin-binding protein) is a caspase substrate and is also cleaved directly by the cytotoxic T lymphocyte protease granzyme B during apoptosis. *Journal of Biological Chemistry.* **275**, 39262-39266.

Brünger, A. (1988). Crystallographic Refinement by Simulated Annealing Application to a 2.8Å Resolution Structure of Aspartate Aminotransferase. *Journal of Molecular Biology*. **203**, 803-816.

Brünger, A. (1992). Free R-value - a novel statistical quantity for assessing the accuracy of crystal structures. *Nature*. **355**, 472-475.

Burgess, W., Jemiolo, D., Kretsinger, R. (1980). Interaction of calcium and calmodulin in the presence of sodium dodecyl-sulfate. *Biochimica et Biophysica Acta*. **623**, 257-270.

Calderwood, D. A., Huttenlocher, A., Kiosses, W. B., Rose, D. M., Woodside, D. G., Schwartz, M. A., Ginsberg, M. H. (2001). Increased filamin binding to beta-integrin cytoplasmic domains inhibits cell migration. *Nature Cell Biology*. **3**, 1060-1068.

Carrington, J., Dougherty, W. (1988). A viral cleavage site cassette: Identification of amino acid sequences required for tobacco etch virus polyprotein processing.

Proceedings of The National Academy of Sciences of The United States of America. **85**, 3391-3395

Castresana, J., Saraste, M. (1995). Hypothesis: Does Vav bind to F-actin through a CH domain? *FEBS Letters.* **374**, 149-151.

Chellaiah, M., Soga, N., Swanson, S., McAllister, S., Alvarez, U., Wang, D., Dowdy, S., Hruska, K. (2000). Rho-A Is Critical for Osteoclast Podosome Organization, Motility, and Bone Resorption. *The Journal of Biology Chemistry*. **275**, 11993–12002.

Collaborative Computational Project, Number 4. (1994). The CCP4 Suite: Programs for Protein Crystallography. *Acta Crystallographica D*. **50**, 760-76.

Corrado, K., Mills, P. L., Chamberlain, J. S. (1994). Deletion Analysis of the Dystrophin-Actin Binding Domain. *FEBS Letters.* 344, 255-260.

Cowtan, K., Zhang, K. (1999). Density modification for macromolecular phase improvement. *Progress in Biophysics & Molecular Biology*. **72**, 245-270.

Cunningham, C., Gorlin, J., Kwiatkowski, D., Hartwig, J., Janmey, P., Byers, H., Stossel T. (1992). Actin-Binding Protein Requirement for Cortical Stability and Efficient Locomotion. *Science*. **255**, 325-327.

Dabrowska, R., Goch, A., Osinska, H., Szpacenko, A., Sosnski, J. (1985). Dual Effect of Filamin on Actomyosin Atpase Activity. *Journal of Muscle Research and Cell Motility.* **6**, 29-42.

D'Addario, M., Arora, P. D., Fan, J., Ganss, B., Ellen, R. P., McCulloch, C. A. G. (2001). Cytoprotection against Mechanical Forces Delivered through B1 Integrins Requires Induction of Filamin A. *The Journal of Biology Chemistry*. **276**, 31969–31977.

Dalkilic, I., Schienda, J., Thompson, T. G. Kunkel1, L. M. (2006). Loss of FilaminC (FLNc) Results in Severe Defects in Myogenesis and Myotube Structure. *Molecular and Cellular Biology.* **26**, 6522–6534.

Dandapani, S., Sugimoto, H., Matthews, B., Kolb, R., Sinha, S., Gerszten, R., Zhou, J., Ingber, D., Kalluri, R., Pollak, M. (2006). α-Actinin-4 Is Required for Normal Podocyte Adhesion. *The Journal of Biological Chemistry.* **282**, 467–477.

Davis, I., Leaver-Fay, A., Chen, V., Block, J., Kapral, G., Wang, X., Murray, L., Arendall, W., Snoeyink, J., Richardson, J., Richardson, D. (2007). MolProbity: all-atom contacts and structure validation for proteins and nucleic acids. *Nucleic Acids Research*. **35**:W375-W383.

Doherty, G., McMahon, H. (2008). Mediation, modulation, and consequences of membrane-cytoskeleton interactions. *Annual Review of Biophysics.* **37**, 65-95.

Dubreuil, R. R. (1991). Stucture and Evolution of the Actin Cross-linking Proteins. *Bioessays.* **13**, 219-226.

Dyson, J., O'Malley, C., Becanovic, J., Munday, A., Berndt, M., Coghill, I.,. Nandurkar, H., Ooms, L., Mitchell, C. (2001). The SH2-Containing Inositol Polyphosphate 5-Phosphatase, SHIP-2, Binds Filamin and Regulates Submembraneous Actin. *The Journal of Cell Biology*. **155**, 1065-1079.

Emery, A. (2002). The muscular dystrophies. *Lancet*. **359**: 687-695.

Emsley, P., Cowtan, K. (2004). Coot: Model-Building Tools for Molecular Graphics. *Acta Crystallographica D*. **60**, 2126-2132

Engler, A., Humbert, P., Wehrle-Haller, B., Weaver, V. (2009). Multiscale Modeling of Form and Function. *Science.* **324**, 208-21.

Fabbrizio, E., Bonetkerrache, A., Leger, J. J., Mornet, D. (1993). Actin Dystrophin Interface. *Biochemistry.* **32**, 10457-10463.

Feng, Y. Y., Walsh C. A. (2004). The many faces of filamin: A versatile molecular scaffold for cell motility and signalling. *Nature Cell Biology.* **6**, 1034-1038.

Fersht, A. (1972). Conformational equilibria in α- and δ-chymotrypsin : The energetics and importance of the salt bridge. *Journal of Molecular Biology*. **64**, 497-509.

Finn, R., Tate, J., Mistry, J., Coggill, P., Sammut, J., Hotz, H., Ceric, G., Forslund, K., Eddy, S., Sonnhammer, E., Bateman, A. (2008). The Pfam protein families database. *Nucleic Acids Research.* **36**, D281-D288.

Fox, J. W., Lamperti, E. D., Eksioglu, Y. Z., Hong, S. E., Feng, Y.Y., Graham, D. A., Scheffer, I. E., Dobyns, W. B., Hirsch, B. A., Radtke, R. A., Berkovic, S. F., Huttenlocher, P. R., Walsh, C. A. (1998). Mutations in filamin 1 prevent migration of cerebral cortical neurons in human periventricular heterotopia. *Neuron*. **21**, 1315-1325.

Franz-Odendaal, T., Hall, B., Witten, P. (2006). Buried Alive: How Osteoblasts Become Osteocytes. *Developmental Dynamics*. **235**, 176-190.

Franzot, G., Sjoblom, B., Gautel, M., Carugo, K. D. (2005). The crystal structure of the actin binding domain from alpha-actinin in its closed conformation: Structural insight into phospholipid regulation of alpha-actinin. *Journal of Molecular Biology.* **348**, 151-165.

Friedl, P., Bröcker E. (2000). The biology of cell locomotion within three-dimensional extracellular matrix. *Cellular and Molecular Life Sciences.* **57**, 41–64.

Fucini, P., Renner, C., Herberhold, C., Noegel, A. A., Holak, T. A. (1997). The repeating segments of the F-actin cross-linking gelation factor (ABP-120) have an immunoglobulin-like fold. *Nature Structural Biology.* **4**, 223-230.

Fukami, K., Endo, T., Imamura, M., Takenawa, T. (1994). Alpha-actinin and vinculin are PIP(2)-binding proteins involved in signaling by tyrosine kinase. *Journal of Biological Chemistry*. **269**, 1518-1522.

Fukami, K., Sawada, N., Endo, T., Takenawa, T. (1996). Identification of a phosphatidylinositol 4,5-bisphosphate-binding site in chicken skeletal muscle alpha-actinin. *Journal of Biological Chemistry*. **271**, 2646-2650

Furuhashi, K., Inagaki, M., Hatano, S., Fukami, K., Takenawa, T. (1992). Inositol phospholipid-induced suppression of F-actin-gelating activity of smooth muscle actin. *Biochemical and Biophysical Research Communications*. **184**, 1261-1265.

Furuike, S., Ito, T., Yamazakia, M. (2001). Mechanical unfolding of single filamin A (ABP-280) molecules detected by atomic force microscopy. *FEBS Letters*. **498**, 72-75.

Galkin, V., Orlova, A., VanLoock, M. S., Rybakova, I. N., Ervasti, J. M., Egelman, E. H. (2002). The utrophin actin-binding domain binds F-actin in two different modes: implications for the spectrin superfamily of proteins. *Journal of Cell Biology.* **157**, 243-251.

Galkin V., Orlova, A., Cherepanova, O., Lebart M., Egelman, E. (2008). High-resolution cryo-EM structure of the F-actin-fimbrin/plastin ABD2 complex. *Proceedings of the National Academy of Sciences of the United States of America*. **105**, 1494-1498.

Gillies R., Didier, N., Denton, M. (1986). Determination of Cell Number in Monolayer Cultures. *Analytical Biochemistry*. **159**, 109-113.

Gimona, M., Djinovic-Carugo, K., Kranewittera, W. J., Winderc, S. J. (2002). Functional plasticity of CH domains. *FEBS Letters.* **513**, 98-106.

Gimona, M., Mital, R. (1998). The single CH domain of calponin is neither sufficient nor necessary for F-actin binding. *Journal of Cell Science***. 111**, 1813-1821.

Glogauer, M., Arora, P., Chou, D., Janmey, P. A., Downey, G. P., McCulloch, C. A. G. (1998). The role of actin-binding protein 280 in integrin-dependent mechanoprotection. *Journal of Biological Chemistry*. **273**, 1689-1698.

Goldmann W. H. (2001). Phosphorylation of filamin (ABP-280) regulates the binding to the lipid membrane, integrin, and actin. *Cell Biology International*. **2**, 805-808.

Goldsmith, S. C., Pokala, M., Shen, W. Y., Fedorov, A. A., Matsudaira, P., Almo, S. C. (1997). The structure of an actin-crosslinking domain from human fimbrin. *Nature Structural Biology*. **4**, 708-712.

Gomez-Garre, P., Seijo, M.; Gutierrez-Delicado, E., Castro del Rio, M., de la Torre, C., Gomez-Abad, C., Morales-Corraliza, J., Puig, M., Serratosa, J. (2006). Ehlers-Danlos syndrome and periventricular nodular heterotopia in a Spanish family with a single FLNA mutation. *Journal of Medical Genetics.* **43**, 232-237.

Gopalakrishna, R., Anderson, W. (1982). Ca^{2+} -induced hydrophobic site on calmodulin - application for purification of calmodulin by phenyl-sepharose affinity-chromatography. *Biochemical and Biophysical Research Communications.* **104**, 830-836

Gorlin, J. B., Yamin, R., Egan, S., Stewart, M.,. Stossel, T. P., Kwiatkowski, D. J., Hartwig, J. H. (1990). Human Endothelial Actin-Binding Protein (ABP-280, Nonmuscle Filamin) - a Molecular Leaf Spring. *Journal of Cell Biology.* **111**, 1089-1105.

Gupta, R., Ahmad, F., (1999). Protein Stability: Functional Dependence of Denaturational Gibbs Energy on Urea Concentration. *Biochemistry.* **38**, 2471-2479.

Hanahan, D., Jessee, J., Bloom, F. R. (1991). Plasmid Transformation of Escherichia coli and Other Bacteria. *Methods in Enzymology*. **204**, 63-113.

Hanein, D., Volkmann, N., Goldsmith, S., Michon, A. M., Lehman, W., Craig, R., DeRosier, D., Almo, S., Matsudaira, P. (1998). An atomic model of fimbrin binding to F-actin and its implications for filament crosslinking and regulation. *Nature Structural Biology.* 5, 924-924.

Hart, A., Morgan, J., Schneider, J., West, K., McKie, L., Bhattacharya, S., Jackson, I., Cross. S. (2006). Cardiac malformations and midline skeletal defects in mice lacking filamin A. *Human Molecular Genetics*. **15**, 2457–2467.

Hastie, L. E., Patton, W. F., Hechtman, H. B., Shepro, D. (1998). Metabolites of the phospholipase D pathway regulate H_2O_2-induced filamin redistribution in endothelial cells. *Journal of Cellular Biochemistry*. **68**, 511-524.

Hayashi, K., Altman, A. (2006). Filamin A Is Required for T Cell Activation Mediated by Protein Kinase C- θ^1. *Journal of Immunology*. **177**, 1721-1728.

Hemmings, L., Kuhlman, P. A., Critchley, D. R. (1992). Analysis of the Actin-Binding Domain of Alpha-Actinin by Mutagenesis and Demonstration That Dystrophin Contains a Functionally Homologous Domain. *Journal of Cell Biology*. **116**, 1369-1380.

Hidalgo-Bravo, A., Pompa-Mera, E. N., Kofman-Alfaro, S., Gonzalez-Bonilla, C. R., Zenteno, J. C. (2005). A novel filamin A D203Y mutation in a female patient with otopalatodigital type 1 syndrome and extremely skewed X chromosome inactivation. *American Journal of Medical Genetics*. **136A**, 190-193.

Hjalm, G., MacLeod, R. J., Kifor, O., Chattopadhyay, N., Brown, E. M. (2001). Filamin-A Binds to the Carboxyl-terminal Tail of the Calcium-sensing Receptor, an Interaction That Participates in CaR-mediated Activation of Mitogen-activated Protein Kinase. *The Journal of Biological Chemistry*. **276**, 34880–34887.

Hock, R. S., Davis, G., Speicher, D. W. (1990). Purification of Human Smooth-Muscle Filamin and Characterization of Structural Domains and Functional Sites. *Biochemistry.* **29**, 9441-9451.

Holm, L., Kaariainen, S., Rosenstrom, P., Schenkel, A. (2008) Searching protein structure databases with DaliLite v.3. *Bioinformatics*. **24**, 2780-2781.

Jackson, W. M., Jaasma, M. J., Tang, R. Y., Keaveny, T. M. (2008). Mechanical loading by fluid shear is sufficient to alter the cytoskeletal composition of osteoblastic cells. *American Journal of Physiology-Cell Physiology*. **295**, C1007-C1015.

Johnson, W. Protein secondary structure and circular-dichroism - a practical guide. (1990). *Proteins-Structure Function and Genetics*. **7**, 205-214.

Jones, E., Walker N., Stuart D. (1991). Methodology employed for the structure determination of tumour necrosis factor, a case of high non-crystallographic symmetry. *Acta Crystallographica A*. **47**, 753-770.

Jones, S., Thornton, J. M. (1996). Principles of protein-protein interactions. *Proceedings of the National Academy of Sciences of the United States of America*. **93**, 13-20.

Jurdica, P., Saltelb, F., Chabadela, A., Destaing, O. (2006). Podosome and sealing zone: Specificity of the osteoclast model. *European Journal of Cell Biology*. **85,** 195–202.

Kabsch, W. J. (1993). Automatic processing of rotation diffraction data from crystals of initially unknown symmetry and cell constants. *Journal of Applied Crystallography*. **26**, 795-800.

Kakita, A., Hayashi, S., Moro, F., Guerrini, R., Ozawa, T., Ono, K., Kameyama, S., Walsh, C. A., Takahashi, H. (2002). Bilateral periventricular nodular heterotopia due to filamin 1 gene mutation: widespread glomeruloid microvascular anomaly and dysplastic cytoarchitecture in the cerebral cortex. *Acta Neuropathologica.* **104**, 649-657.

Kaplan, J. M., Kim, S. H., North, K. N., Rennke, H., Correia, L. A., Tong, H. Q., Mathis, B. J., Rodriguez-Perez, J. C., Allen, P. G., Beggs, A. H., Pollak, M. R. (2000). Mutations in ACTN4, encoding alpha-actinin-4, cause familial focal segmental glomerulosclerosis. *Nature Genetics*. **24**, 251-256.

Keep, N. H., Winder, S. J., Carolyn, A., Moores, S. W., Norwood, F. L. M., Kendrick-Jones, J. (1999). Crystal structure of the actin-binding region of utrophin reveals a head-to-tail dimer. *Structure with Folding & Design.* **7**, 1539-1546.

Kelly, S., Jess, T., Price, N. (2005). How to study proteins by circular dichroism. *Biochimica et Biophysica Acta.* **1751**, 119-139.

Klaile, E., Müller, M., Kannicht, C., Singer, B., Lucka, L. (2005). CEACAM1 functionally interacts with filamin A and exerts a dual role in the regulation of cell migration. *Journal of Cell Science*. **118**, 5513-5524.

Klein, M. G., Shi, W. X., Klein, M. G., Shi, W., Ramagopal, U., Tseng, Y., Wirtz, D Kovar, D. R., Staiger, C. J. Almo1, S. C. (2004). Structure of the actin crosslinking core of fimbrin. *Structure.* **12**, 999-1013.

Knubovets, T., Osterhout, J., Connolly, P., Klibanov. A. (1999). Structure, thermostability, and conformational flexibility of hen egg-white lysozyme dissolved in glycerol. *Proceedings of the National Academy of Sciences of the United States of America.* 96, 1262–1267.

Korenbaum, E., Rivero, F. (2002). Calponin homology domains at a glance. *Journal of Cell Science*. **115**, 3543-3545.

Koteliansky, V. E., Shirinsky, V. P., Gneushev, G. N., Smirnov, V. N. (1981). Filamin, a High Relative Molecular Mass Actin-Binding Protein from Smooth Muscles, Promotes Actin Polymerisation. *FEBS Letters*. **136**, 98-100.

Krakow, D., Robertson, S. P., King, L. M., Morgan, T., Sebald, E. T., Bertolotto, C., Wachsmann-Hogiu, S., Acuna, D., Shapiro, S. S., Takafuta, T., Aftimos, S., Kim, C. A., Firth, H., Steiner, C. E., Cormier-Daire, V., Superti-Furga, A., Bonafe, L., Graham, J. M., Grix, A., Bacino, C. A., Allanson, J., Bialer, M. G., Lachman, R. S., Rimoin, D. L., Cohn, D. H. (2004). Mutations in the gene encoding filamin B disrupt vertebral segmentation, joint formation and skeletogenesis. *Nature Genetics.* **36**, 405-410.

Kuhlman, P. A., Hemmings, L., Critehley, D. R. (1992). The Identification and Characterization of an Actin-Binding Site in Alpha-Actinin by Mutagenesis. *FEBS Letters.* **304**, 201-206.

Lad, Y, Jiang, P., Ruskamo, S., Harburger, D., Ylaänne, J., Campbell, I., Calderwood, D. (2008). Structural basis of the migfilin-filamin interaction and competition with integrin β tails. *The Journal of Biological Chemistry*. **283**, 35154–35163.

Laskowski, R., MacArthur, M., Moss, D., Thornton, J. (1993). PROCHECK: a program to check the stereochemical quality of protein structures. *The Journal of Applied Crystalography.* **26**, 283-291.

Lavinder, J., Hari, S., Sullivan, B., Magliery, T. (2009). High-Throughput Thermal Scanning: A General, Rapid Dye-Binding Thermal Shift Screen for Protein Engineering. *Journal of the American Chemical Society*. **131**, 3794–3795.

Laemmli, U. (1970). Cleavage of structural proteins during the assembly of the head of bacteriophage T4. *Nature.* **227**, 680-685.

Lebart, M. C., C. Mejean, Casanova, D., Audemard, E., Derancourt, J., Roustan, C., Benyamin, Y. (1994). Characterization of the Actin-Binding Site on Smooth-Muscle Filamin. *Journal of Biological Chemistry.* **269**, 4279-4284.

Lee, S., Weins, A., Hayes, D., Pollak, M., Dominguez, R. (2008). Crystal Structure of the Actin-Binding Domain of α-Actinin-4 Lys255Glu Mutant Implicated in Focal Segmental Glomerulosclerosis. *Journal of Molecular Biology*. **376**, 317–324.

Lehman, W, Craig, R., Kendrick-Jones, J., Sutherland-Smith, A. J. (2004). An open or closed case for the conformation of calponin homology domains on F-actin? *Journal of Muscle Research and Cell Motility.* **25**, 351–358.

Leslie, A.G.W. (1992). Recent changes to the MOSFLM package for processing film and image plate data. *Newsletter on Protein Crystallography*, No. 26.

Leung, C., Liem, R., Parry, D., Green, K. (2001). The plakin family. *Journal of Cell Science.* **114**, 3409-3410.

Levine, B. A., Moir, A. J. G., Audemard, E., Mornet, D., Patchell, V. B., Perry, S. V. (1990). Structural Study of Gizzard Caldesmon and Its Interaction with Actin - Binding Involves Residues of Actin Also Recognized by Myosin Subfragment-1. *European Journal of Biochemistry*. **193**, 687-696

Levine, B. A., Moir, A. J. G., Patchell, V.B., Perry, S.V. (1992). Binding-Sites Involved in the Interaction of Actin with the N-Terminal Region of Dystrophin. *FEBS Letters.* **298**, 44-48.

Liang, C., Park, A., Guan, J. (2007). In vitro scratch assay: a convenient and inexpensive method for analysis of cell migration in vitro. *Nature Protocols*. **2**, 329-333.

Liu, G. P., Thomas, L., Warren, R. A., Enns, C. A., Cunningham, C. C., Hartwig, J. H., Thomas, G. (1997). Cytoskeletal protein ABP-280 directs the intracellular trafficking of furin and modulates proprotein processing in the endocytic pathway. *Journal of Cell Biology*. **139**, 1719-1733.

Loo, D. T., Kanner, S. B., Aruffo, A. (1998). Filamin binds to the cytoplasmic domain of the beta(1)-integrin - Identification of amino acids responsible for this interaction. *Journal of Biological Chemistry.* **273**, 23304-23312.

Lorenzi, M., Gimona, M. (2008). Synthetic actin-binding domains reveal compositional constraints for function. *International Journal of Biochemistry & Cell Biology*. **40**, 1806-1816

Loy, C. J., Sim, K. S. Yong, E. L. (2003). Filamin-A fragment localizes to the nucleus to regulate androgen receptor and coactivator functions. *Proceedings of the National Academy of Sciences of the United States of America.* **100**, 4562-4567.

Matthews, B. (1968). Solvent content of protein crystals. *Journal of Molecular Biology*. **33**, 491-497.

McCoy, A., Grosse-Kunstleve, R., Storoni, L., Read, R. (2005). Likelihood-enhanced fast translation functions. *Acta Crystallographica Section D*. **61**, 458-464.

McCoy, A. J., Fucini, P., Noegel, A. A., Stewart, M. (1999). Structural basis for dimerization of the Dictyostelium gelation factor (ABP120) rod. *Nature Structural Biology*. **6**, 836-841

Mejean, C., Lebart, M. C., Boyer, M., Roustan, C., Benyamin, Y. (1992). Localization and Identification of Actin Structures Involved in the Filamin Actin Interaction. *European Journal of Biochemistry.* **209**, 555-562.

Mejean, C., Lebart, M. C., Roustan, C., Benyamin, Y. (1995). Inhibition of ACTIN-dystrophin interaction by inositide phosphate. *Biochemical and Biophysical Research Communications.* **210**, 152-158

Moens, P., Bagatolli, L. (2007). Profilin binding to sub-micellar concentrations of phosphatidylinositol (4,5) bisphosphate and phosphatidylinositol (3,4,5) trisphosphate. *Biochimica et Biophysica Acta*. **1768**, 439–449.

Moores, C. A., Kendrick-Jones, J. (2000). Biochemical characterisation of the actin-binding properties of utrophin. *Cell Motility and the Cytoskeleton.* **46**, 116-128.

Moro, F., Carrozzo, R., Veggiotti, P., Tortorella, G., Toniolo, D., Volzone, A., Guerrini, R. (2002). Familial periventricular heterotopia - Missense and distal truncating mutations of the FLN1 gene. *Neurology.* **58**, 916-921.

Morris, G., Man, N., Huyen, N., Pereboev, A., Kendrick-Jones, J., Winder, S. (1999). Disruption of the utrophin-actin interaction by monoclonal antibodies and prediction of an actin-binding surface of utrophin. *Biochemical Journal.* **337**, 119-123.

Murray, J., Davies, K., Harper, P., Meredith, L, Mueller C., Williamson, R. (1982). Linkage relationship of a cloned DNA-sequence on the short arm of the X-chromosome to duchenne muscular-dystrophy. *Nature*. **300**, 69-71.

Murshudov, G., Vagin, A., Dodson, E. (1997). Refinement of macromolecular structures by the maximum-likelihood method. *Acta Crystallographica D.* **53**, 240-255.

Nagano, T, Yoneda, T., Hatanaka, Y., Kubota, C., Murakami, F., Sato, M. (2002). Filamin A-interacting protein (FILIP) regulates cortical cell migration out of the ventricular zone. *Nature Cell Biology*. **4**, 495-501.

Nagano, T., Morikubo, S., Sato, M. (2004). Filamin A and FILIP (Filamin A interacting protein) regulate cell polarity and motility inneocortical subventricular and intermediate zones during radial migration. *Journal of Neuroscience*. **24**, 9648-9657.

Nakamura, F., Hartwig, J. H., Stossel, T. P., Szymanski, P. T. (2005). Ca^{2+} and Calmodulin Regulate the Binding of Filamin A to Actin Filaments. *The Journal of Biological Chemistry*. **280**, 32426–32433.

Nakamura, F., Osborn, T. M., Hartemink, C. A., Hartwig, J. H., Stossel, T. P. (2007). Structural basis of filamin A functions. *Journal of Cell Biology*. **179**, 1011-1025.

Niesen, F., Berglund, H., Vedadi, M. (2007). The use of differential scanning fluorimetry to detect ligand interactions that promote protein stability. *Nature Protocols*. **2**, 2212-2221.

Niederman, R., Amrein, P. C., Hartwig, J. (1983). 3-Dimensional Structure of Actin-Filaments and of an Actin Gel Made with Actin-Binding Protein. *Journal of Cell Biology.* **96**, 1400-1413.

Nomachi, A., Nishita, M., Inaba, D., Enomoto, M., Hamasaki, M., Minami, Y. (2008). Receptor Tyrosine Kinase Ror2 Mediates Wnt5a-induced Polarized Cell Migration by Activating c-Jun N-terminal Kinase via Actin-binding Protein Filamin A. *The Journal of Biological Chemistry.* **283**, 27973–27981.

Norwood, F. L. M., Sutherland-Smith, A. J., Keep, N. H., Kendrick-Jones, J. (2000). The structure of the N-terminal actin-binding domain of human dystrophin and how mutations in this domain may cause Duchenne or Becker muscular dystrophy. *Structure with Folding & Design.* **8**, 481-491.

Notredame, C., Higgins, D., Heringa, J. (2000). T-Coffee: A novel method for multiple sequence alignments. *Journal of Molecular Biology*. **302**, 205-217.

Ohta, Y., Stossel, T. P., Hartwig, J. H. (1991). Ligand-Sensitive Binding of Actin-Binding Protein to Immunoglobulin-G Fc Receptor-I (Fc-Gamma-Ri). *Cell.* **67**, 275-282.

Ohta, Y., Hartwig, J. H. (1996). Phosphorylation of actin-binding protein 280 by growth factors is mediated by p90 ribosomal protein S6 kinase. *Journal of Biological Chemistry*. **271**, 11858-11864.

Ohta, Y., Suzuki, N., Nakamura, S., Hartwig, J. H., Stossel, T. P. (1999). The small GTPase RalA targets filamin to induce filopodia. *Proceedings of the National Academy of Sciences of the United States of America.* **96**, 2122-2128.

Olson, E., Walsh, C. (2002). Smooth, rough and upside-down neocortical development. *Current Opinion in Genetics & Development*. **12**, 320-327.

Osborn, T. (2007). Mechanism of F-actin crosslinking by filamin A and the anti-inflammatory functions of plasma gelsolin in bodily fluids. Thesis. Göteborg University.

Perutz M., Raidt H. (1975). Stereochemical basis of heat-stability in bacterial ferredoxins and in hemoglobin-A2. *Nature*. **255**, 256-259.

Perutz, M. (1978). Electrostatic effects in proteins. *Science.* 201, 1187-1191.

Pettersen, E., Goddard, T., Huang, C., Couch, G., Greenblatt, D., Meng, E., Ferrin, T. (2004). UCSF Chimera - A Visualization System for Exploratory Research and Analysis. *Journal of Computational Chemistry*. **25**, 1605-1612

Poussaint, T. Y., Fox, J. W., Dobyns, W. B., Radtke, R., Scheffer, I. E., Berkovic, S. F., Barnes, P. D., Huttenlocher, P. R., Walsh, C. A. (2000). Periventricular nodular heterotopia in patients with filamin-1 gene mutations: neuroimaging findings. *Paediatric Radiology*. **30**, 748-755.

Prior, T., Papp, A., Snyder, P., Burghes, A., Bartolo, C., Sedra, M., Western, L., Mendell, J. (1993). A missense mutation in the dystrophin gene in a Duchenne muscular-dystrophy patient. *Nature Genetics*. **4**, 357-360.

Ramachandran G., Ramakrishnan C., Sasisekharan V. (1963). Stereochemistry of polypeptide chain configurations. *Journal of Molecular Biology.* **7**, 95-99.

Read, R.J. (2001). Pushing the boundaries of molecular replacement with maximum likelihood. *Acta Crystallographica D.* **57**, 1373-1382.

Revenu, C., R. Athman, R., Robine, S., Louvard, D. (2004). The co-workers of actin filaments: From cell structures to signals. *Nature Reviews Molecular Cell Biology*. **5**, 635-646.

Reynolds, C., Damerell, D., Jones, S. (2009). ProtorP: a protein-protein interaction analysis server. *Bioinformatics*. **25**, 413-416.

Rice, L., Shamoo, Y., Brünger, A. (1998). Phase Improvement by Multi-Start Simulated Annealing Refinement and Structure-Factor Averaging. *Journal of Applied Crystallography*. **31**, 798-805.

Roberts, R. G., Gardner, R. J., Bobrow, M. (1994). Searching for the 1 in 2,400,000: A review of dystrophin gene point mutations. *Human Mutation*. **4**, 1-11.

Robertson, S. P., Twigg, S. R. F., Sutherland-Smith, A. J., Biancalana, V., Gorlin, R. J., Horn, D., Kenwrick, S. J., Kim, C. A., Morava, E., Newbury-Ecob, R., Orstavik, K. H., Quarrell, O. W. J., Schwartz, C. E., Shears, D. J., Suri, M., Kendrick-Jones, J., Wilkie, A. O. M. (2003). Localized mutations in the gene encoding the cytoskeletal protein filamin A cause diverse malformations in humans. *Nature Genetics.* **33**, 487-491.

Robertson, S. P. (2005). Filamin A: phenotypic diversity. *Current Opinion in Genetics & Development*. **15**, 301-307

Robertson, S. P. (2007). Otopalatodigital syndrome spectrum disorders: otopalatodigital syndrome types 1 and 2, frontometaphyseal dysplasia and Melnick-Needles syndrome. *European Journal of Human Genetics*. **15**, 3-9.

Sarkisian, M., Bartley C., Chi, H., Nakamura, F., Hashimoto-Torii K., Torii M., Flavell R., Rakic, P. (2006). MEKK4 signalling regulates filamin expression and neuronal migration. *Neuron*. 52, 789-801.

Saltel, F., Destaing, O., Bard, F., Eichert, D., Jurdic, P. (2004). Apatite-mediated Actin Dynamics in Resorbing Osteoclasts. *Molecular Biology of the Cell*. **15**, 5231–5241.

Sarkisian, M., Bartley, C., Rakic, P. (2008). Trouble making the first move: interpreting arrested neuronal migration in the cerebral cortex. *Trends in Neurosciences*. **31**, 54-61.

Sawyer, G., Clark, A., Robertson, S., Sutherland-Smith, A. (2009). Disease-associated Substitutions in the Filamin B Actin Binding Domain Confer Enhanced Actin Binding Affinity in the Absence of Major Structural Disturbance: Insights from the Crystal Structures of Filamin B Actin Binding Domains. *Journal of Molecular Biology*. **390**, 1030-1047.

Schomaker V., Trueblood K. (1998). Correlation of Internal Torsional Motion with Overall Molecular Motion in Crystals. *Acta Crystallographica B*. **54**, 507-514.

Schultz, J., Milpetz, F., Bork, P., Ponting, C. (1998). SMART, a simple modular architecture research tool: Identification of signalling domains. *Proceedings of the National Academy of Science of the USA*. **95**, 5857-5864.

Seck, T. Baron, R., Horne, W. (2003). Binding of filamin to the C-terminal tail of the calcitonin receptor controls recycling. *Journal of Biological Chemistry*. **278**, 10408-10416.

Sharma, C. P., Ezzell, R. M., Arnaout, M. A. (1995). Direct Interaction of Filamin (Abp-280) with the Beta-2-Integrin Subunit Cd18. *Journal of Immunology*. **154**, 3461-3470.

Sharma, C. P. Goldmann, W. H. (2004). Phosphorylation of actin-binding protein (ABP-280; filamin) by tyrosine kinase p56(lck) modulates actin filament cross-linking. *Cell Biology International.* **28**, 935-941.

Sheen, V., Dixon, P., Fox, J., Hong, S., Kinton, L., Sisodiya, S., Duncan, J., Dubeau, F, Scheffer, I., Schachter, S., Wilner, A., Henchy, R., Crino, P., Kamuro, K., DiMario, F., Berg, M., Kuzniecky, R., Cole, A., Bromfield, E., Biber, M., Schomer, D., Wheless, J., Silver, K., Mochida, G., Berkovic, S., Andermann, F., Andermann, E., Dobyns, W., Wood, N., Walsh, C. (2001). Mutations in the X-linked filamin 1 gene cause periventricular nodular heterotopia in males as well as in females. *Human Molecular Genetics.* **10**, 1775-1783.

Sheen, V. L., Feng, Y., Graham, D., Takafuta, T., Shapiro, S. S., Walsh, C. A. (2002). Filamin A and Filamin B are co-expressed within neurons during periods of neuronal migration and can physically interact. *Human Molecular Genetics*. **11**, 2845-2854.

Sheen, V. L., Jansen, A., Chen, M. H., Parrini, E., Morgan, T., Ravenscroft, R., Ganesh, V., Underwood, T., Wiley, J., Leventer, R., Vaid, R. R., Ruiz, D. E., Hutchins, G. M., Menasha, J., Willner, J., Geng, Y., Gripp, K. W., Nicholson, L., Berry-Kravis, E., Bodell, A., Apse, K., Hill, R. S., Dubeau, F., Andermann, F., Barkovich, J., Andermann, E., Shugart, Y. Y., Thomas, P., Viri, M., Veggiotti, P., Robertson, S., Guerrini, R.,

Walsh, C. A. (2005). Filamin A mutations cause periventricular heterotopia with Ehlers-Danlos syndrome. *Neurology.* **64**, 254-262.

Shoichet, B., Baase, W., Kuroki, R., Matthews B. (1995). A Relationship Between Protein Stability and Protein Function. *Proceedings of the National Academy of Sciences of the United States of America.* **92**, 452-456.

Smith P., Krohn, R., Hermanson, G., Mallia, A., Gartner, F., Provenzano, M., Fujimoto, E., Goeke, N., Olson B., Klenk D. (1985). Measurement of protein using bicinchoninic acid. *Analytical Biochemistry*. **150**, 76-85.

Stahlhut, M., van Deurs, B. (2000). Identification of Filamin as a Novel Ligand for Caveolin-1: Evidence for the Organization of Caveolin-1–associated Membrane Domains by the Actin Cytoskeleton. *Molecular Biology of the Cell.* **11**, 325–337.

Stossel, T. P., Condeelis, J., Cooley, L., Hartwig, J. H., Noegel, A., Schleicher, M., Shapiro, S. S. (2001). Filamins as integrators of cell mechanics and signalling. *Nature Reviews Molecular Cell Biology.* **2**, 138-145.

Sutherland-Smith, A. J., C. A. Moores, Norwood, F. L. M., Hatch, V., Craig, R., Kendrick-Jones, J., Lehman, W. (2003). An atomic model for actin binding by the CH domains and spectrin-repeat modules of utrophin and dystrophin. *Journal of Molecular Biology.* **329**, 15-33.

Takafuta, T., Wu, G. X., Murphy, G. F., Shapiro, S.S. (1998). Human beta-filamin is a new protein that interacts with the cytoplasmic tail of glycoprotein Ib alpha. *Journal of Biological Chemistr*y. **273**, 17531-17538.

Thompson, J., Higgins, D., Gibson, T. (1994). CLUSTAL W: improving the sensitivity of progressive multiple sequence alignment through sequence weighting, position-specific gap penalties and weight matrix choice. *Nucleic Acids Research*. **22**, 4673-4680.

Travis, M., van der Flier, A., Kammerera, R., Moulda, A., Sonnenberg, A., Humphries, M. (2004). Interaction of filamin A with the integrin b7 cytoplasmic domain: role of alternative splicing and phosphorylation. *FEBS Letters*. **569**, 185-190.

Tyler, J. M., Anderson, J. M. Branton, D. (1980). Structural Comparison of Several Actin-Binding Macromolecules. *Journal of Cell Biology.* **85**, 489-495.

Tu, Y., Wu, S., Shi, X., Chen, K., Wu, C. (2003). Migfilin and Mig-2 Link Focal Adhesions to Filamin and the Actin Cytoskeleton and Function in Cell Shape Modulation
Cell. **113**, 37-47.

Vadlamudi, R. K., Li, F. Adam, L., Nguyen, D., Ohta, Y., Stossel, T. P. Kumar, R. (2002). Filamin is essential in actin cytoskeletal assembly mediated by p21-activated kinase 1. *Nature Cell Biology.* **4**, 681-690.

van der Flier, A., Sonnenberg, A. (2001). Structural and functional aspects of filamins. *Biochimica et Biophysica Acta-Molecular Cell Research.* **1538**, 99-117.

Volkmann, N., DeRosier, D., Matsudaira, P., Hanein, D. (2001). An Atomic Model of Actin Filaments Cross-linked by Fimbrin and Its Implications for Bundle Assembly and Function. *Journal of Cell Biology*. **153**, 947-956.

Vorgerd, M., van der Ven, P., Bruchertseifer, V., Löwe, T., Kley, R., Schröder, R., Lochmüller, H., Himmel, M., Koehler, K., Fürst, D., Huebner, A. (2005). A Mutation in the Dimerization Domain of Filamin C Causes a Novel Type of Autosomal Dominant Myofibrillar Myopathy. *American Journal of Human Genetics*. **77**, 297–304.

Way, M., Pope, B., Cross, R., Kendrick-Jones, J., Weeds, A. (1992). Expression of the N-terminal domain of dystrophin in *E. coli* and demonstration of binding to F-actin. *FEBS Letters*. **301**, 243-245.

Weihing, R. R. (1988). Actin-Binding and Dimerization Domains of Hela-Cell Filamin. *Biochemistry.* **27**, 1865-1869.

Weins, A., Schiondorff, J. S., Nakamura, F., Denker, B. M., Hartwig, J. H., Stossel, T. P., Pollak, M. R. (2007). Disease-associated mutant alpha-actinin-4 reveals a mechanism for regulating its F-actin-binding affinity. *Proceedings of The National Academy Of Sciences Of The United States Of America*. **104**, 16080-16085.

Winder, S. J. (1997). The membrane-cytoskeleton interface: the role of dystrophin and utrophin. *Journal of Muscle Research and Cell Motility.* **18**, 617-629.

Winn, M., Isupov M., Murshudov, G. (2000). Use of TLS parameters to model anisotropic displacements in macromolecular refinement. *Acta Crystallographica D.* **57**, 122-133

Woo, M. S., Ohta, Y., Rabinovitz, I., Stossel, T. P., Blenis, J. (2004). Ribosomal S6 kinase (RSK) regulates phosphorylation of filamin A on an important regulatory site. *Molecular Cell Biology.* **24**, 3025-3035.

Xu, W. F., Xie, Z. W., Chung, D. W., Davie, E. W. (1998). A novel human actin-binding protein homologue that binds to platelet glycoprotein Ib alpha. *Blood.* **92**, 1268-1276.

Yamazaki, M., Furuike, S., Ito, T. (2002). Mechanical response of single filamin A (ABP-280) molecules and its role in the actin cytoskeleton. *Journal of Muscle Research and Cell Motility*. **23**, 525-534.

Yang, F., Gustafson, K. R., Boyd, M. R., Gronenborn, A. M., Clore, G. M., Wlodawer, A. (1999). Crystal structure of a potent HIV-inactivating protein cyanovirin-N shows domain-swapping. *Biophysical Journal.* **76**, A137-A137.

Yao, J., Lee, T. C., Kos, C. H., Henderson. J. M., Allen, P. G., Denker, B. M., Pollak, M. R. (2004). α-Actinin-4-mediated FSGS: an inherited kidney disease caused by an aggregated and rapidly degraded cytoskeletal protein. *PLoS Biology.* **2**, 787-794 .

Yeh, A., McMillan, A., Stowell, M. (2005). Rapid and simple protein-stability screens: application to membrane proteins. *Acta Crystallographica D.* **D62**, 451–457

Yuan, Y., Shen, Z. (2001). Interaction with BRCA2 Suggests a Role for Filamin-1 (hsFLNa) in DNA Damage Response. *The Journal of Biological Chemistry.* **276**, 48318–48324.

Zhang, D., Herring, J. A., Swaney, S. S., McClendon, T. B., Gao, X., Browne, R. H., Rathjen, K. E., Johnston, C. E., Harris, S., Cain, N. M., Wise, C. A. (2006). Mutations responsible for Larsen syndrome cluster in the FLNB protein. *Journal of Medical Genetics.* **43**, e24.

Zhang, W., Han, S. W., McKeel, D. W., Goate, A., Wu, J. Y. (1998). Interaction of Presenilins with the Filamin Family of Actin-Binding Proteins. *The Journal of Neuroscience.* **18**, 914–922.

9 Appendix

9.1 Gel Filtration Standard Curve

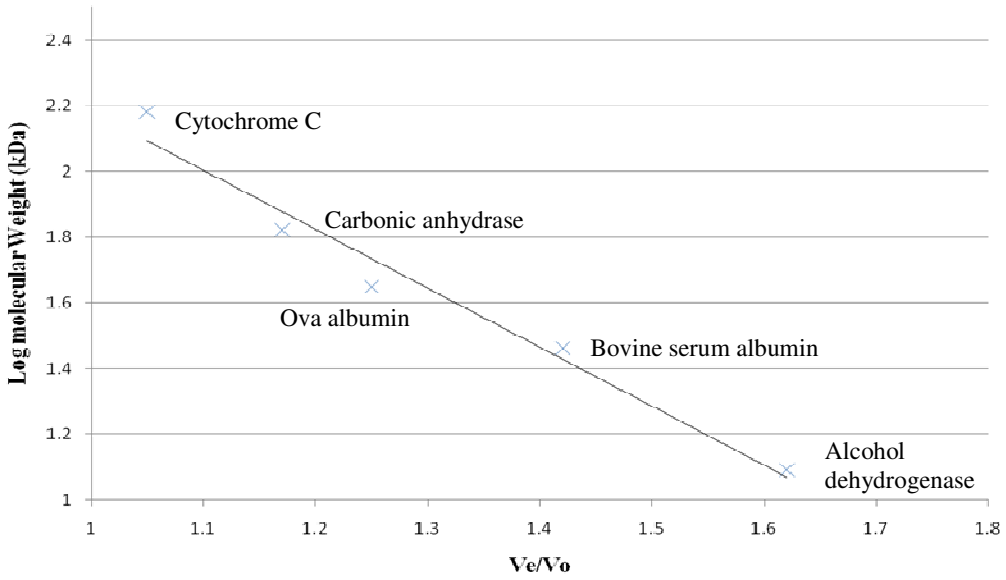

Figure 9-1. Calibration of the Superdex 75 Gel Filtration Column.

The column was calibrated using the standards;

Cytochrome C (12.4 kDa)

Carbonic anhydrase (29 kDa)

Ova albumin (45 kDa)

Bovine serum albumin (66 kDa)

Alcohol dehydrogenase (150 kDa)

The void volume, (Vo), was determined by β-amylase, (200 kDa). The standards, (and samples), were injected and run in 50 mM K_2HPO_4/KH_2PO_4, pH 8, 150 mM NaCl buffer.

9.2 Densitometry of Coomassie Stain with Filamin A ABD Standards

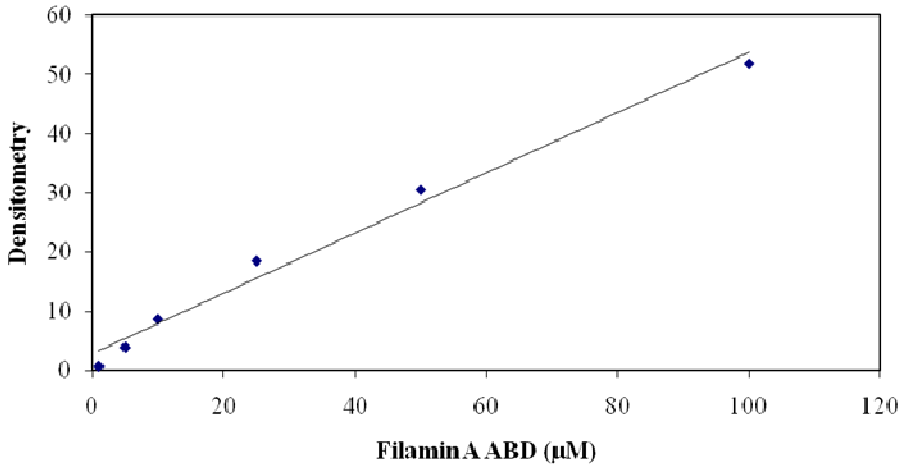

Figure 9-2. Calibration of the Linearity of Coomassie Stain in SDS PAGE Analysis.
Samples were run in a 12% SDS gel, stained and the density of the protein bands in the supernatant and pellet fractions was determined using the QuantityOne software (Biorad).

9.3 BSA Standard of the BCA Assay

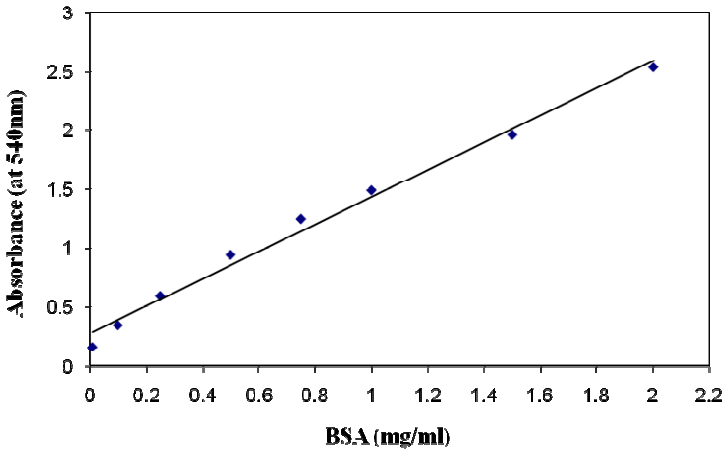

Figure 9-3. Standard Curve of BSA for the BCA Assay.

Standards were made up from 0-2mg/mL to construct a standard curve for the BSA assay to determine the concentration of the unknown protein samples.